

POLITECNICO DI TORINO

Collegio di Ingegneria Chimica e dei Materiali
Corso di Laurea Magistrale in Ingegneria dei Materiali

Tesi di Laurea Magistrale

**Passivation of metals (Co, Cu) with
Self-Assembled Monolayers for area-selective
Atomic Layer Deposition**



Relatore

prof. Marco Sangermano

Candidato

Giuseppe Nappo

Anno accademico 2018-2019

TABLE OF CONTENTS

LIST OF FIGURES	pag. IV
LIST OF TABLES	pag. VIII
RIASSUNTO	pag. IX
INTRODUCTION	pag. 1
CHAPTER 1. BACKGROUND	pag. 3
• 1.1 DOWNWARD SCALING OF DEVICES	pag. 3
• 1.2 INTERCONNECT SCALING ISSUES	pag. 5
- 1.2.1 Physical issues of interconnects scaling.....	pag. 5
- 1.2.2 Technological issues of interconnects scaling.....	pag. 11
CHAPTER 2. AREA SELECTIVE ATOMIC LAYER DEPOSITION	pag. 16
• 2.1 ATOMIC LAYER DEPOSITION	pag. 16
- 2.1.1 Introduction to the process	pag. 16
- 2.1.2 Binary ALD	pag. 17
- 2.1.3 ALD pros and cons	pag. 17
- 2.1.4 Process parameters	pag. 18
- 2.1.5 Growth mechanism	pag. 19
- 2.1.6 ALD precursors	pag. 20
• 2.2 AREA SELECTIVITY.....	pag. 22
- 2.2.1 General considerations	pag. 22
- 2.2.2 Selectivity (S)	pag. 24
- 2.2.3 Inherent area-selectivity	pag. 25

- 2.2.4 Functionalization by area-deactivation.....	pag. 27
- 2.2.5 Selectivity issues and further developments	pag. 28
CHAPTER 3. SELF-ASSEMBLED MONOLAYERS	pag. 30
• 3.1 GENERALITIES ABOUT SAMS.....	pag. 30
- 3.1.1 SAMs structure	pag. 30
- 3.1.2 SAMs growth mechanisms	pag. 32
- 3.1.3 SAMs from liquid phase	pag. 34
• 3.2 THIOLS SELF-ASSEMBLED MONOLAYERS	pag. 35
- 3.2.1 Basic notions.....	pag. 35
- 3.2.2 Alkanethiols	pag. 36
CHAPTER 4. EXPERIMENTAL METHOD.....	pag. 38
• 4.1 PROCEDURAL STEPS	pag. 38
- 4.1.1 Preparation of the samples	pag. 38
- 4.1.2 Glassware cleaning	pag. 39
- 4.1.3 Preparation of the ODT solution	pag. 40
- 4.1.4 SAM deposition by spin coating	pag. 40
- 4.1.5 Characterization of the samples.....	pag. 42
- 4.1.6 Thermal study of the samples	pag. 43
- 4.1.7 ALD attempts.....	pag. 43
• 4.2 PROCEDURAL TECHNIQUES	pag. 45
- 4.2.1 Spectroscopic Ellipsometry (SE)	pag. 45
- 4.2.2 Water droplet Contact Angle measurement (WCA).....	pag. 46
- 4.2.3 Atomic Force Microscopy (AFM)	pag. 48
- 4.2.4 Cyclic Voltammetry (CV)	pag. 49
- 4.2.5 Rutherford Backscattering Spectroscopy (RBS)	pag. 51
CHAPTER 5. COBALT: RESULTS AND DISCUSSION.....	pag. 53
• 5.1 SPIN COATING	pag. 53

- 5.1.1 ODT [different ways for solution deposition] – spinning	pag. 53
- 5.1.2 ODT [2 min] – spinning [different rpm]	pag. 54
- 5.1.3 ODT [different wetting times] – spinning	pag. 55
- 5.1.4 Annealing test.....	pag. 55
- 5.1.5 ODT – rinsing – spinning	pag. 55
- 5.1.6 Pre-treatment _{EtOH} – ODT – rinsing – spinning	pag. 56
- 5.1.7 Pre-treatment _{DMAB} – Pre-treatment _{EtOH} – ODT – rinsing – spinning.....	pag. 56
- 5.1.8 Pre-treatment _{DMAB} – Pre-treatment _{EtOH} – ODT – rinsing – spinning [other attempts].....	pag. 57
- 5.1.9 Pre-treatment _{DMAB} – Pre-treatment _{EtOH} – ODT [wet annealing] – rinsing – spinning	pag. 58
• 5.2 POST SPIN COATING	pag. 61
- 5.2.1 Thermal study on the best Co sample	pag. 61
- 5.2.2 ALD on the best Co sample	pag. 63
CHAPTER 6. COPPER: RESULTS AND DISCUSSION	pag. 65
• 6.1 SPIN COATING	pag. 65
- 6.1.1 Pre-treatment _{EtOH} – ODT – rinsing – spinning	pag. 65
- 6.1.2 Pre-treatment _{EtOH} – ODT [wet annealing] – rinsing – spinning	pag. 66
- 6.1.3 Pre-treatment _{EtOH} – ODT – rinsing – spinning – annealing	pag. 67
• 6.2 POST SPIN COATING	pag. 69
- 6.2.1 Thermal study on the best Cu sample	pag. 69
- 6.2.2 ALD on the best Cu sample	pag. 70
CONCLUSIONS	pag. 74
REFERENCES.....	pag. 75

LIST OF FIGURES

1.1	IC front- and back- end	pag. 5
1.2	Simplified structure for RC analysis.....	pag. 6
1.3	Simplified diagram of copper interconnect scaling	pag. 9
1.4	Plot of cobalt and copper resistivities versus trench critical dimension.....	pag. 10
1.5	General fabrication method of a vertical interconnect access.....	pag. 12
1.6	Comparison between a conventional nano-patterning technique and area selective atomic layer deposition	pag. 14
1.7	VIA filling	pag. 15
2.1	Typical ALD process	pag. 17
2.2	Plot of ALD growth rate versus temperature	pag. 19
2.3	Proposed classification of ALD processes based on the initial growth per cycle	pag. 20
2.4	Selectivity window and nucleation delay	pag. 25
2.5	Area selective deposition of W on silicon substrate	pag. 26
2.6	Silicon-selective ZnO ALD using ODPAs-SAMs as blocking layer on copper	pag. 27
2.7	Selectivity improving approach by monomers regeneration in ZnO ALD	pag. 28
3.1	SAM structure	pag. 30
3.2	SAMs growth mechanism	pag. 33
3.3	Dipping methodology for growing SAMs from liquid phase	pag. 34
3.4	ODT molecular structure	pag. 36
3.5	Schematic view of a single chain of an alkanethiol adsorbed on a substrate	pag. 37
4.1	Picture of the spin coater	pag. 41
4.2	Picture of the heat pulse	pag. 43
4.3	Arrangement of the coupons in the reactor used to perform the Hf _x N _y ALD .	pag. 44
4.4	Representation of the change in polarization of an incident light beam on a sample.....	pag. 45
4.5	Picture of the Woollam RC2 ellipsometer	pag. 46

4.6	Schematic of a liquid drop spread on a solid surface	pag. 47
4.7	Picture of the water contact angle tool.....	pag. 47
4.8	Representation of atomic force microscopy working principle	pag. 48
4.9	Picture of the experimental setup for the CV.....	pag. 51
5.1	Results for two different ways of depositing the ODT solution on the coupons.....	pag. 54
5.2	Results for coupons spun at different rpm.....	pag. 54
5.3	Results for coupons spun after different contact times of ODT solution	pag. 55
5.4	Results, at different ODT solution contact times, for coupons rinsed with EtOH after spinning	pag. 56
5.5	Results, at different ODT solution contact times, for coupons pre-treated with EtOH and rinsed with EtOH before spinning	pag. 56
5.6	Results, at different ODT solution contact times, for coupons pre-treated with DMAB solution and EtOH, and rinsed with EtOH before spinning	pag. 57
5.7	Thicknesses from SE curves, at different ODT solution contact times, for coupons pre-treated with DMAB solution and EtOH, treated with wet-annealing at different temperatures, and rinsed with EtOH before spinning.....	pag. 58
5.8	WCA values, at different ODT solution contact times, for coupons pre-treated with DMAB solution and EtOH, treated with wet-annealing at different temperatures, and rinsed with EtOH before spinning	pag. 58
5.9	AFM images for coupons pre-treated with DMAB solution and EtOH, treated with wet-annealing (at different temperatures and contact times) and rinsed with EtOH before spinning	pag. 59
5.10	CV voltammograms for bare cobalt and 4 coupons pre-treated with DMAB solution and EtOH, treated with wet-annealing (at different temperatures and contact times) and rinsed with EtOH before spinning	pag. 60
5.11	Percentage coverage values for 4 coupons pre-treated with DMAB solution and EtOH, treated with wet-annealing (at different temperatures and contact times) and rinsed with EtOH before spinning	pag. 61

5.12	Thermal study, carried on at 6 different temperatures, for a Co coupon pre-treated with DMAB solution and EtOH, treated with wet-annealing (at 40°C, for 6 minutes) and rinsed with EtOH before spinning	pag. 62
5.13	CV results of thermal study, carried on at 6 different temperatures, for a Co coupon pre-treated with DMAB solution and EtOH, treated with wet-annealing (at 40°C, for 6 minutes) and rinsed with EtOH before spinning	pag. 62
5.14	Plot of thickness change experienced by 4 different coupons versus number of cycles of Hf _x N _y ALD performed at 120°C	pag. 63
5.15	Plot of thickness change experienced by 4 different coupons versus number of cycles of Hf _x N _y ALD performed at 150°C	pag. 64
6.1	Results, at different ODT solution contact times, for coupons pre-treated with EtOH and rinsed with EtOH before spinning	pag. 65
6.2	CV results, at different ODT solution contact times, for coupons pre-treated with EtOH and rinsed with EtOH before spinning	pag. 66
6.3	Results, at different ODT solution contact times, for coupons pre-treated with EtOH, treated with wet-annealing (at 40°C) and rinsed with EtOH before spinning	pag. 67
6.4	Results, at different ODT solution contact times, for coupons pre-treated with EtOH, rinsed with EtOH before spinning and annealed after spinning...	pag. 67
6.5	Roughness profiles with related parameters of three distinct sections of a blanket copper coupon and an ODT-treated copper coupon before and after the annealing	pag. 68
6.6	CV results, at different ODT solution contact times, for coupons pre-treated with EtOH, rinsed with EtOH before spinning and annealed after spinning.....	pag. 68
6.7	Results of thermal study, carried on at 5 different temperatures, for a Cu coupon pre-treated with EtOH, treated with ODT solution (at 25°C, for 1 minute), rinsed with EtOH before spinning and annealed after spinning	pag. 69
6.8	CV results of thermal study, carried on at 5 different temperatures, for a Cu coupon pre-treated with EtOH, treated with ODT solution (at 25°C, for 1 minute), rinsed with EtOH before spinning and annealed after spinning ...	pag. 70

6.9	Plot of thickness change experienced by 4 different coupons versus number of cycles of Hf_xN_y ALD performed at 120°C	pag. 70
6.10	Plot of thickness change experienced by 4 different coupons versus number of cycles of Hf_xN_y ALD performed at 150°C	pag. 71
6.11	Plot of Hf amount on growth and non-growth areas versus number of cycles of Hf_xN_y ALD performed at 120°C	pag. 72
6.12	Plot of Hf amount on growth and non-growth areas versus number of cycle of Hf_xN_y ALD performed at 125°C	pag. 72

LIST OF TABLES

1.1	List of conductive elemental metals with related values of resistivity and mean free path at room temperature.....	pag. 8
2.1	List of materials grown by ALD	pag. 21
3.1	Combinations of head groups and substrates employed in forming SAMs ...	pag. 31
5.1	Roughness values for bare cobalt and 4 coupons pre-treated with DMAB solution and EtOH, treated with wet-annealing (at different temperatures and contact times) and rinsed with EtOH before spinning	pag. 60
6.1	Selectivity values for the 8 different ALD performed	pag. 73

RIASSUNTO

Passivazione di metalli (Co, Cu) con monostrati auto-assemblanti per deposizione atomica a strati area-selettiva

Introduzione

L'obiettivo del lavoro sperimentale svolto ai fini di questa tesi è stato quello di ottenere una passivazione efficace di superfici metalliche di cobalto e rame, mediante l'impiego di monostrati auto-assemblanti di octadecantiolo depositato attraverso tecnica di rivestimento per rotazione, in modo da impedire la deposizione atomica a strati di nitruro di hafnio.

Capitolo 1. Retrosceca

1.1 Riduzione delle dimensioni dei dispositivi

Nel 1975, durante un meeting internazionale sui dispositivi elettronici, Gordon E. Moore (cofondatore della *Fairchild Semiconductor* e della *Intel*) affermò che "il numero di transistor per chip sarebbe raddoppiato ogni due anni", arguta previsione che in seguito diventò nota come **legge di Moore**. La dichiarazione racchiudeva in sé un concetto molto importante, divenuto forza motrice dell'industria elettronica, ovvero la miniaturizzazione esponenziale (e la conseguente evoluzione) dei circuiti integrati. Le ragioni che hanno generato questo fenomeno sono essenzialmente due: il tornaconto economico (più un chip è piccolo e più se ne possono realizzare a partire da uno stesso wafer) ed il miglioramento delle performance (più componenti si realizzano nello stesso chip, maggiori le funzionalità di quest'ultimo).

Nonostante gli enormi vantaggi derivanti dalla riduzione delle dimensioni circuitali, le industrie stanno oggi affrontando una serie di problemi che limitano ulteriori sviluppi. Tali problemi sono sia di natura fisica (le proprietà fisiche, al di sotto di una certa soglia, non scalano più in maniera proporzionale alle dimensioni) che di natura tecnologica (vincoli imposti dalle tecniche produttive umane).

La tecnica più utilizzata e largamente diffusa per la progettazione dei circuiti integrati si chiama CMOS. La realizzazione di un circuito attraverso la tecnologia CMOS comprende due fasi ben distinte: la fabbricazione del front-end e la fabbricazione del back-end. Il **front-end** è

la porzione del chip dove vengono costruiti i componenti attivi, come i transistor, i condensatori, i resistori e così via. Il **back-end** invece viene costruito sopra al front-end e si compone di una serie di strati sovrapposti contenenti materiale dielettrico e fili di materiale conduttore. Il compito di questi fili è quello di connettere elettricamente i dispositivi del front-end ed è per questo motivo che sono più propriamente detti **interconnessioni**. Le interconnessioni sono di due tipi, locali e globali. Le interconnessioni locali sono fisicamente prossime al front-end, poiché posizionate nei livelli più bassi del back-end, e sono per questo molto piccole; quelle globali si trovano nei livelli superiori e risultano quindi più grandi e distanziate. Quando si parla di miniaturizzazione dei circuiti si tende a porre l'accento sui transistor, o comunque sul front-end. E' tuttavia molto importante scalare anche le dimensioni del back-end (quindi delle interconnessioni), poiché ciò contribuisce in egual misura alle prestazioni dei dispositivi.

1.2 Problemi relativi alla riduzione delle interconnessioni

Per decenni le interconnessioni sono state prodotte in alluminio, ma negli anni '90 si è passati al **rame** (Cu) per via delle sue migliori proprietà. Oggigiorno, però, il rame si sta rivelando inadeguato alle crescenti esigenze di miniaturizzazione, a causa di due effetti che scaturiscono dalla riduzione delle dimensioni fisiche: l'incremento di resistenza e l'acuirsi dell'elettromigrazione.

- 1) La **resistenza** di un'interconnessione a sezione trasversale A e resistività ρ è data dalla seconda legge di Ohm ($R = \rho L/A$). La resistività di un conduttore cresce al diminuire della sua sezione. Questo incremento è proporzionale al cammino libero medio degli elettroni del materiale: più il cammino libero medio è alto, infatti, più gli elettroni subiscono dispersione (*scattering*) nel momento in cui si trovano confinati in aree ridotte, con un conseguente aumento della resistività. Il rame ha una resistività (ρ_{Cu}) bassa se paragonata a quella di altri metalli, tuttavia il suo cammino libero medio (λ_{Cu}) è elevato, pertanto quando le dimensioni delle interconnessioni diventano paragonabili a λ_{Cu} (o addirittura minori), ρ_{Cu} subisce un'impennata (e lo fa di conseguenza R).
- 2) L'**elettromigrazione** è un fenomeno diffusivo a cui sono soggetti i cationi di un materiale metallico, a seguito del trasferimento di quantità di moto da parte degli elettroni di conduzione. L'elettromigrazione è direttamente proporzionale alla

diffusività del materiale, la quale a sua volta dipende da diversi fattori, come temperatura assoluta di fusione e struttura cristallina.

Il **cobalto** (Co) presenta di norma una resistività maggiore rispetto a quella del rame ($\rho_{Cu} < \rho_{Co}$) però possiede un cammino libero medio considerevolmente più basso. Ciò comporta che, al di sotto di una certa sezione A, la sua resistività cresce in maniera più blanda rispetto a quanto non faccia quella del rame. Inoltre la sua più alta temperatura di fusione unitamente ad una particolare struttura cristallina (definita a grani di bamboo) fanno sì che la sua diffusività sia minore, implicando una maggiore resistenza al fenomeno dell'elettromigrazione. Alla luce di ciò, si intuisce facilmente che il cobalto potrebbe essere il candidato ideale per rimpiazzare il rame nella fabbricazione delle interconnessioni. E' bene sottolineare che la sostituzione non avverrebbe ovunque, ma riguarderebbe solo le interconnessioni locali (che sono più piccole), mentre per le interconnessioni globali si ricorrerebbe in ogni caso all'uso del rame. Sono dunque queste le motivazioni che hanno indirizzato questo lavoro di tesi allo studio di entrambi i sopracitati metalli.

La miniaturizzazione, comunque, non affronta soltanto sfide relative al rimpicciolimento dei componenti, ma anche inerenti ad un corretto **allineamento** degli stessi gli uni sugli altri, ad esempio nel complesso di strati del back-end. Le tecniche di fabbricazione tradizionali impiegano approcci *top-down* che si avvalgono di processi litografici, i quali non sono esenti da errori. Durante la litografia, infatti, possono verificarsi dei disallineamenti che, nel caso delle interconnessioni, portano alla riduzione delle sezioni di collegamento tra un componente e l'altro, con conseguente degradazione delle performance. La necessità di eliminare i problemi di posizionamento ha dato un forte impulso allo sviluppo di approcci *bottom-up* che consentano processi **auto-allineanti**. Uno dei sopradetti approcci, che ha riscosso una crescente attenzione nell'ultimo ventennio, è quello della **deposizione atomica a strati area-selettiva** (AS ALD), su cui si concentra questo lavoro di tesi. Grazie alla possibilità di depositare materia in specifiche zone di interesse, l'AS ALD permette di superare i limiti della litografia tradizionale.

Capitolo 2. Deposizione atomica a strati area-selettiva

2.1 Deposizione atomica a strati

La deposizione atomica a strati (*atomic layer deposition*), brevemente indicata con l'acronimo ALD, è una tecnica di deposizione che consente la crescita di film sottili su

substrati solidi. In una deposizione atomica a strati il substrato di interesse viene esposto a specie chimiche gassose, denominate precursori, similmente a quanto avviene nella deposizione chimica da vapore (CVD). Al contrario della CVD, tuttavia, i precursori non vengono mai inseriti simultaneamente nella camera di reazione, ma sono inviati separatamente, in una serie di impulsi (*pulses*) consecutivi. Tra due impulsi successivi è necessario eseguire una **depurazione** (*purge*) del reattore con gas inerte, al fine di rimuovere le molecole di precursore in eccesso ed eventuali sottoprodotti di reazione. Ad ogni impulso il precursore inviato interagisce con i siti reattivi esposti dalla superficie in una maniera **auto-limitante**: quando i siti terminano, infatti, termina anche la reazione. Solitamente in una deposizione atomica a strati vengono impiegati soltanto due precursori, che possiamo indicare in maniera generica con A e B; la sequenza “*pulse A – purge – pulse B – purge*” è denominata **ciclo** ed è schematicamente rappresentata in *figura 1*.

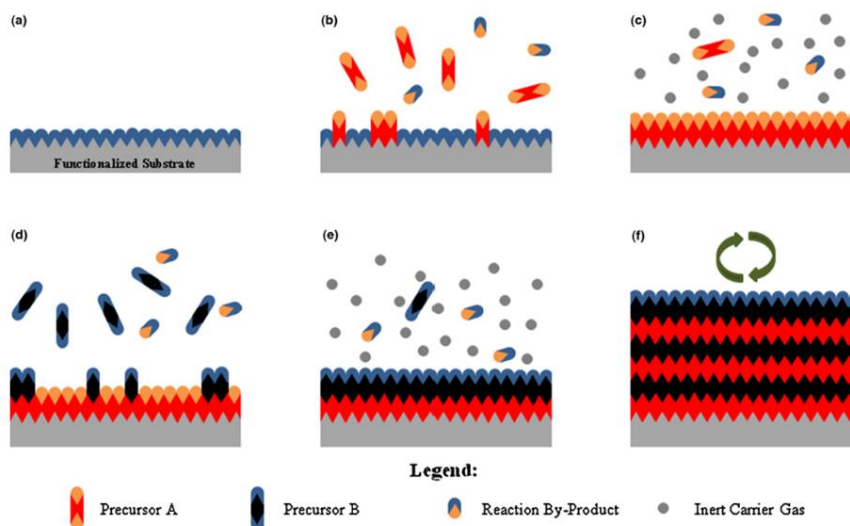


Figura 1: rappresentazione schematica della tipica deposizione atomica a strati.

La tecnica dell'ALD offre diversi vantaggi. Innanzitutto, grazie all'opportunità di selezionare il numero di cicli, garantisce un controllo dello spessore del film depositato a livello dell'Ångstrom. In secondo luogo, dato che le reazioni si sviluppano fino ad esaurimento dei siti reattivi presenti in superficie, consente di depositare film continui e privi di difetti. Inoltre, non è un processo a linea di vista in quanto anche se le zone più esposte del substrato reagiscono prima delle altre, la natura auto-limitante delle reazioni fa sì che, prima o poi, anche le parti più nascoste reagiscano, con il risultato di ottenere film

geometricamente conformi al solido sottostante. Queste qualità la rendono davvero ideale per l'industria dei semiconduttori.

2.2 Selettività areale

Nell'industria dei semiconduttori si ha a spesso a che fare con substrati "compositi", cioè composti da materiali differenti (*patterned*): un singolo strato di back-end, ad esempio, è costituito sia da metalli che da dielettrici. Una deposizione di un film su un substrato composito si definisce area-selettiva se avviene solo su determinate zone del substrato stesso. Le zone in cui la deposizione deve verificarsi e quelle in cui non deve verificarsi sono rispettivamente chiamate **zone di crescita** (*growth areas*) e **zone di non crescita** (*growth areas*). La grandezza fisica che esprime l'efficacia di una deposizione area-selettiva è denominata **selettività**. Dette θ_{GA} e θ_{NGA} le quantità di materiale presente dopo la deposizione nelle zone di crescita e di non crescita, la selettività si calcola nel modo seguente:

$$S = \frac{\theta_{GA} - \theta_{NGA}}{\theta_{GA} + \theta_{NGA}} \quad \text{Eq. 1}$$

Realizzare una deposizione con $S = 1$, ovvero perfettamente area-selettiva, non è possibile in quanto, dopo un certo intervallo di tempo, anche nelle zone di non crescita inizierà a depositarsi qualcosa. Relativamente ad una deposizione atomica a strati, il numero di cicli entro il quale la deposizione si arresta alle sole zone di crescita è chiamato **finestra di selettività**.

Esistono diversi meccanismi in grado di rendere area-selettiva un'ALD e sono di seguito elencati.

- 1) Si utilizzano precursori naturalmente selettivi verso le zone di crescita, cioè che dimostrino particolare affinità chimica nei confronti di queste ultime, ma nessuna affinità verso le zone di non crescita. Questo metodo è limitato a poche combinazioni di materiali e comunque non possiede un'ampia finestra di selettività.
- 2) Si opera una **funzionalizzazione** del substrato, che può essere localmente attivato o localmente disattivato. Nel primo caso si appone qualcosa sulle zone di crescita che favorisca la deposizione; nel secondo caso si appone qualcosa sulle zone di non crescita che la ostacoli.

Al giorno d'oggi si tende ad operare attraverso il meccanismo di funzionalizzazione per disattivazione. Vari sono i materiali che possono essere adoperati a questo scopo, tuttavia

negli ultimi anni la tendenza sempre più diffusa è quella di impiegare **monostrati auto-assemblanti** (*self-assembled monolayers*) che vengono collocati nelle zone di non crescita prima della deposizione e, in un secondo momento, opportunamente rimossi. In un lavoro di *Hashemi et al.*, per esempio, l'acido octadecilfosfonico (ODPA) è stato adottato per ottenere una deposizione atomica a strati di ossido di zinco (ZnO) area-selettiva nei confronti della silice, su substrati composti di rame e silice (Cu/SiO₂). L'ODPA, attaccandosi al Cu ma non a SiO₂, ha funto da barriera passivante che ha prevenuto la deposizione dell'ossido sul rame (si veda la *figura 2*).

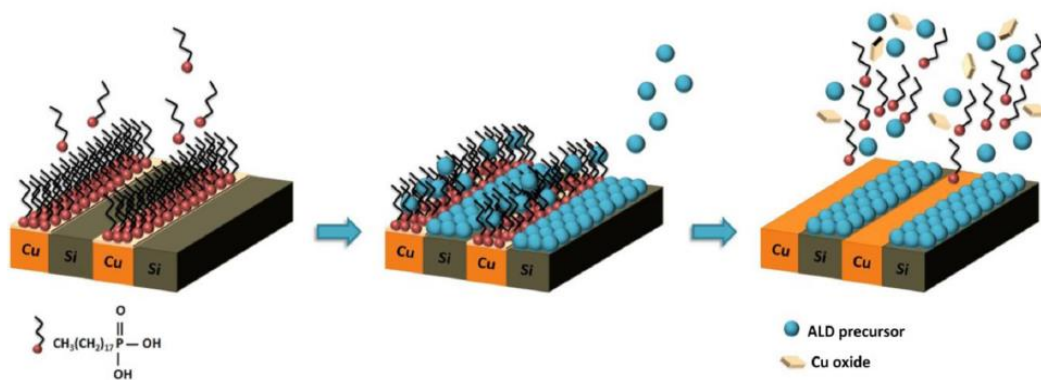


Figura 2: ALD di ZnO area selettiva verso SiO₂ su substrato composito Cu/SiO₂.

Capitolo 3. Monostrati auto-assemblanti

3.1 Generalità sui monostrati auto-assemblanti

L'espressione monostrati auto-assemblanti (SAMs) si riferisce a disposizioni ordinate di molecole organiche che spontaneamente si assemblano in strati su determinate superfici solide. Tale processo è il risultato di un adsorbimento chimico e pertanto le molecole auto-assemblanti devono mostrare una certa affinità nei confronti del substrato.

All'interno della struttura delle molecole precorritrici dei SAMs è possibile individuare tre parti costitutive, come rappresentato in *figura 3*.

- Il **gruppo di testa** (*head group*) è il gruppo funzionale responsabile del legame chimico con la superficie.
- La **coda** (*tail o backbone*) è una catena idrocarburica, solitamente alifatica satura. Tra le catene di molecole adiacenti si instaurano forze attrattive di diverso tipo (solitamente di Van der Waals) che determinano l'impaccamento del monostrato.
- Il **gruppo finale** (*end group*) è l'unità strutturale che viene esposta dalla superficie dopo il chemisorbimento, caratterizzando quindi le proprietà finali della stessa.

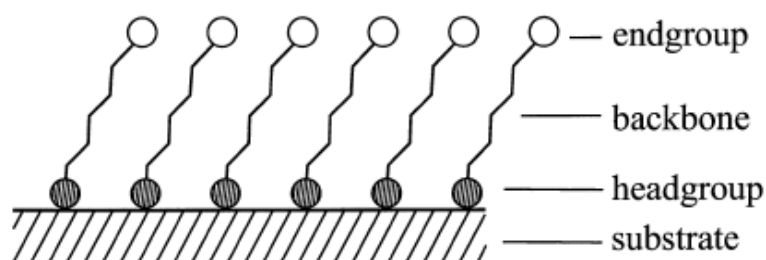


Figura 3: struttura di un SAM.

Le molecole auto-assemblanti possono essere depositate sostanzialmente in due modi: da fase liquida o da fase vapore. La deposizione da fase liquida, detta anche **immersione**, è il metodo tradizionalmente impiegato per la formazione dei SAMs e consiste, per l'appunto, nell'immersione del solido da rivestire in una soluzione contenente le molecole auto-assemblanti. Si tratta di una metodologia semplice, ma anche dispendiosa in termini di solvente e precursore, nonché di tempo; in aggiunta, risulta poco utilizzabile industrialmente. La deposizione da fase vapore, al contrario, è facile da integrare nei processi industriali, ma è decisamente più costosa per via dell'apparato strumentale richiesto, senza contare che non tutte le molecole precorritrici possono essere facilmente evaporate. E' in questo contesto che si inserisce la metodologia adoperata nel suddetto lavoro di tesi: il **rivestimento per rotazione** (*spin coating*). Come l'immersione, anche il rivestimento per rotazione fa uso di soluzione liquida, tuttavia richiede quantità minori di solvente e precursore, è molto più rapido e si dimostra idoneo a livello industriale. Al contrario della deposizione da fase vapore, inoltre, risulta poco costoso.

I parametri che influiscono sulla buona riuscita dell'adsorbimento del precursore sul substrato dalla soluzione liquida sono svariati e tra di essi si ricordano la natura del solvente, la pulizia del substrato, la purezza della soluzione e la concentrazione del precursore stesso.

3.2 Monostrati auto-assemblanti di tioli

Nella grande varietà di composti utilizzati per la generazione dei SAMs, i composti organo-solfonici giocano un ruolo fondamentale, siccome lo zolfo mostra una grande affinità sia verso la maggioranza dei metalli che verso alcuni semiconduttori. I tioli, in particolar modo, sono stati quelli più ampiamente studiati e, non a caso, costituiscono l'archetipo dei monostrati auto-assemblanti. La categoria di tioli più semplice è senza dubbio quella degli n-alcantioli, molecole con formula di struttura $\text{CH}_3(\text{CH}_2)_n\text{SH}$. Il SAM utilizzato in questa tesi, l'**octadecantiolo** (ODT), appartiene a questo gruppo di composti.

Capitolo 4. Metodo sperimentale

4.1 Passi procedurali

Gli esperimenti di questo lavoro di tesi sono stati condotti presso la sede principale di IMEC, noto centro belga di ricerca e sviluppo. Ciascun esperimento si è articolato nei punti di seguito descritti.

1. **Preparazione dei campioni metallici.** I campioni, piccoli quadrati di lato 3 cm denominati *coupon*, venivano tagliati a partire da wafer metallici prodotti direttamente in IMEC, e poi conservati all'interno di una camera bianca.
2. **Pulizia della vetreria.** Essendo la purezza della soluzione di partenza un requisito fondamentale per la riuscita del SAM, gli oggetti di vetro destinati alla preparazione della stessa subivano, a cadenza mensile, una pulizia profonda. Becher, matraccio e contenitori venivano trattati con acqua regia e soluzione piranha, rispettivamente destinate alla rimozione dei contaminanti metallici ed organici. Subito prima della preparazione della soluzione, inoltre, gli oggetti sopracitati erano sottoposti ad un'altra pulizia, meno aggressiva, consistente in tre energici risciacqui con solventi organici.
3. **Preparazione della soluzione di ODT.** La soluzione veniva preparata mescolando una certa quantità di ODT (soluto) in etanolo (solvente). L'operazione era rigorosamente svolta in una scatola a guanti ad atmosfera inerte, al fine di evitare reazioni indesiderate dell'ODT con l'ossigeno. La scelta del solvente è ricaduta sull'etanolo poiché, oltre a poter solvatare un grande varietà di alcantioli, risulta poco costoso, poco tossico e disponibile con un elevato grado di purezza.
4. **Deposizione del SAM con rivestimento per rotazione.** Il procedimento, eseguito con uno strumento chiamato *spin coater*, era abbastanza semplice. I coupon, dopo essere stati esposti ad un rapido getto di azoto atto a rimuovere eventuali particelle contaminanti depositatesi sulla loro superficie, venivano posizionati sullo spin coater, lasciati ad interagire con la soluzione di ODT ed infine rotati. Nel corso degli esperimenti sono state adottate diverse strategie, cambiando di volta in volta determinati parametri o procedimenti, poi spiegati ai *capitoli 5 e 6*.
5. **Caratterizzazione dei campioni.** Dopo la fase di rivestimento, i coupon erano analizzati con diverse tecniche, allo scopo di comprendere se la deposizione del SAM fosse avvenuta con successo. Una prima valutazione era realizzata attraverso misure

di spettroscopia ellissometrica e angolo di contatto. Con la spettroscopia si potevano constatare i cambi di spessore subiti dai coupon dopo lo *spin coating*, rispetto ad un campione preso come riferimento zero. Con l'angolo di contatto, invece, veniva stabilita la bagnabilità dei coupon e confrontata con quella iniziale. I campioni che superavano positivamente questi test preliminari venivano ulteriormente investigati con altre due tecniche: la microscopia a forza atomica e la voltammetria ciclica, che fornivano, rispettivamente, informazioni sulla rugosità superficiale dei coupon e sulla percentuale di copertura del substrato metallico da parte del SAM. Tutte queste tecniche saranno descritte più nel dettaglio nel *paragrafo 4.2*.

6. **Studio di stabilità termica.** I campioni di rame e cobalto che, sulla base delle analisi sperimentali, si erano rivelati efficacemente passivati, sono stati sottoposti ad uno studio termico volto a determinare la stabilità in temperatura dell'ODT chemisorbito. Dopo aver riprodotto più copie dello stesso coupon, esse sono state riscaldate a temperature differenti e successivamente analizzate con le medesime tecniche di caratterizzazione viste in precedenza. Dal raffronto dei risultati ottenuti prima e dopo i vari riscaldamenti, si è arrivati a stabilire l'intervallo di temperatura in cui l'ODT chemisorbito su rame e cobalto risulta stabile, cioè non degrada o desorbe.
7. **Tentativi di deposizione atomica a strati di nitrato di hafnio.** I campioni di Co/Cu ritenuti efficacemente passivati con l'ODT sono stati testati in un reattore per l'ALD di nitrato di hafnio (Hf_xN_y), a temperature comprese nell'intervallo di stabilità dell'ODT stesso. Dal momento che non è stato possibile lavorare su substrati composti di metallo-SiO₂, nel reattore sono stati inseriti coupon rappresentativi di entrambi i materiali. Per ricreare le condizioni di un eventuale substrato composto metallo-SiO₂, i coupon di SiO₂ avevano subito lo stesso identico trattamento di quelli metallici. L'ODT però, non avendo alcuna affinità chimica con SiO₂, non vi si deposita, pertanto i campioni di SiO₂ + ODT erano sostanzialmente campioni di puro SiO₂. La deposizione del nitrato di hafnio sarebbe dovuta avvenire sui campioni di SiO₂ + ODT, ma non su quelli metallici passivati (Co/Cu + ODT). Per verificare ciò, dopo l'ALD i coupon sono stati analizzati nuovamente con la spettroscopia ellissometrica, per stimarne i cambi di spessore e, in caso di risultati soddisfacenti, ulteriormente investigati con la spettroscopia in retrodispersione di Rutherford.

4.2 Tecniche di caratterizzazione

- La **spettroscopia ellissometrica** (SE) sfrutta il cambio di polarizzazione a cui va incontro un fascio di luce incidente quando interagisce con un campione. Il cambio di polarizzazione viene espresso mediante un rapporto di ampiezza ($\tan \Psi$) e una differenza di fase (Δ), grandezze che, inserite in opportuni modelli matematici, permettono di ricavare diverse proprietà del campione, tra cui lo spessore di un film sottile sulla sua superficie.

La presenza del monostrato auto-assemblato di ODT avrebbe dovuto far registrare un aumento di spessore di 2 nm, calcolato considerando la lunghezza delle catene e la loro inclinazione sulla superficie.

- La **misura dell'angolo di contatto** (CA) permette di determinare la bagnabilità di un solido da parte di un liquido. Nel caso in cui il liquido sia l'acqua, la tecnica (WCA) valuta l'idrofilicità, o viceversa l'idrofobicità, del solido stesso.

Dalla letteratura scientifica è noto che su uno strato di ODT ben assemblato sul Cu l'acqua genera angoli di contatto di circa 110°. Purtroppo non è stato possibile reperire un riferimento analogo per l'angolo formato con l'ODT sul Co. In ogni caso ci si aspetta un valore molto simile in quanto gli alcantioli sui metalli danno, in genere, angoli di contatto compresi fra 105° e 115°.

- Nella **microscopia a forza atomica** (AFM) si sonda la superficie di un campione attraverso una microleva (*cantilever*) alla cui estremità è montata una punta acuminata (*tip*). A seconda delle forze attrattive o repulsive che si instaurano fra la punta e la superficie, la microleva subisce piccole deflessioni grazie alle quali è possibile registrare le creste e le valli della superficie scansionata, elaborando così una mappa topografica della stessa.

Seppur in maniera limitata, in questo lavoro di tesi si è fatto un certo utilizzo dell'AFM, perlopiù destinato a misure di rugosità superficiale dei coupon (esprese attraverso i due parametri R_q ed R_a).

- La **voltammetria ciclica** (CV) valuta i processi di ossidazione e riduzione che interessano un campione all'interno di una cella elettrochimica. Il risultato di una CV è un grafico chiamato voltammogramma, che presenta sulle ascisse il potenziale applicato ai capi della cella e sulle ordinate il flusso di corrente che vi scorre all'interno. Nell'ambito di questo progetto, la CV è stata utilizzata per stimare il grado

di copertura percentuale dei SAMs su rame e cobalto: un SAM dall'efficace azione passivante dovrebbe impedire totalmente il passaggio di corrente, generando quindi un voltammogramma piatto. Dal calcolo delle aree sottese ai voltammogrammi, è stato possibile risalire alla copertura mediante la seguente formula:

$$Coverage(\%) = \frac{area_{riferimento} - area_{campione}}{area_{riferimento}} * 100 \quad Eq. 2$$

- La **spettroscopia in retrodiffusione di Rutherford** (RBS) è una tecnica analitica non distruttiva che permette di valutare la composizione chimica superficiale di un materiale. Il principio di funzionamento è molto semplice: un fascio di ioni bombarda la superficie di un campione; gli ioni subiscono scattering elastico; si calcolano le energie e gli angoli di diffusione degli ioni retrodiffusi. Da tali grandezze è possibile risalire agli elementi presenti nel campione e quantificarli.

La RBS è stata utilizzata per valutare la quantità di hafnio depositata sui coupon dopo l'ALD.

Capitolo 5. Cobalto: risultati e discussione

5.1 Spin coating

Inizialmente si è valutato se convenisse versare la soluzione dall'alto, con lo spin coater in esecuzione, o applicarla sui coupon con l'ausilio di una siringa ed aspettare un certo intervallo di tempo prima di avviare lo strumento. Il primo metodo si è rivelato del tutto inefficace, probabilmente a causa del fatto che le molecole di ODT, essendo rapidamente scalzate dal campione per via della rotazione, non riuscivano ad interagire con lo stesso.

Si è poi cercato di capire se la velocità di rotazione dello spin coater incidesse sull'esito della deposizione, ma non sono state trovate correlazioni.

In seguito si è analizzata l'influenza del tempo di contatto della soluzione di ODT sui campioni, testando 4 tempi diversi (30 s, 60 s, 90 s, 120 s). Si è notato, all'aumentare del tempo, un chiaro incremento sia dell'angolo di contatto che dello spessore del film depositato. Con appena 2 minuti di contatto sembrava si potessero già raggiungere dei buoni risultati, tuttavia si è poi constatato che la maggior parte dell'ODT che sembrava depositato era semplicemente fisisorbito. Di conseguenza si è aggiunta una fase di risciacquo dei campioni in etanolo subito prima della rotazione, in modo tale che l'azione del solvente potesse rimuovere inutili molecole fisisorbite. Da quel momento in poi, inoltre, sono stati

adottati tempi di contatto leggermente più lunghi per ogni serie di coupon analizzati (2 min, 4 min, 6 min, 8 min). Essendo i risultati ottenuti con il procedimento “ODT + risciacquo + rotazione” del tutto insoddisfacenti, si è deciso di inserire un pre-trattamento dei campioni in etanolo allo scopo di pulirne la superficie in modo tale da favorire le reazioni con l’ODT. La strategia “pre-trattamento_{EtOH} + ODT + risciacquo + rotazione”, però, non ha apportato particolari miglioramenti.

A quel punto è stato considerato che la presenza di un ossido sulla superficie dei campioni, sicuramente presente per via del loro contatto con l’atmosfera, potesse impedire all’ODT di reagire con il metallo. In virtù di ciò, si è aggiunto un pre-trattamento dei coupon in una soluzione acquosa di DMAB (dimetilammin-borano) a concentrazione 0,5 M che potesse ridurre l’ossido superficiale. La strategia “pre-trattamento_{DMAB} + pre-trattamento_{EtOH} + ODT + risciacquo + rotazione” si è sicuramente rivelata migliore delle precedenti, tuttavia non ha portato ai risultati attesi, ovvero spessore ≈ 2 nm e WCA $\approx 110^\circ$ (si veda *figura 4*).

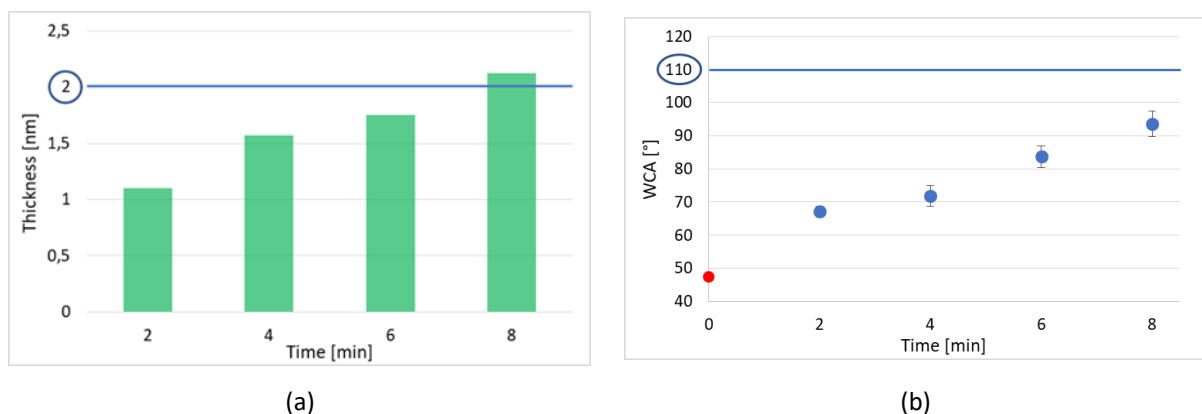


Figura 4: risultati sperimentali, a differenti tempi di contatto di ODT, per campioni pre-trattati con DMAB ed EtOH, e risciacquati con EtOH prima della rotazione. (a) spessori; (b) valori WCA.

Successivamente si è introdotta una metodologia definita “cottura umida”. I campioni, dopo aver subito i vari pre-trattamenti, venivano posti su un piastra riscaldante e la soluzione era versata durante il riscaldamento, affinché le molecole di ODT avessero energia sufficiente per reagire con il cobalto. Sono state testate 4 temperature differenti (30°C, 35°C, 40°C e 45°C) e si sono ottenuti risultati sensibilmente migliori sia in termini di spessori che di WCA (si vedano le *figure 5* e *6*). I coupon migliori, ovvero quelli trattati a 40°C e 45°C per 6 e 8 minuti sono stati più approfonditamente studiati con AFM e CV. Sebbene i risultati dell’AFM fossero positivi, la CV ha evidenziato gradi di copertura molto bassi, inferiori al 40%. Questo

è stato spiegato ipotizzando che un monostrato di ODT si era sì chemisorbito sul metallo, ma fosse tuttavia lasco, non densamente impaccato.

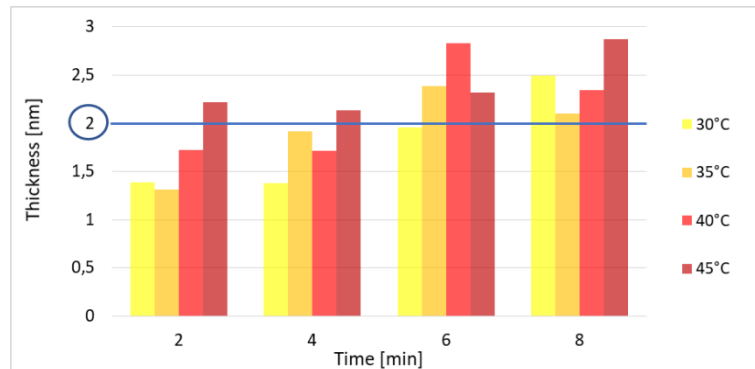


Figura 5: spessori, a differenti tempi di contatto di ODT, per campioni pre-trattati con DMAB ed EtOH, trattati con cottura umida a diverse T , e risciacquati con EtOH prima della rotazione. Il valore di spessore ideale da raggiungere (≈ 2 nm) è evidenziato da una linea blu.

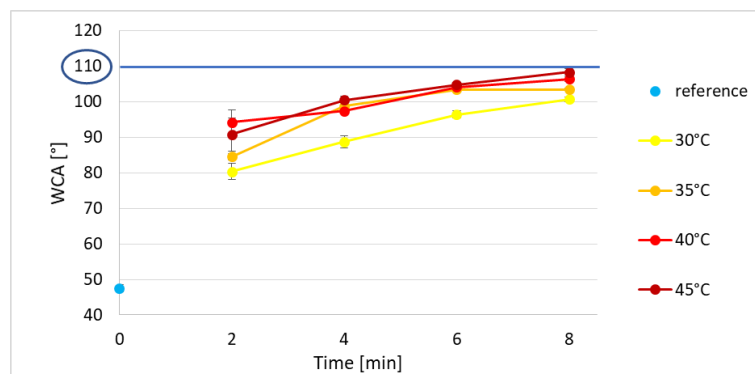


Figura 6: valori di WCA, a differenti tempi di contatto di ODT, per campioni pre-trattati con DMAB ed EtOH, trattati con cottura umida a diverse T , e risciacquati con EtOH prima della rotazione. Il valore di WCA ideale da raggiungere ($\approx 110^\circ$) è evidenziato da una linea blu.

5.2 Post spin coating

Nonostante i risultati della CV non fossero ottimali, è stato comunque effettuato uno studio termico sul campione ritenuto migliore, ovvero quello cotto a 40°C per 6 minuti. I campioni ad 8 minuti, infatti, non mostravano grosse differenze e, a parità di risultati, si è preferito scegliere il processo più rapido. Tra 40°C e 45°C si è preferita la prima opzione perché a 45°C l'etanolo evaporava molto velocemente durante la cottura umida ed era necessario aggiungere continuamente gocce di soluzione per evitare che il coupon restasse asciutto, fenomeno più limitato a 40°C . Dopo aver prodotto 6 copie dello stesso coupon, ognuna di

esse è stata riscaldata per 15 minuti ad una diversa temperatura, rispettivamente 100°C, 125°C, 150°C, 200°C, 250°C e 300°C. Confrontando gli esiti di SE, WCA e CV prima e dopo il riscaldamento, il monostrato di ODT sul cobalto si è rivelato stabile fino a 150°C circa.

Successivamente si sono eseguite diverse deposizioni atomiche a strati: a 120°C e 150°C (concordi con l'intervallo di stabilità termica dell'ODT su Co), a 10, 20, 30 e 40 cicli. Per ognuna delle deposizioni la spettroscopia ellissometrica ha permesso di osservare una crescita lineare del nitrato di hafnio tanto sui campioni di SiO₂ quanto su quelli di Co + ODT, rivelando quindi una passivazione del tutto inefficace.

Capitolo 6. Rame: risultati e discussione

6.1 Spin coating

Contrariamente al caso del cobalto, l'ODT ha mostrato sin da subito una grande affinità con il rame. Semplicemente versando la soluzione sui coupon per ridotti intervalli di tempo (30 s, 1 min, 2 min, 4 min), infatti, si sono ottenuti spessori ben superiori a 2 nm ed angoli di contatto prossimi ai 120° (si veda la *figura 7*).

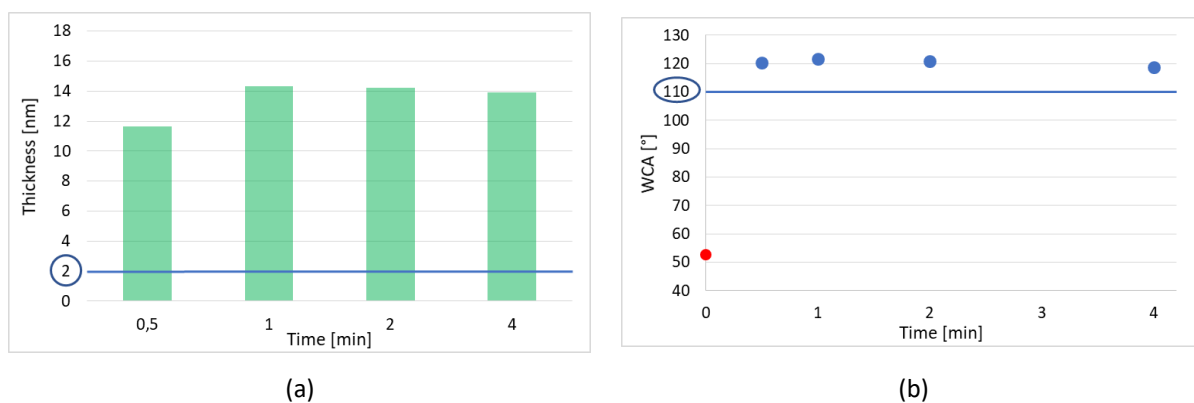
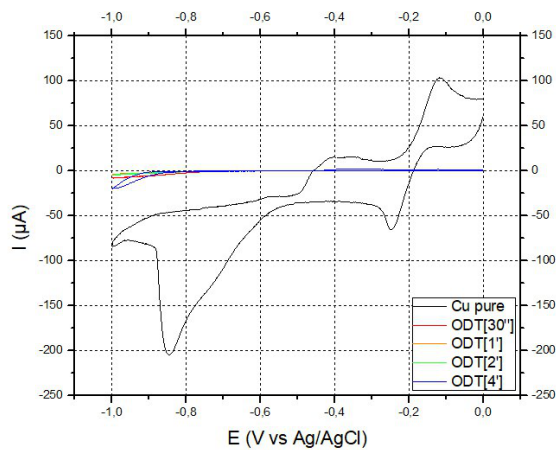


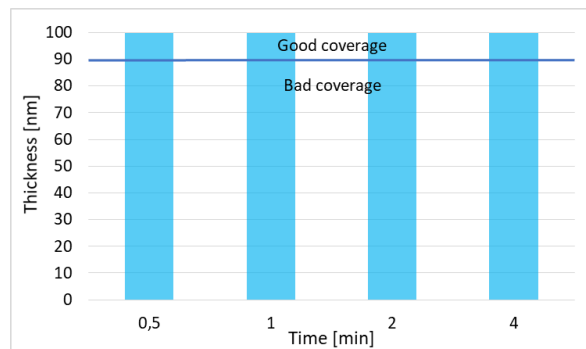
Figura 7: risultati sperimentali, a differenti tempi di contatto di ODT, per campioni pre-trattati con EtOH, e risciacquati con EtOH prima della rotazione. (a) spessori; (b) valori WCA

Essendo i risultati inconciliabili con l'ipotesi di un monostrato, si è facilmente concluso che l'octadecantiolo sul rame produca un multistrato.

Eseguendo misurazioni di CV, si sono ottenuti voltammogrammi piatti e coperture superiori al 99,99% (si veda la *figura 8*).



(a)



(b)

Figura 8: risultati della CV, a differenti tempi di contatto di ODT, per campioni pre-trattati con EtOH, e risciacquati con EtOH prima della rotazione. (a) Voltammogrammi; (b) valori di copertura percentuale.

Per tentare di ridurre l'altezza del multistrato, si è operata una cottura a media temperatura (140°C) per 15 min. Quest'ultima ha comportato diversi effetti: una riduzione di spessore (probabilmente per l'evaporazione delle molecole fisisorbite); una diminuzione del WCA, che ha finalmente approssiato il valore ideale di 110°; una levigatura della superficie, come testimoniato dai valori di rugosità registrati all'AFM.

6.2 Post spin coating

Come per il cobalto, anche per il rame si è poi eseguito lo studio volto a determinare la stabilità termica dell'ODT. Si sono testate 5 differenti temperature (100°C, 150°C, 200°C, 250°C, 300°C) su altrettante copie di un campione tenuto a contatto con l'ODT per 1 minuto e successivamente ricotto. Confrontando gli esiti di SE, WCA e CV prima e dopo il riscaldamento, il monostrato di ODT sul cobalto si è rivelato stabile fino a 150°C circa.

Inseguito sono state effettuate diverse deposizioni atomiche a strati: a 120°C e 150°C (concordi con l'intervallo di stabilità termica dell'ODT su Cu), a 10, 20, 30 e 40 cicli. La spettroscopia ellissometrica ha rivelato crescita lineare di Hf_xN_y sui coupon di SiO_2 , ma non su quelli di Cu + ODT. I campioni sono quindi stati analizzati con la tecnica RBS, i cui risultati sono presentati nelle figure 9 e 10. Conoscendo il quantitativo esatto di hafnio sulle zone di crescita (SiO_2) e su quelle di non crescita (Cu + ODT) si è potuto calcolare la selettività delle varie deposizioni per mezzo dell'equazione 1. La selettività, in media, è risultata maggiore del 90%, segno di un'ottima passivazione del rame da parte del monostrato auto-assemblante di ODT.

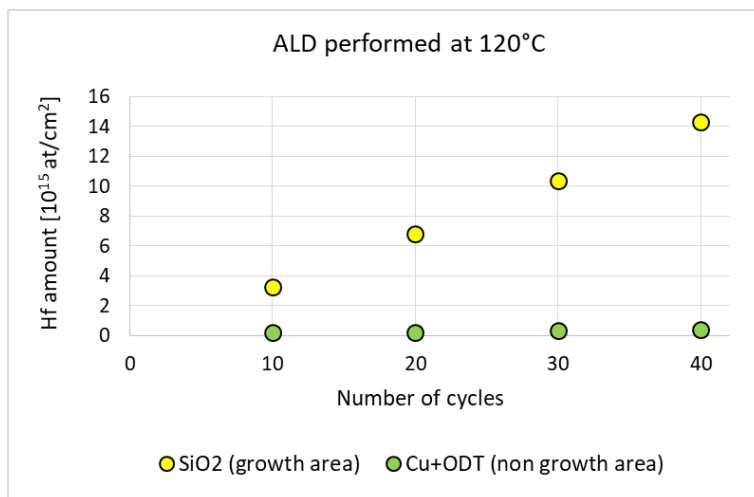


Figura 9: quantitativo di hafnio sulle zone di crescita e di non crescita in funzione del numero di cicli di una deposizione atomica a strati di Hf_xN_y eseguita a 120°C.

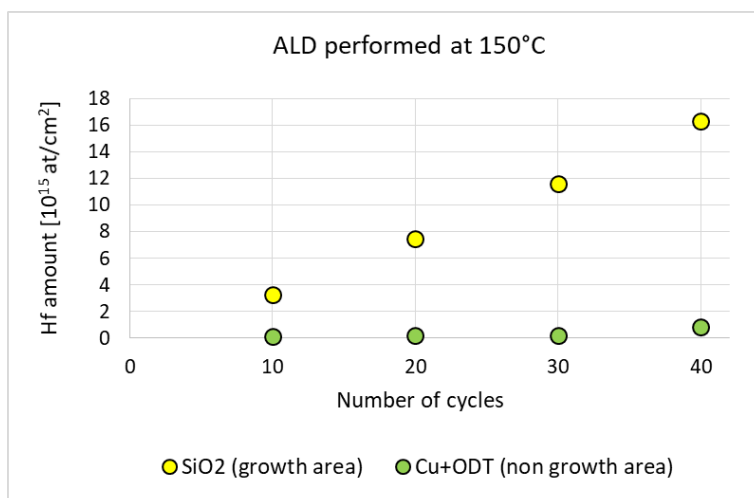


Figura 10: quantitativo di hafnio sulle zone di crescita e di non crescita in funzione del numero di cicli di una deposizione atomica a strati di Hf_xN_y eseguita a 150°C.

Conclusioni

L'obiettivo di questo lavoro è stato quello di ottenere una passivazione efficace di Cu e Co mediante un monostrato di ODT, al fine di bloccare l'ALD di Hf_xN_y . La deposizione dell'ODT sul Co si è rivelata molto ardua e, alla fine, si è certamente avuta la formazione di un monostrato, ma non abbastanza denso da prevenire l'ALD. Al contrario, l'ODT è stato facilmente depositato sul Cu, seppur in forma di multistrato. L'azione passivante dell'ODT sul Cu è stata poi valutata con delle deposizioni di prova di Hf_xN_y , che sono risultate, in media, selettive al 90%.

INTRODUCTION

Complementary Metal Oxide Semiconductor technology, simply known as CMOS technology, is the most popular and worldwide spread fabrication methodology employed for the construction of integrated circuits (ICs), which are used in practically all the electronic applications.

Over the last three decades, CMOS technology has undergone an extraordinary evolution characterized by a continuous *downward scaling* trend, which has led to an increasingly pronounced miniaturization of devices. Microelectronics industry has benefited enormously from this process: among the major advantages they may be included the lower costs of manufacturing, an increased speed of data transfer, a boosted computer processing power. Unfortunately, sustaining the downscaling tendency nowadays is becoming more and more challenging, because of two main kinds of limitations which arise during fabrication.

The first are physical, since the properties of matter below a certain threshold do not scale together with the physical dimensions.

The latter are technological, due to the constraints of traditional *top-down approaches*; the usage of photolithography, for example, entails problems of misalignment which are not acceptable when the dimensions involved are in the order of few tens of nanometers.

The research for *bottom-up approaches* has proved to be a good strategy to solve many issues related to the conventional techniques. One of them, *Area Selective Atomic Layer Deposition (AS-ALD)*, has recently gained a lot of attention due to its disruptive potential in allowing self-alignment and thickness control at the nanometric level.

Atomic Layer Deposition is a vacuum deposition technique which enables to grow thin, smooth, very conformal and defects-free films onto solid substrates; by the exposition of a substrate to alternated gaseous reactants, in a series of sequential and non-overlapping pulses, ALD builds up a film in a layer-by-layer fashioned way.

Area Selective, instead, means that the deposition does not involve the whole surface, but it occurs only in pre-determined regions of interest, feature which turns out to be essential when dealing with patterned samples, as in this study.

If, in a patterned sample, one material shows chemical affinity towards the substance to be deposited whereas the others don't, area selectivity is inherently surface-dependent. If not, the selectivity can be achieved through *functionalization* of the substrate, either activating the growth areas, or deactivating the non-growth areas.

Activation aims to promote/enhance the selectivity where it is needed while deactivation consists of passivating the regions where ALD should not take place with something that prevents the deposition. The most widely used materials for the second purpose are *Self-Assembled Monolayers* (SAMs).

Self-assembled monolayers are organic molecules which spontaneously assemble in ordered layers on the surfaces of solid materials, as a result of a chemisorption process. Among the great variety of compounds which belong to this family, *alkanethiols* have been extensively studied and employed, and they now have a prominent role.

The target of this thesis project was to successfully passivate *cobalt* and *copper* surfaces by octadecanethiol self-assembled monolayers (ODT SAMs) deposited by *spin-coating*, in order to block atomic layer deposition of hafnium nitride (Hf_xN_y ALD).

The study focused on the abovementioned metals for a reason: copper is currently employed for the construction of ICs wires, whereas cobalt shows some properties which qualify it as a possible replacement for the first one.

The initial part of the work aimed to reach a good passivation of the metals, trying different experimental pathways. Each attempt was followed by the characterization of the samples, performed with Water Contact Angle (WCA), Spectroscopic Ellipsometry (ES), Atomic Force Microscopy (AFM) and Cyclic Voltammetry (CV) techniques.

In the second part of the work the most promising samples underwent an ALD, being subsequently analyzed with Spectroscopic Ellipsometry (ES) and Rutherford Backscattering Spectroscopy (RBS) techniques to verify if deposition was effectively prevented.

CHAPTER 1. BACKGROUND

1.1 DOWNWARD SCALING OF DEVICES

During the '60s *Gordon E. Moore*, head of research and development (R&D) at Fairchild Semiconductor, noticed that the number of components in a chip was literally doubling every year, changing from one transistor in 1959 to 64 transistors in 1965.

In the 1975, at the International Electron Devices Meeting (IEDM) organized by the Institute of Electrical and Electronics Engineers (IEEE), Moore, revising what he had previously observed, predicted that the number of transistors on a chip would have doubled every 2 years from that moment on. He made the revision because he was expecting a significant slowdown in device and circuit innovation.

Moore's statement at that meeting became known as **Moore's law**. The original prediction underwent a lot of changes and nowadays many popular variations of it exist. The accuracy of the original Moore's law and its subsequent derivatives is difficult to check, but the important thing they all have in common is the belief that chip progress happens exponentially.

But which are the causes behind this exponential downscaling?

The primary driving force is the financial gain. The goal of every manufacturing community is maximizing the profit minimizing in the meantime the production costs; it is obvious that the smaller a transistor is, the more of them can be fabricated in one single wafer.

The second main reason is the improvement of ICs performance. With the integration of more individual components on a single chip, the functionality increases, leading to the minimization of the data flow delay which occurs when the individual functions are isolated in different integrated systems [1].

However, besides the tremendous benefits of transistor technology scaling, industry is facing a lot of circuit design implications. Before addressing this topic, it is worth to have a look at the ICs fabrication process. The most popular and worldwide spread technology for the realization of integrated circuits is the **CMOS technology**, where the acronym CMOS stands for complementary metal oxide semiconductor. The fabrication of an integrated circuit using

CMOS technology goes through two important steps: the front-end of line (FEOL) process flow and the back-end of line (BEOL) process flow [2].

The **front-end** is the portion of the IC where individual components such as transistors, capacitors and resistors are created.

The **back-end** is fabricated on top of the front-end and it is constituted by several layers of dielectric materials containing a metal wiring scheme, and bonding sites for the chip-to-package connections.

The purpose of the metal wires is to connect electrically the devices of the front-end, that's why they are also known as **interconnects**. The presence of a multitude of layers stems from the fact that there is simply not enough space on the chip surface to create all those interconnects in a single layer, therefore chip manufacturers build complex multi-level vertical stacks. The lower-levels lines, called local interconnects, are very close to the transistors and they need to be small, i.e. thin and short, since they attach/join to components which are really small themselves and closely packed together. The higher-levels lines, named global interconnects, travel between different blocks of the circuit thus they usually are thick, long and widely separated [3].

The first layer of the back-end, the nearest one to the devices of the front-end, is called pre-metal dielectric (PMD) layer. Vertical circular holes are created in the dielectric of the PMD layer: these holes are called contacts, because they are filled with metal and allow the electrical contact between the devices of the front-end and the wiring scheme of the back-end.

The first layer on top of the PMD is called first inter metal dielectric (IMD1) layer and it contains the first interconnects, which develop horizontally and are named trenches. When two trenches in the IMD1 are going to cross each other but they are not allowed to connect, one of them must go one level up, in order to avoid the intersection, hence an upper inter metal dielectric layer is created, IMD2. To make the metal lines of the IMD1 connect with other lines in the IMD2, vertical connections must be realized, conceptually similar to the contacts previously described; these vertical lines are called VIAs, which stands for vertical interconnect accesses.

The iteration of this process gives rise to the stack of layers which is exactly the back-end, schematically depicted in *figure 1.1*.

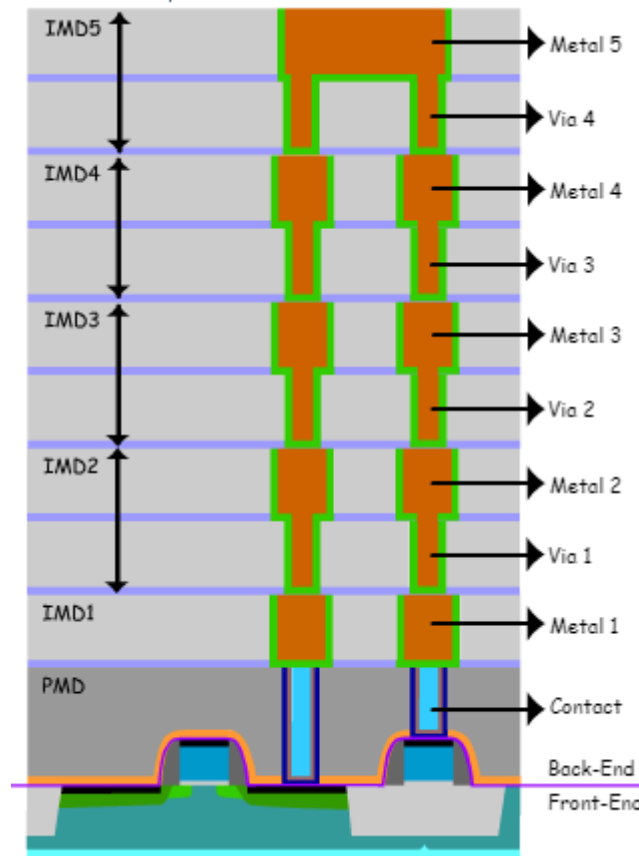


Figure 1.1: IC front- and back- end [4].

As previously anticipated, downscaling is not that easy: first, because shrinking is not simply a matter of squeezing in all directions, since properties do not scale together with the physical dimensions; secondly, because many technological problems arise with the conventional fabrication techniques commonly deployed so far [5]. Next paragraphs will provide an overview of this subject, referring to the only case of interconnects; the downward scaling of the transistors (and the other active devices of the front-end), in fact, must be accompanied by the simultaneous scaling of the components of the back-end, such as the interconnects (trenches and VIAs), because they equally contribute to the overall performance of integrated circuits.

1.2 INTERCONNECT SCALING ISSUES

1.2.1 Physical issues of interconnects scaling

For decades interconnects have been produced in aluminum but, in the late '90s, with the progressive shrinking of IC size, aluminum properties revealed themselves not suitable

any more and chipmakers switched to **copper** because of its lower resistivity and improved reliability and durability.

Nowadays conventional copper interconnects are facing, in their turn, a significant roadblock to further downscaling due to two major issues: **RC time constant increase** and degradation of **electromigration (EM) reliability** [3].

The RC time constant of an RC circuit is defined, to be rigorous, as the time required to charge the circuit capacitor, through the resistor, from an initial charge voltage of 0 to approximately 63.2% of the value of an applied DC (Direct Current) voltage. In a simpler way the RC constant, also indicated with the letter τ , is equal to the product of the circuit resistance (R) and the circuit capacitance (C).

The **electrical resistance** of a material measures the difficulty for an electric current to flow through a particular cross-section of that material.

The **capacitance** of a material, instead, refers to the ability of the material itself to store electrical charge.

Figure 1.2 shows an example of structure for RC analysis; the two parallelepipeds on top of the SiO₂ dielectric layer represent metal interconnects.

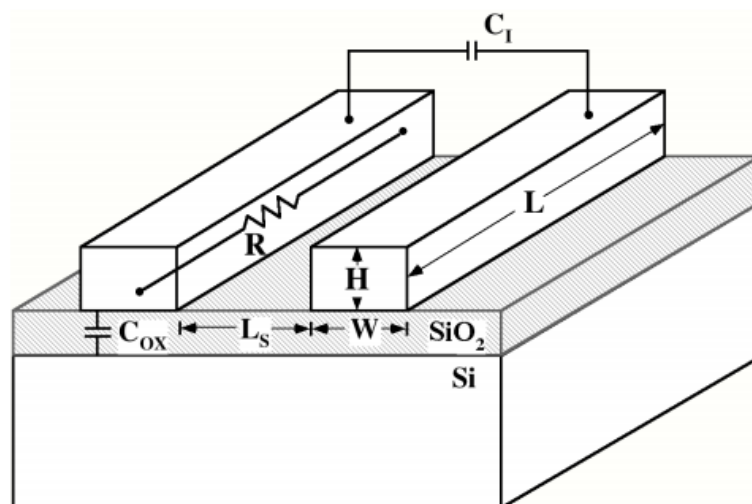


Figure 1.2: simplified structure for RC analysis [6].

In order to obtain fast devices, the RC time constant should be as low as possible, because device speed is inversely proportional to it. In a few words, the lower the τ , the faster the chips. By referring to the picture above, let's consider one at a time the two contributions to the τ , namely C and R.

- The capacitance between the interconnects can be calculated as follows [6]:

$$C_I = k_{ox}\epsilon_0 \frac{HL}{L_s} \quad \text{Eq. 1.1}$$

where k_{ox} is the dielectric constant of the oxide, ϵ_0 is the permittivity of free space and L_s is the distance between the two metal lines, while H and L are line height and length respectively.

As it can be seen from the formula, the capacitance is function of the distance between the lines and the insulating dielectric material surrounding them. Reducing circuit size (i.e. making L_s smaller) brings to higher capacitances, which may provoke undesired cross-talks, meaning that the signal in one metal line influences the signal in a neighboring line, with consequent malfunctioning of the device.

The development of low-k materials has significantly reduced capacitance ($k_{ox} \downarrow \Rightarrow C \downarrow$). Today dielectrics own an average k of approximately 2.5, definitively lower than the 4.2 of pure silicon dioxide; although various methods exist to achieve lower values, the resulting ultra-low-k films become increasingly fragile as the k value decreases, placing a limit to further improvements [3].

- As regards the electrical resistance (R), considering each interconnect of *figure 1.2* as a homogeneous conductor with constant transversal section (A), R is given by the second *Ohm's law*:

$$R = \rho \frac{L}{A} = \rho \frac{L}{WH} \quad \text{Eq. 1.2}$$

where ρ is the conductor electrical resistivity, while L, W and H are respectively its length, width and height.

As it is possible to observe in *table 1.1* [7], copper has one of the lowest bulk electrical resistivity among metals but, at the same time, a long electron mean free path, which is the average distance travelled by an electron in between two consecutive collisions. The longer the mean free path is in a material, the more resistivity increases as area is reduced, because electrons find themselves so "area-

constrained” that they begin to scatter far more often at grain boundaries and surfaces [8]. Copper electron mean free path is large, therefore it is strongly affected by cross-sectional area, entailing a remarkable increase in resistivity when area shrinks. BEOL scaling implicates a decrease of both length ($L \downarrow$) and cross sectional area ($A \downarrow$) and this last, in turn, involves a huge increase of resistivity for copper interconnects ($\rho_{Cu} \uparrow$); since L contribution to R ($L \downarrow \Rightarrow R \downarrow$) is negligible if compared with the other two ($A \downarrow, \rho_{Cu} \uparrow \Rightarrow R \uparrow$), it is clear that the sum of all these effects translates into higher resistance values. High values of R mean reduction of electron flow, thus slowdown of devices.

Table 1.1: List of conductive elemental metals sorted in alphabetical order, with related values of resistivity (ρ) and mean free path (λ) at room temperature. For hexagonal structures (Co, Ru) the two listed values of λ are for transport perpendicular and parallel to the hexagonal axis [7].

Element	Symbol	$\rho_{\text{Room}} [\mu\Omega \cdot \text{cm}]$	$\lambda_{\text{Room}} [\text{nm}]$
Aluminum	Al	2.650	18.9
Cobalt	Co	6.2	11.8/7.77
Copper	Cu	1.678	39.9
Gold	Au	2.214	37.7
Ruthenium	Ru	7.8	6.594/4.88
Silver	Ag	1.587	53.3
Tungsten	W	5.28	15.5

Electromigration is the transport of material in a conductor due to the diffusion of cations¹, which is caused by the momentum transfer from the electrons to the cations against which they collide. The current density induced by electromigration (J_{EM}) is dependent on the effective diffusivity (D_{eff}) of atoms in the crystal lattice, according to the equation below:

$$J_{EM} = nv_d = n \left(\frac{D_{eff}}{k_B T} \right) F_{EM} \quad \text{Eq. 1.3}$$

¹Metallic lattices consist of aligned positive ions immersed in a "cloud" of delocalized electrons.

where n is the charge-carrier number density, v_d the drift velocity, k_b is the Boltzmann constant and F_{EM} is the electromigration driving force [9, 10].

The formation of hillocks and voids, caused by the accumulations and depletions of atoms due to electromigration, provokes the deterioration of the interconnects, with the risks of short and open circuits and a consequent reduction of devices reliability [10].

Fabricating a copper interconnect involves the creation of different layers surrounding the bulk conducting copper precisely to mitigate the electromigration phenomenon, typically a tantalum nitride barrier (which prevents metal diffusion into the dielectric) and a tantalum liner (which improves the TaN barrier adherence to the Cu) [3]. The chances to reduce these layers are limited because they need to have good barrier properties, this meaning they require a minimum thickness of around 1.5/2nm per side [11]. It is therefore obvious that the thinning of the line width primarily depends on the thinning of Cu core, as shown in *figure 1.3*, with dramatic effects on resistance, especially below the 11nm technology node².

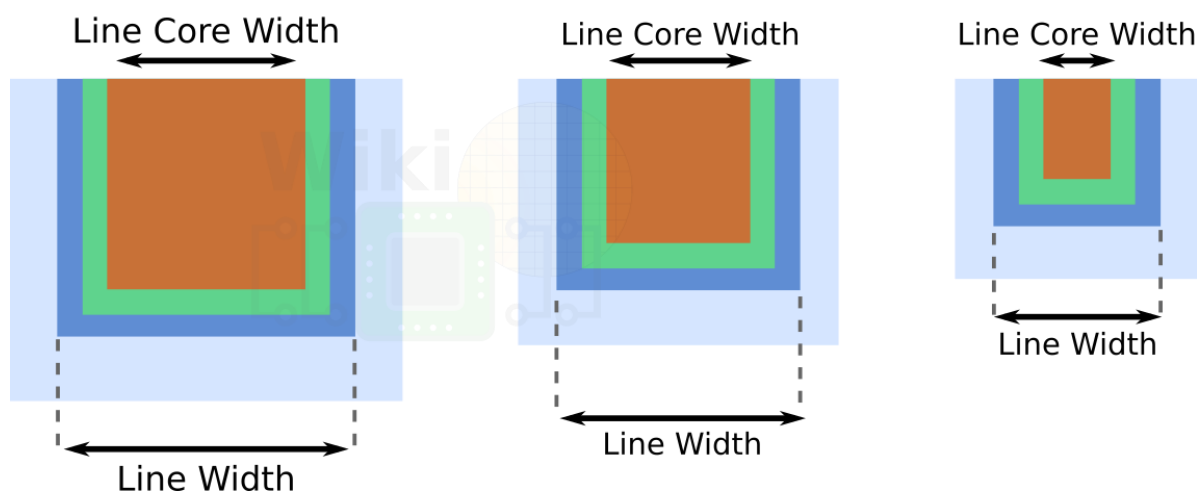


Figure 1.3: Simplified diagram of copper interconnect scaling [12].

In the last few years industry has proposed several solutions to overcome the problems emerged with copper interconnects, and the most promising strategy at the moment seems to be the replacement of copper with other transition metals, such as cobalt (Co) and

²Technology nodes, or simply nodes, indicate “semiconductors generations”. Technically speaking, a node is the minimum feature size in a semiconductor manufacturing process: each generation of semiconductors is designed by a certain number of technology nodes, usually expressed in nm.

ruthenium (Ru). Since this thesis will deal with **cobalt**, the latter will be the only one to be taken into analysis.

It has been already pointed out that electrical resistivity increases as the cross-sectional area decreases, but the ascending trend is different for each metal, according to their electron mean free paths.

Cobalt has higher bulk resistivity than copper but, on the other hand, its electron mean free path is considerably lower. *Figure 1.4* presents cobalt and copper resistivity curves against trench critical dimension, which is the smallest geometrical feature to be considered for the component, i.e. width. Looking at the curves, it may be noticed that below 10 nm cobalt resistivity (ρ_{Co}) raises more slowly than copper resistivity (ρ_{Cu}) meaning that ρ_{Co} , normally higher than ρ_{Cu} , becomes lower. Since resistance R is directly proportional to resistivity ρ , using cobalt it would be possible to obtain interconnects with lower resistance with respect to the traditional copper ones [12].

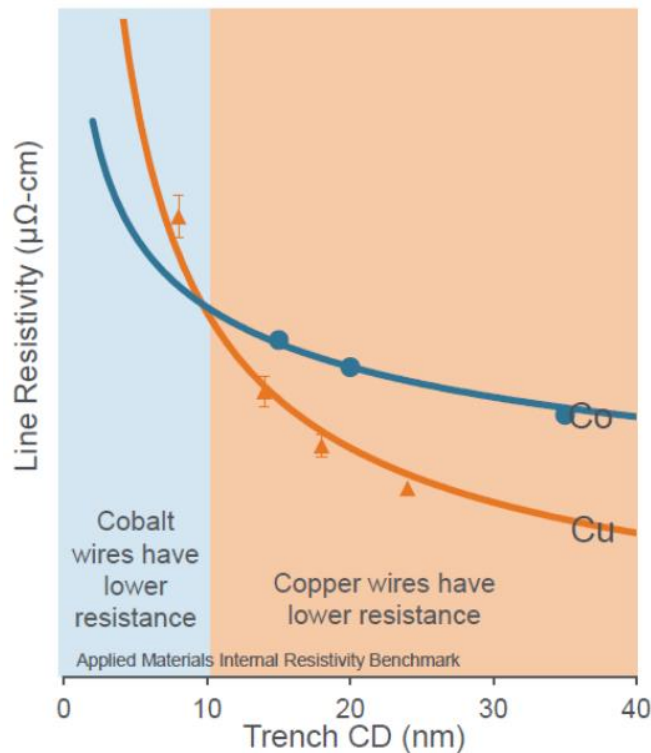


Figure 1.4: plot of cobalt and copper resistivities versus trench critical dimension [3].

Moreover, it has been demonstrated that for cobalt, in contrast to the case of copper, a single film as thin as one-nanometer is enough to serve as both the liner and the barrier,

because of the less tendency of cobalt to diffuse with respect to copper. This fact is due to the dependency of metals diffusivity on melting temperature (T_m) and crystal structure [9]. First, cobalt T_m is higher than copper T_m , implying a greater activation energy required for diffusion. Secondly, as regards the crystal structure, transmission electron microscope images have revealed that nanometric cobalt presents bamboo grains that copper loses when scaled down below 90 nm [13]; this bamboo-grains structure (which consists of crystallites that expand across the entire width of the interconnect and are aligned in the direction of current flow) plays a critical role in retarding diffusion. In a few words, cobalt diffusivity is smaller than copper one ($D_{Co} < D_{Cu}$) leading, by virtue of *equation 1.3*, to a smaller electromigration-induced current density ($J_{EM,Co} < J_{EM,Cu}$), thus cobalt proves to have better electromigration reliability.

However, it is worth to highlight that despite the benefits cobalt could provide, it would not replace copper entirely but just in the first layers, where there are local interconnects and dimensions at stake are very small (in the order of few dozens of nanometers) [12]. For global interconnects, that run longer distances and are more detached from each other, it makes sense to continue using copper, and this is the reason why it will be investigated in this thesis work as well as cobalt.

1.2.2 Technological issues of interconnects scaling

Currently the back-end of line process flow relies almost completely on top-down approaches, which oblige to employ, iteratively, lithography and etching steps to create the complex stack of layers of the back-end [14].

As stated before, close attention must be given to the fabrication of trenches and VIAs, because they are proving to be an obstacle to further downscaling [5].

Let's now consider, for instance, the standard (top-down) procedure for the realization of a VIA: as shown in *figure 1.5*, six main steps are required [15].

- 1) Lithography, necessary for the following etching step. The substrate is coated with a photosensitive organic material called photoresist, or simply resist; a patterned mask capable of blocking light is then placed onto the resist, so that only its unmasked regions will be exposed to light. Successively, a solvent referred to as developer is applied to the surface. The organic material in the unmasked areas will be degraded

by light and the developer will dissolve it away, leaving behind a coating in the masked areas³.

2) Etching, in order to create the hole of the VIA.

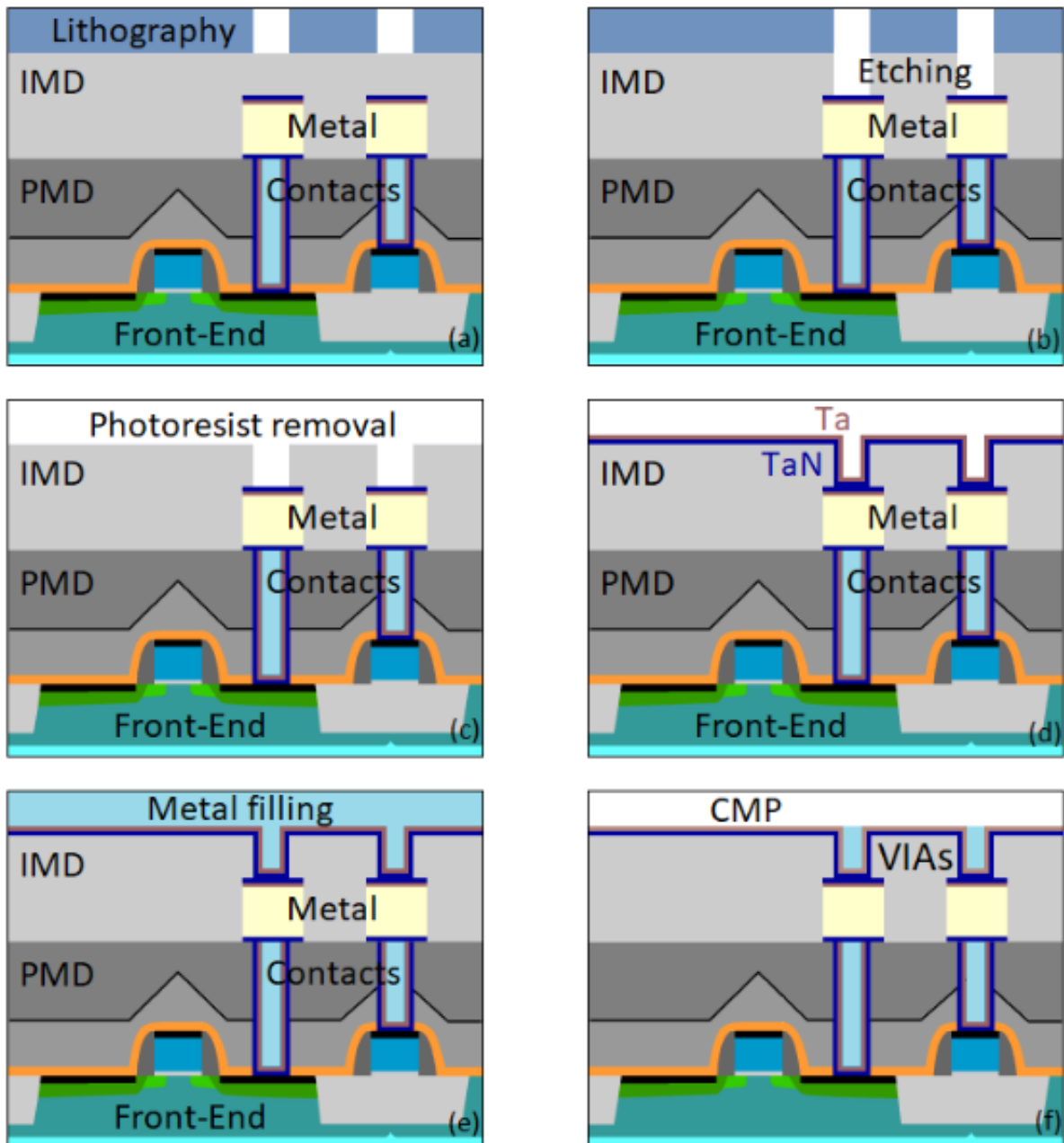


Figure 1.5: general fabrication method of a Vertical Interconnect Access. (a) Lithography; (b) etching; (c) photoresist removal; (d) deposition of TaN barrier and Ta liner; (e) filling with metal; (f) chemical mechanical polishing [4].

³The previous explanation concerns the use a *positive photoresist*. In the case of a *negative photoresist* the organic material in the unmasked areas will be strengthened by light (because of either polymerization or cross-linking) and the developer will dissolve away the regions which did not undergo light exposure.

- 3) Photoresist removal, to take away the light sensitive organic material used in the lithography step.
- 4) Deposition of TaN barrier layer and Ta liner, whose functions have been already discussed in the previous paragraph.
- 5) Filling of the hole with conductive metal, to create the Vertical Interconnect Access. (This is a two-step process: first a nucleation layer is deposited, usually by chemical vapor deposition, then the bulk layer is formed, typically by electrochemical deposition)
- 6) Chemical mechanical polishing, for removing the excess of metal from the wafer surface.

With downscaling, the rising challenge is not only fabricating smaller components, but also make them align properly when they need to be stacked one above the other; considering the VIA fabrication explained above, it's easy to understand that this task should be theoretically fulfilled by lithography.

The effectiveness of photolithography depends on the alignment of the substrate to be processed with respect to the mask used in the optical exposure. Unfortunately, misalignments always occur, due to various causes. The maximum error in alignment is called **edge placement error**, usually indicated with the acronym EPE; EPE should be smaller than one-fourth of the critical dimension [14].

In the case of the Vertical Interconnect Access, alignment errors entail a reduction of the section in contact with the underlying metallic layer, with a consequent increase in resistivity and a deterioration of performance.

The need for eliminating the edge placement errors of top-down processing has led to an increasing demand for development of bottom-up approaches, which enable self-alignment and avoid going through the numerous steps of traditional (top-down) nanopatterning techniques.

One of such bottom-up approaches, that has gained more and more attention in the last two decades, is the **area selective atomic layer deposition (AS-ALD)**.

ALD is a deposition technique which allows to grow thin films on solid surfaces in a bottom-up fashioned way, building them up layer-by-layer, with promising and unique capabilities for sub 45 nm CMOS technology [16].

A deposition technique is said area-selective when it aims to limit the deposition to some specific areas of interest, in such a way that the substrate is prevented to be fully coated. The locations where the deposition should and should not take place are usually referred to as **growth** and **non-growth areas** respectively.

The disruptive potential of AS-ALD in aligning two materials on top of each other is shown in *figure 1.6*, where there is a comparison with a conventional patterning pathway which makes use of lithography and etching [14]. Both ALD and area-selectivity, however, will be thoroughly discussed in *chapter 2*.

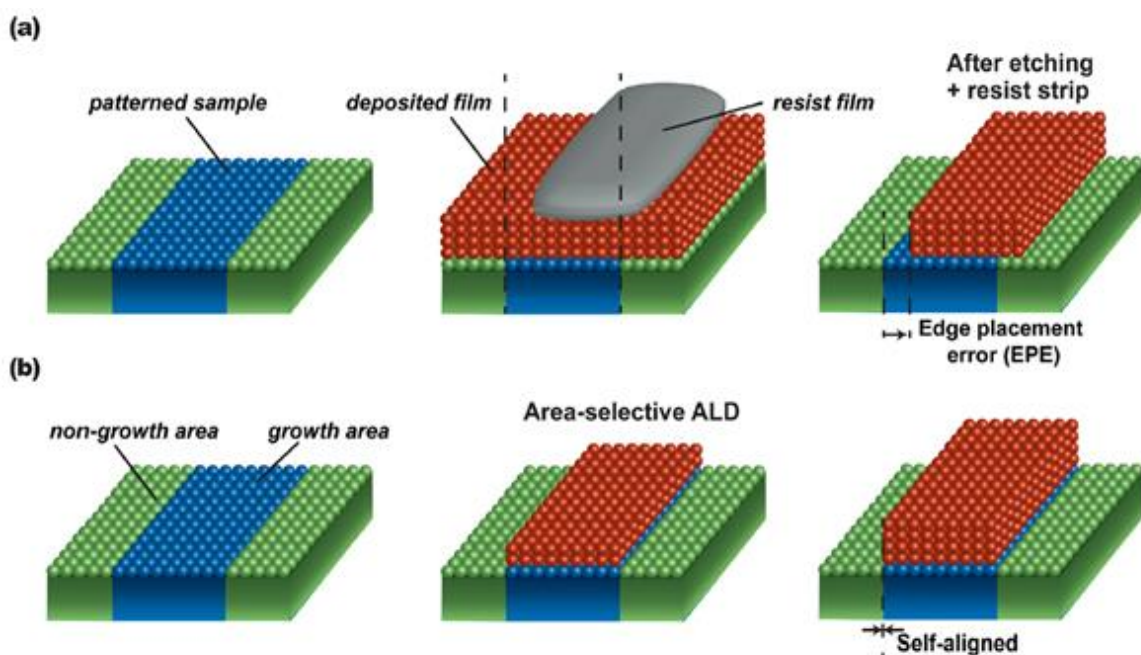


Figure 1.6: (a) conventional patterning pathway, which consists of film deposition, lithography and etching; (b) area-selective atomic layer deposition, that enables self-alignment by making the deposition occur only where it is required [14].

The edge placement error is not the only problem that arises during VIA fabrication. During the filling of the VIA, in fact, the usage of traditional top-down deposition techniques may provoke the formation of defects, which obviously deteriorate the properties of the metal [17].

The most common examples of such defects are the so-called voids and seams, which are respectively represented in *figure 1.7 (b)* and *(c)*. Basically, both voids and seams are gaps which develop as result of incomplete/irregular filling, interrupting the continuity of the

metal; the only difference between voids and seams is the shape of the gap, which is in any case located in the center of the VIA channel.

Once again, the usage of a bottom-up approach could be the solution to the problem: the area selective ALD technique turns out to be the right strategy to not simply mitigate, but even eliminate the incomplete filling defects, since it builds structures layer-by-layer and permits to reach a good fill, like shown in *fig 1.7 (a)*.

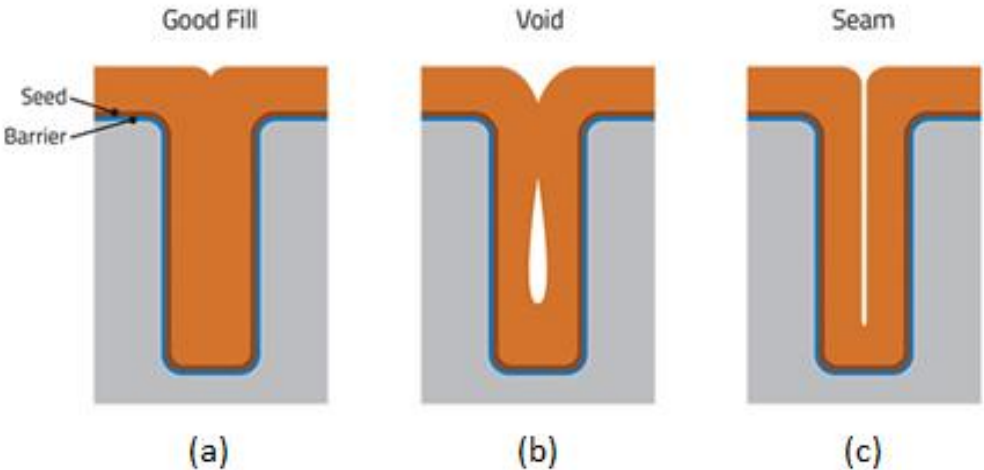


Figure 1.7: VIA filling.

(a) Good VIA filling; (b) void formation during VIA filling; (c) seam formation during VIA filling [4].

CHAPTER 2. AREA SELECTIVE ATOMIC LAYER DEPOSITION

2.1 ATOMIC LAYER DEPOSITION

2.1.1 Introduction to the process

Atomic layer deposition (ALD) is a vacuum deposition method used to grow thin films on solid substrates.

Historically speaking, ALD has been developed independently twice, in the '60s in the Soviet Union, under the name of "molecular layering" (ML), and during the '70s in Finland, when the Finnish engineer *Tuomo Suntola*, in order to deposit ZnS for electroluminescent displays, invented a technique which was named "atomic layer epitaxy" (ALE) [18, 19]. For some reasons, the latter discovery is nowadays the most commonly acknowledged origin of ALD.

The acronym ALD began to replace ALE only after the year 2000, when semiconductor industry started using the technique massively. After all, the term epitaxy⁴ was no longer adequate, since the materials deposited were usually amorphous or polycrystalline.

Atomic layer deposition consists of exposing the substrate of interest, conveniently located in a vacuum chamber, to alternated gaseous species referred to as **precursors**, similarly to what happens in the chemical vapor deposition (CVD). In contrast to CVD, however, the precursors are never present simultaneously in the reactor, but they are inserted separately, in a series of sequential, non-overlapping pulses. In each pulse the molecules of the injected precursor react with the exposed surface; the individual reactions between gas and substrate are actually half-reactions, because they make up only one part of the whole film synthesis. Every half-reaction occurs in a self-limiting way: the molecules, in fact, can interact only with the finite number of reactive sites presented by the surface and once all the reactive sites of the surface are consumed, the reaction terminates. After a reactive step, a purging step must always follow in order to remove excess reactant molecules and any by-products of the reaction; inert gases are used to this purpose, generally N₂ or Ar [20]. When describing an ALD process it is important to specify both pulse times (the times the surface is being exposed to each gaseous species) and purge times (the times left in between

⁴Deposition of a monocrystalline overlayer upon a crystalline substrate which determines its orientation.

two consecutive dosing steps, to let unwanted molecules evacuate the chamber). The set of doses and purges represents an ALD **cycle**. By changing the number of cycles, it is possible to vary the thickness of the deposited film. ALD processes are often described in terms of their **growth per cycle**. Theoretically the growth per cycle (GPC) should be one monolayer per cycle but, in the practice, it can vary between 0.1 Å/cycle and 2 Å/cycle depending on process parameters, precursors reactivity, surface size and so on [18].

2.1.2 Binary ALD

The most part of atomic layer depositions requires the exposure of the substrate to only two precursors, let's say *A* and *B*, often indicated as “reactant” and “co-reactant”: the sequence “pulse A – purge – pulse B – purge” represents the cycle of the binary ALD, which is schematically portrayed in *figure 2.1*.

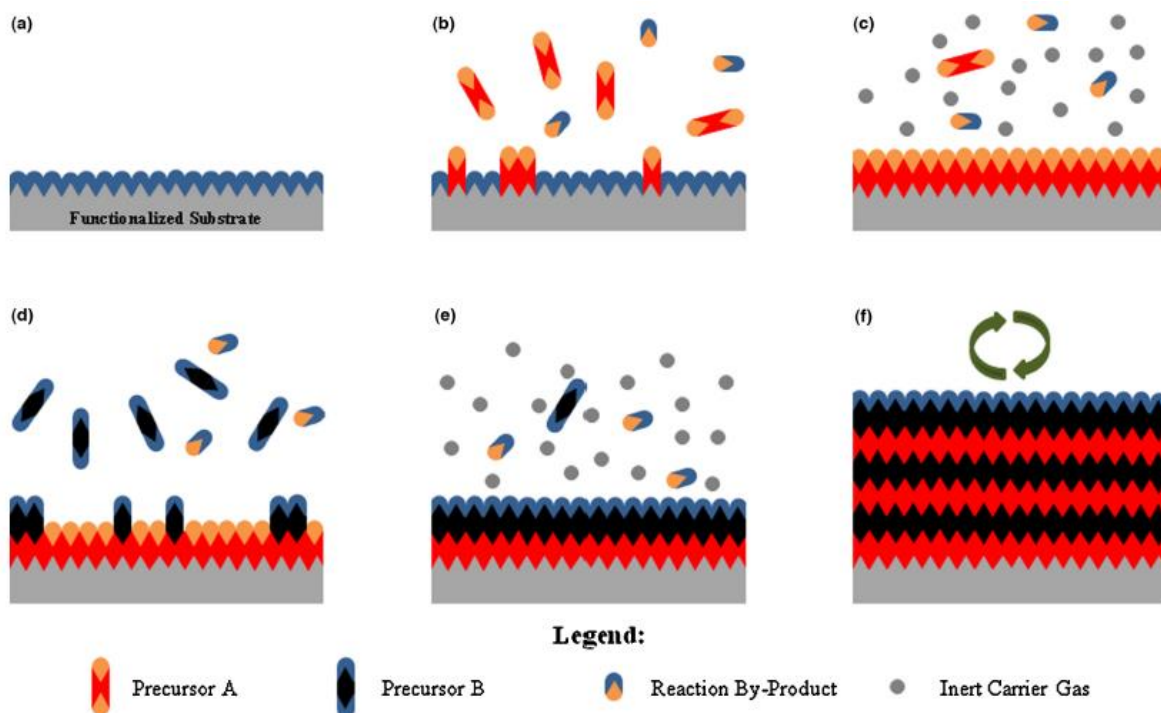


Figure 2.1: typical ALD process. (a) The substrate to be coated is placed in the reactor. (b) Precursor A is pulsed, and it reacts with the surface; (c) excess A precursor and reaction by-products are purged away. (d) Precursor B is pulsed, and it reacts with the surface; (e) excess B precursor and reaction by-products are purged away. (f) The cycle is repeated until the desired thickness is achieved [20].

2.1.3 ALD pros and cons

The advantages of ALD are several and the most important ones are listed below [21].

- It allows a precise thickness control at the Ångstrom level, due to the opportunity to select the number of cycles.
- Films deposited by ALD tend to be very continuous, smooth and pinhole-free, since reactions develop completely during each cycle and no sites of the surface remain unfilled during film growth.
- The self-limiting nature of the reactions produce an excellent coverage of the substrate, leading to films which result extremely conformal to the geometry of the underlying structures, even for complex and high aspect-ratio substrates. In other words, it is not a line-of-sight process (such as PVD), in fact even if some surface areas react before than others (for example because of inhomogeneous precursor fluxes), the global reaction between precursor and substrate won't stop until it has reached completion even in the areas less exposed.

Miniaturization process in the semiconductor industry has led to the necessity of continuous, defect-free films that must be deposited with high conformality and controlled thickness. No other techniques could satisfy these requirements as good as ALD.

The biggest weakness of ALD is the slow deposition rate, which derives from the long times involved in pulsing and purging, as well as the layer-by-layer nature of the deposition itself. Most ALD rates fall within a range of 100÷300 nm/h [20]. However, these rates strongly depend on the reactors design and the substrates (big and/or high aspect ratio substrates clearly need more time to be coated). CVD and PVD are certainly faster techniques, but they suffer from non-uniformity and non-conformality, respectively due to rapid surface reactions and shadowing effects.

2.1.4 Process parameters

The most important parameter in the ALD technique is the deposition temperature. ALD processes are carried at modest temperatures (normally below 350°C), more specifically in a well-defined range, which is denominated **ALD temperature window** and varies according to the precursors and the substrate involved [20].

Staying inside the window assures a self-controlled and saturated growth, whereas exceeding the limits of the window leads to no layer formation because of different effects, as shown in *figure 2.2*.

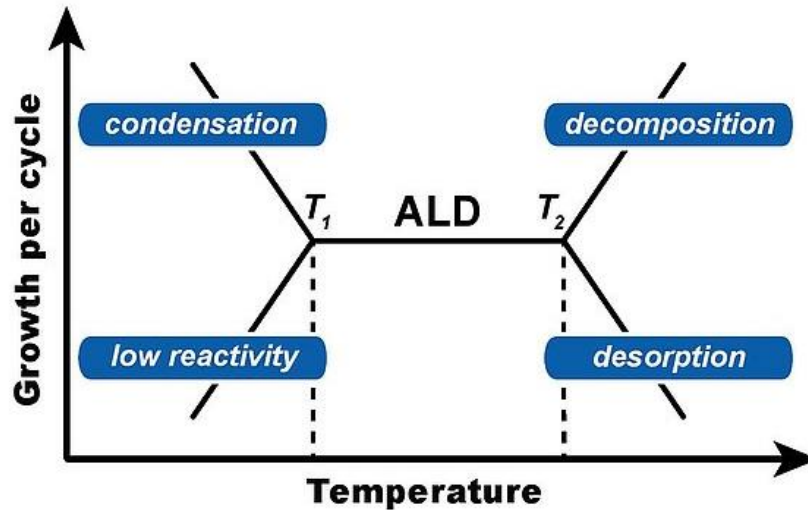


Figure 2.2: plot of ALD growth rate versus temperature. Temperature window is defined by T_1 and T_2 .

- If the temperature is too low, either the thermal energy is not enough to overcome the activation energy of the reaction (low reactivity), or the precursor condensates on the surface through a non-ALD type deposition (condensation).
- If the temperature is too high, either the precursor thermally decomposes (decomposition), or it rapidly desorbs from the surface (after having been chemisorbed) because of too much thermal energy (desorption).

Other parameters to be considered for an atomic layer deposition are pulse and purge times, which indicate, respectively, the quantity of reactant and inert gas that enters the reactor chamber per cycle [22].

Short pulse time implicates incomplete reaction between precursor and surface sites of the substrate, which results in poor quality and uniformity of the film. On the other hand, long pulse time produces waste of precursor and can make some reactant particles stick to the top layer, event that compromises the reaction of the successive cycle. Besides, short purge time is not enough to clean up completely the by-products, whereas long purge time may provoke the entry of impurities.

2.1.5 Growth mechanism

Concerning the kinetic of the process, different growth mechanisms have been identified, in relation to what happens to the growth per cycle (GPC). The only differences in the trend of the GPC are registered in the very beginning of the growth, when the substrate is not fully

covered yet: with the increasing extent of deposition, in fact, the original substrate gives way to the first layer of the film to be deposited and the growth per cycle is expected to become constant in any case. As it can be observed in *figure 2.3*, the GPC can be classified as constant [2.3(a)], substrate enhanced [2.3(b)] or substrate inhibited [2.3(c)] [23].

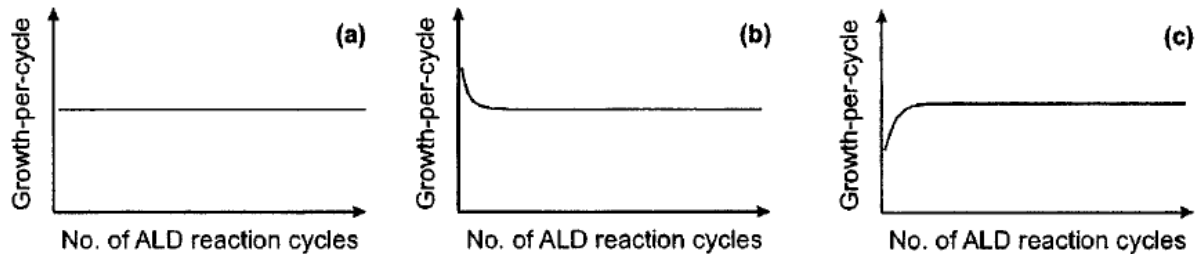


Figure 2.3: proposed classification of ALD processes based on the initial growth per cycle.

(a) Constant GPC; (b) substrate enhanced GPC; (c) substrate inhibited GPC [23].

When the GPC is constant, the ALD is said steady. It is important to notice that in a steady ALD the physical quantity that stays constant is the amount of material deposited versus the number of ALD cycles, while in a steady CVD it is the amount of material deposited versus time (i.e. the growth rate) to be constant. In the substrate enhanced ALD, the GPC is higher in the beginning with respect to the steady state, while in the substrate inhibited ALD, the GPC is lower, but it gradually increases until it reaches the steady state.

At the origin of the third growth mechanism (GPC substrate inhibited) a model of islands growth has been proposed. According to this model, the substrate is not really reactive towards the ALD precursors, except for some active defective-areas: nucleation starts at these defective points and create “islands” which continue to grow regularly, i.e. laterally and symmetrically from the center [23].

2.1.6 ALD precursors

As it can be clearly noticed consulting scientific journals, there is a wide variety of materials that can be grown through atomic layer deposition, among which metals, semiconductors and insulators, in both crystalline and amorphous phases. *Table 2.1* summarizes elements and various compounds (binary oxides, nitrides, sulfides) that can be obtained by the technique [20]. Basically, the main limitation to the realization of a material via ALD is the availability of reactants that can interact with the surface through the appropriate chemical

pathway, in order to obtain that material. Precursors should be easily available or synthesized and not very expensive; furthermore, they should be volatile enough to be in the gas phase either at room temperature or upon moderate heating and, once in the gaseous state, they should not decompose until they have reached the surface of interest. Finally, they must react with surface groups rapidly and they should interact aggressively with each other to reach the saturation stage in a short time and ensure a reasonable deposition time [20, 24].

Table 2.1: list of materials grown by ALD [20].

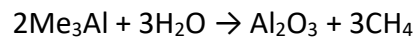
Elements	Compounds		
	Oxides (E_xO_y)	Nitrides (E_xN_y)	Sulfides (E_xS_y)
C, Al, Si, Ti, Fe, Co, Ni, Cu, Zn, Ga, Ge, Mo, Ru, Rh, Pd, Ag, Ta, W, Os, Ir, Pt	Li, Be, B, Mg, Al, Si, P, Ca, Sc, Ti, V, Cr, Mn, Fe, Co, Ni, Cu, Zn, Ga, Ge, Sr, Y, Zr, Nb, Ru, Rh, Pd, In, Sn, Sb, Ba, La, Ce, Pr, Nd, Sm, Eu, Gd, Tb, Dy, Ho, Er, Tm, Yb, Lu, Hf, W, Ir, Pt, Pb, Bi	B, Al, Si, Ti, Cu, Ga, Zr, Nb, Mo, In, Hf, T, W	Ca, Ti, Mn, Cu, Zn, Sr, Y, Cd, In, Sn, Sb, Ba, La, W

All sorts of reactants in accordance with the aforementioned requirements have been tried in atomic layer depositions. The non-metal precursors are usually hydrides (H_2O , H_2S , NH_3 , AsH_3). H_2O and H_2S show reactivity at reasonable temperatures ($T < 500^\circ C$) and formation of suitable surface species to anchor the metal precursor, while NH_3 and AsH_3 have more limited reactivity. Among the metal precursors it is possible to remember metal halides (especially chlorides, widely applied for oxide, nitride and sulfide films formation), metal alkyls (which in some cases behave almost ideally in the formation of oxide and sulfide films), metal alkoxides, electropositive metals compounds and metal alkyl amides (as precursors for nitride films) [22].

To give a more practical example of reactants (and reactions) involved in a typical atomic layer deposition, it is possible to analyze one of the first substances grown by this technique,

namely aluminium oxide (Al₂O₃), which also is one of the most used materials in electronics applications [25].

Many reactions pathways exist, but two reactants are needed in any case, the first containing aluminum and the second containing oxygen. The most studied aluminum source is trimethylaluminum (Me₃Al), which has been employed by different research groups using various oxygen sources, such as water (H₂O), hydrogen peroxide (H₂O₂), nitrogen dioxide (NO₂) and ozone (O₃) [25, 26]. The reaction with water is:



The highest growth rate obtained with this route is about 1.2 Å/cycle, with a deposition temperature between 150°C and 450°C. With H₂O₂ the growth rate is in the same order, but using other sources it is lower.

Aluminium chloride (AlCl₃) has also been used as aluminum source, coupled with H₂O, O₂ or alcohols as oxygen sources. The growth rate in this case is typically in the range 0.4 – 0.9 Å/cycle, but it is variable not only according to the co-reactant chosen for AlCl₃, but also to the reactor and the deposition temperature.

Water has been tested also with dimethylaluminum chloride (Me₂AlCl), giving a maximum growth rate of 0.8 Å/cycle at 250°C [26].

2.2 AREA SELECTIVITY

2.2.1 General considerations

As mentioned in *chapter 1*, area-selectivity is the essential requirement to make ALD occur in predetermined locations of a patterned substrate (the so-called growth areas), in such a way to enable self-aligning processes which would improve the current technology for the BEOL production.

When considering the generic layer of the back-end, growth and non-growth areas simply reflect the different materials presented by the layer itself. Since these materials are usually characterized in function of their electrical properties as metals or dielectrics, selective depositions can be distinguished with acronyms which recall these properties: MoM (metal-

on-metal), MoD (metal-on-dielectric), DoD (dielectric-on-dielectric) and DoM (dielectric-on-metal) [14].

Like all the other chemical depositions, ALD proceeds through a mechanism of nucleation and growth.

In order to achieve a uniform deposition in the desired growth regions and no deposition at all in the desired non-growth regions, the nucleation step must be selective, property which can be obtained with different approaches.

1. Selectivity may be inherently surface-dependent, meaning that some sites of the substrate naturally react with the precursors and some others don't, as a result of different chemical affinities.
2. Selectivity may be achieved by a **functionalization** of the substrate.

The substrate can be:

- a) locally activated, meaning that there is something in the growth regions that promotes the nucleation;
- b) locally deactivated (or inhibited), meaning that there is something onto the non-growth regions that prevents the nucleation.

The current tendency is to operate through a deactivation mechanism (*approach 2b*). Conventional lithographic materials, such as patternable polymers, can be used to block reaction sites and prevent ALD film growth, as long as they result thermally stable and unreactive [27]. Recently the thinnest possible blocking layers, namely self-assembled monolayers (SAMs), have been proved very suitable functionalizing units, but this subject will be discussed more thoroughly later. First, it is worth to remember that a deposition, regardless of the type, takes place if it is energetically favorable and this happens when the change in *Gibbs free energy* (ΔG) is negative [28]. The variation of Gibbs free energy is related to the changes in enthalpy (ΔH) and entropy (ΔS) according to the *equation 2.1*:

$$\Delta G = \Delta H - T\Delta S \quad \text{Eq. 2.1}$$

Depending on the values of ΔH and ΔS , different situations can be distinguished.

- If $\Delta H < 0$ and $\Delta S > 0$, ΔG is necessarily < 0 and the reaction is spontaneous, independently from T (this is the case of substrates which show chemical affinity towards the deposited substance).

- If $\Delta H > 0$ and $\Delta S < 0$, ΔG is positive and the reaction is thermodynamically forbidden (this is the case of substrates which do not show chemical affinity towards the deposited substance).
- If both ΔH and ΔS are positive ($\Delta H > 0$ and $\Delta S > 0$), the reaction occurs only if T is high enough.
- If both ΔH and ΔS are negative ($\Delta H < 0$ and $\Delta S < 0$), the reaction occurs only if T is low enough.

The purpose of functionalization by activation is to expose, in growth areas, surface groups which make the reaction between substrate and precursors energetically favorable. Vice versa, the purpose of functionalization by deactivation is to expose, in the non-growth areas, surface groups which make the reaction between substrate and precursors energetically forbidden or strongly unfavorable.

2.2.2 Selectivity (S)

The physical quantity which expresses the effectiveness of an area-selective deposition is called **selectivity** (S). For a given patterned substrate, defining as θ_{GA} and θ_{NGA} the amounts of material present after the deposition on growth and non-growth areas, the generally accepted formula for selectivity (S), is [14, 29]:

$$S = \frac{\theta_{GA} - \theta_{NGA}}{\theta_{GA} + \theta_{NGA}} \quad \text{Eq. 2.2}$$

S varies between -1 and +1 and some applications in nanoelectronics might require a selectivity as high as 0,99999999 [14]. In the very ideal case $\theta_{NGA} = 0$ and $S = 1$, which means, in other words, a perfect selective deposition. In practical terms θ_{NGA} is always bigger than 0 and, basing on the literature regarding many AS-ALD approaches, for a film few nanometers thick a selectivity value of 0.99 appears already a difficult, but in some cases achievable, target [14].

But why is $\theta_{NGA} > 0$ in any case? Because some deposition always occurs in the non-growth areas, due to defectivity of selectivity.

The time it takes for the deposition to start in the non-growth areas is defined as **nucleation delay**, while the number of cycles before the nucleation starts is defined as **selectivity**

window [14]. Figure 2.4 gives a visual representation of what nucleation delay and selectivity window are.

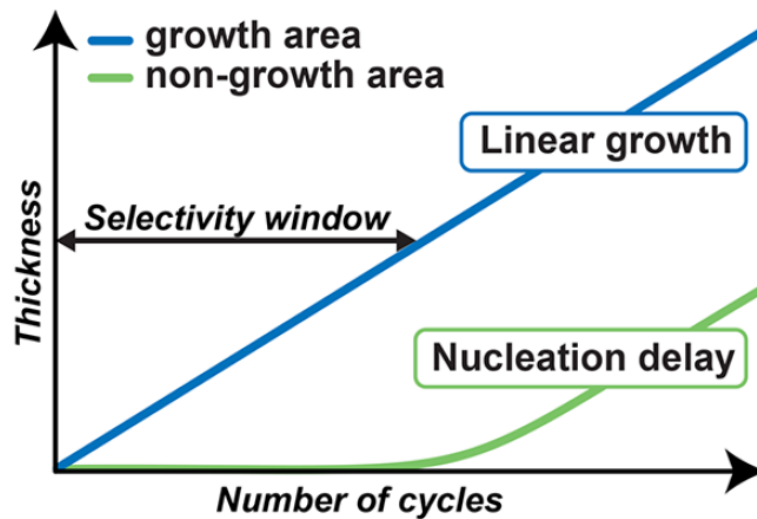


Figure 2.4: nucleation behavior on the growth and non-growth areas and selectivity window [14].

The larger the nucleation delay, the bigger the selectivity window; a wide selectivity window translates into higher values of S , meaning more chances to get a very good deposition result.

As it can be seen in the picture, in the growth area the layer thickness increases from the very beginning of ALD process, in a linear fashion. In the non-growth area, instead, the thickness at first is equal to 0 but, at the end of the window, it starts to increase with the same linear trend. Selectivity is a function of number of cycles, therefore of film thickness. This implies that there are basically two ways to evaluate different ALD processes: either comparing S values for a specific target thickness, or comparing the thickness that can be obtained when limiting S to a specific maximum value.

2.2.3 Inherent area-selectivity

As it could be easily realized, the inherently selective deposition is peculiar for some specific combinations of substrates and precursors, hence the deployment on a broad scale of this approach is limited.

It has been observed, for example, that tungsten ALD is more energetically favorable on silicon (Si) rather than on silica (SiO₂) and this allows a selective deposition of tungsten on

the first material, even if after several ALD cycles this selectivity is lost. The process is schematically depicted in *figure 2.5*.

Using tungsten hexafluoride (WF_6) as the tungsten source, the two reactions involved in the process are:

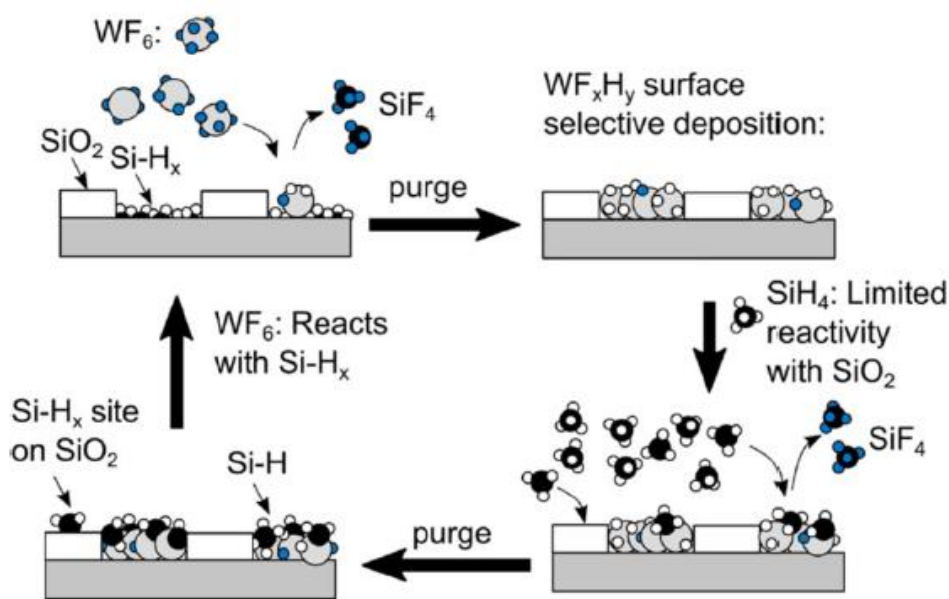
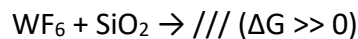
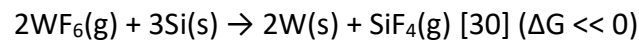


Figure 2.5: area selective deposition of tungsten on silicon substrate [4].

Several of these naturally selective processes exploit the large difference in chemical character between hydroxyl-terminated ($-\text{OH}$) and hydrogen-terminated surfaces ($-\text{H}$). This typically leads metal oxides to selectively deposit onto hydroxylated silicon (Si-OH) and avoid H-terminating silicon (Si-H), which experiences a nucleation delay. For example, in a study by *Longo et al.* about titanium dioxide (TiO_2) ALD (using titanium tetrachloride and water as precursors), after 25 cycles the growth of TiO_2 was detected on the OH -terminated Si but not on the H-terminated Si, thus revealing selectivity. However, the selectivity window of metal oxides is small: in the same study, for instance, the hafnium dioxide (HfO_2) ALD [using tetrakis-(dimethylamido)-hafnium and water as reactants] registered a loss of selectivity after just 10 cycles [14].

2.2.4 Functionalization by area-deactivation

As previously anticipated, a common way employed nowadays for the functionalization consists of using self-assembled monolayers, molecules that allow to modify the physical and chemical properties of both metallic and dielectric surfaces.

SAMs are deposited before the ALD and are conveniently removed afterwards, when they are not needed anymore. In literature there is plenty of articles of groups which have investigated many combinations of substrates, passivating SAMs and ALD materials.

For instance, octadecylphosphonic acid (ODPA) has been successfully used by *Hashemi et al.* to direct the area selective ALD on a pattern made by metal and metal oxide [31]. It was found that ODPA forms a well-packed layer on copper in a variety of states (i.e. Cu, CuO, Cu₂O) but, at the same time, it does not attach on SiO₂ at room temperature. It was therefore possible to operate a selective ALD of zinc oxide (ZnO) on patterned samples of copper and silicon dioxide (Cu/SiO₂): after the functionalization of the copper with the ODPA, the ZnO had no choice other than growing only onto SiO₂; by this method films up to 36 nm in thickness were formed. After the deposition of zinc oxide on silica, the SAM needed to be removed from copper; since the electrochemical dissolution of self-assembled molecules could not be taken into account (because it is not compatible with many electronic fabrication processes), a mild etchant was used to selectively remove the copper oxide (Cu₂O) to which the SAM was attached. A schematic representation of the process is given in *figure 2.6*.

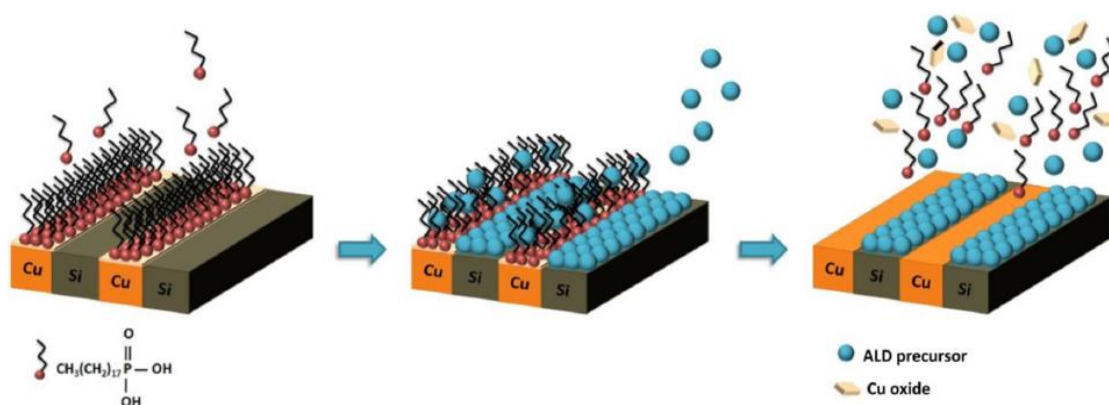


Figure 2.6: silicon-selective ZnO ALD using ODPA-SAMs as blocking layer on Cu, with consequent selective removal of SAMs using an etchant [31].

2.2.5 Selectivity issues and further developments

The power of an area selective ALD process like the one previously described (*paragraph 2.2.3*) relies on the possibility to appropriately designate precursors (for the atomic layer deposition) and SAMs (for the passivation of the non-growth area) for a specific patterned substrate. Unfortunately, as discussed in *paragraph 2.2.1* it is always unavoidable that some deposition occurs where it should not, i.e. the non-growth area. This is often due to the modifications that non-growth area itself may undergo when exposed to the ALD reactants: even the mild H_2O , for instance, is sufficiently reactive to alter H-terminated Si. Moreover, the approaches based on the use of SAMs are for a large part limited by the thermal stability of SAMs themselves: for some species desorption or degradation starts already at 100°C , with dramatic consequences for the passivating layer, which experiences pinholes formation with subsequent loss of selectivity.

A solution to these challenges is to implement correction steps during the ALD, such as the ones presented below [14].

- SAMs regeneration: it consists in the iterated regeneration of the monomers of which the passivating layer is made up. *Hashemi et al.*, in their work about the AS-ALD of ZnO on SiO_2 exposed in the earlier paragraph, were able to achieve the regeneration by delivering DDT (dodecanethiol) SAMs in the vapor phase after every 150 cycles of ZnO; the group reached a final zinc oxide film thickness of 81 nm, considerably higher with respect to the value obtained without the implementation of regeneration. *Figure 2.7* shows a schematic representation of the approach.

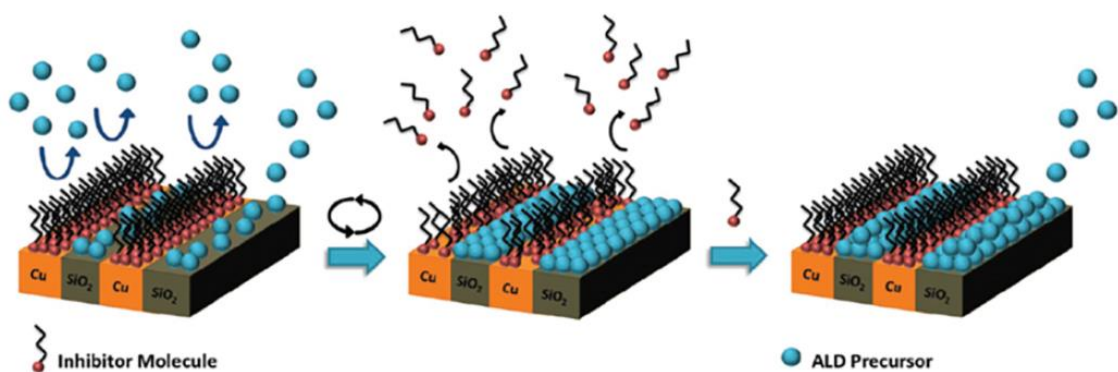


Figure 2.7: selectivity improving approach by monomers regeneration in AS-ALD of ZnO on SiO_2 [14].

- Repeating functionalization: instead of repeating regeneration after a certain number of ALD cycles, like in the previous case, the functionalization step is performed after each ALD cycle, creating a super-cycle of alternated atomic layer deposition (on growth areas) and self-assembled monolayers passivation (on non-growth areas).
- Selective etching: it combines the AS-ALD with a selective etching of the material on the non-growth areas. It seems a promising strategy to reach the very high selectivity values required for reliable semiconductor processing.

CHAPTER 3. SELF-ASSEMBLED MONOLAYERS

3.1 GENERALITIES ABOUT SAMs

3.1.1 SAMs structure

The expression self-assembled monolayers, simply known as SAMs, refers to ordered arrays of organic molecules which spontaneously assemble themselves in layers on the surfaces of solid materials [32].

The defining feature of the process is the chemisorption: SAMs form thanks to the strong interaction between the solid surface of interest and the molecules, which show a specific affinity towards the surface itself. The strength of the bonds creates monolayers that exhibit much more stability with respect to the Langmuir-Blodgett films⁵, a closely related class of polymeric layers which originate from the physisorption of the molecules onto the substrate. Conceptually speaking, self-assembled monolayers are not so different from surfactant monolayers, made up by well-known amphiphilic molecules which are at the basis of all detergency applications. The main feature that distinguishes the self-assembling molecules from the ordinary surfactants is the fact they are not merely constituted by hydrophilic heads and hydrophobic tails, but they have a slightly more complex structure (see *figure 3.1*), since they are tailored such to have favorable and specific properties [33].

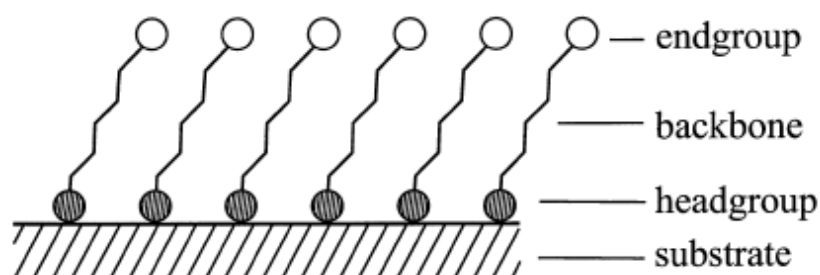


Figure 3.1: SAM structure [34].

As it can be seen from the *figure 3.1* in the typical self-assembling molecule (precursor of the

⁵Langmuir-Blodgett films are prepared by transferring Langmuir films onto solid substrates. Langmuir films simply consist of amphiphilic molecules spread on the surface of a liquid.

self-assembled monolayer) it is possible to identify three different parts, which are listed below with a brief explanation of their peculiar characteristics.

- **Head group:** functional group responsible for the chemical bond with the surface. Since the distinctive trait of SAMs systems is the coupling between the substrate and the head group (while the rest of the molecule can be essentially freely chosen), this “chemisorption pair” is often used to classify SAMs systems themselves [34]. Some of the most famous are summarized in *table 3.1* [35].
- **Backbone or tail:** hydrocarbon chain of various length, usually aliphatic and saturated, which separates the two ends of the molecule. Different kinds of lateral attractive forces establish among adjacent chains, reducing the total energy of the system. The maximization of these interactions (mostly Van der Waals forces, but also hydrogen bonds in some cases) determines the tightest possible packaging for the organic layer, within the geometric constraints imposed by steric hindrance of head groups [35].
- **End group:** structural unit which will be exposed after the chemisorption by the surface, determining its new and final properties.

Table 3.1: combinations of head groups and substrates employed in forming SAMs [35].

Organic compounds class	Head group	Substrates used
Alcohols	R-OH	Fe _x O _y , SiH, Si
Amines	R-NH ₂	Stainless steel 316L, FeS ₂ , CdSe, Mica, YBa ₂ Cu ₃ O _{7-δ}
Isonitriles	R-C≡N	Ag, Au
Carboxylic acids	R-COOH	Fe _x O _y , Ni, Ti/TiO ₂ , α-Al ₂ O ₃
Organosilicon derivatives		
- alkylsilanes	R-SiH ₃	HfO ₂ , PtO, TiO ₂ , ZrO ₂
- alkylchlorosilanes	R-SiCl ₃	HfO ₂ , PtO, TiO ₂ , ZrO ₂
Organosulfur derivatives		
- dialkyl sulfides	R-S-R'	Au
- dialkyl disulfides	R-SS-R'	Ag, Au, CdS, Pd
- alkanethiols	R-SH	Ag, AgS, Au, AuAg, AuCu, CdTe, CdSe, CdS, Cu, FePt, GaAs, Ge, Hg, HgTe, InP, Ir, Ni, PbS, Pd, PdAg, Pt, Ru, Zn, ZnSe, ZnS
Organophosphorus derivatives		
- phosphine oxides	R ₃ -P=O	Co, CdS, CdSe, CdTe
- phosphonates	R-(PO)(OH) ₂	Al, Al-OH, GaAs, GaN, Mica, TiO ₂ , ZrO ₂ , CdSe, CdTe

The interest in SAMs has witnessed tremendous growth in the past few decades. The ease of their preparation, the tunability of surface properties through the modification of their chemical structure, the huge variety of molecules that can be employed (as it can be seen from the *table 3.1*), their use as building or blocking unities in more complex structure and last but not least, the possibility to obtain high quality layers, make SAMs really attractive in a wide range of applications in biotechnology, tribology, electrochemistry, micro- and nano-electronics [34, 36].

3.1.2 SAMs growth mechanisms

The deposition of SAMs precursors, with the consequent chemisorption that eventually leads to the formation of the monolayers, can occur essentially in two ways, either from the gaseous or the liquid phase.

The traditional deposition route is from liquid solution. Growth from the gaseous phase is usually more expensive, due to the experimental setup that requires a vacuum chamber, but it offers some advantages too, such as a better cleanliness of the environment and a better control of the temperature of the process [34].

The mechanisms of SAMs growth on surfaces are several and many of them are still under investigation. Although they vary according to the molecules, the substrates and the deposition route (either from gas or liquid) involved, it is possible to define a common behavior, summarized in the *picture 3.2* [33].

The first step is clearly the transport of adsorbate molecules throughout the fluid at the solid interface, which can imply some combination of diffusive and convective transfer phenomena. This is followed by the adsorption on the substrate, with an evolution of the molecular order and an increase of surface coverage depending on some adsorption rate.

1. In the very early stages of the adsorption, SAMs must be pictured as a low-density vapor phase, in which mobile and isolated adsorbed molecules are conformationally disordered and randomly distributed on the surface (see *A1* and *B1* in *fig 3.2*).
2. At a later stage, two qualitatively different growth process can occur:
 - The monolayer can enter a region of coexistence between the vapor phase and a high-density condensed phase or, in other words, a solid phase (see *A2* in *fig 3.2*). Islands of solid phase will nucleate and grow, surrounded by

isolated adsorbed molecules in the vapor phase. These solid domains will eventually coalesce together to cover the substrate entirely (see A3 in fig 3.2).

- The monolayer can enter a region of coexistence between the vapor phase and a low-density condensed phase, which may consist of either a disordered 2D liquid [see B2(a) in fig. 3.2], or an ordered phase with lower density than the solid one, such as a lying-down phase [see B2(a') in fig. 3.2] where the axis of the molecules is parallel to the surface plane.

After that the vapor phase is completely converted [see B2(b) and B2(b') in fig. 3.2] to the low-density condensed phase (either the 2D liquid or the lying-down phase), solid islands [see B2(c) and B2(c') in fig. 3.2] surrounded by the aforementioned low-density phase will start to nucleate and grow, ending up joining together in a solid layer (see B3 in fig 3.2).

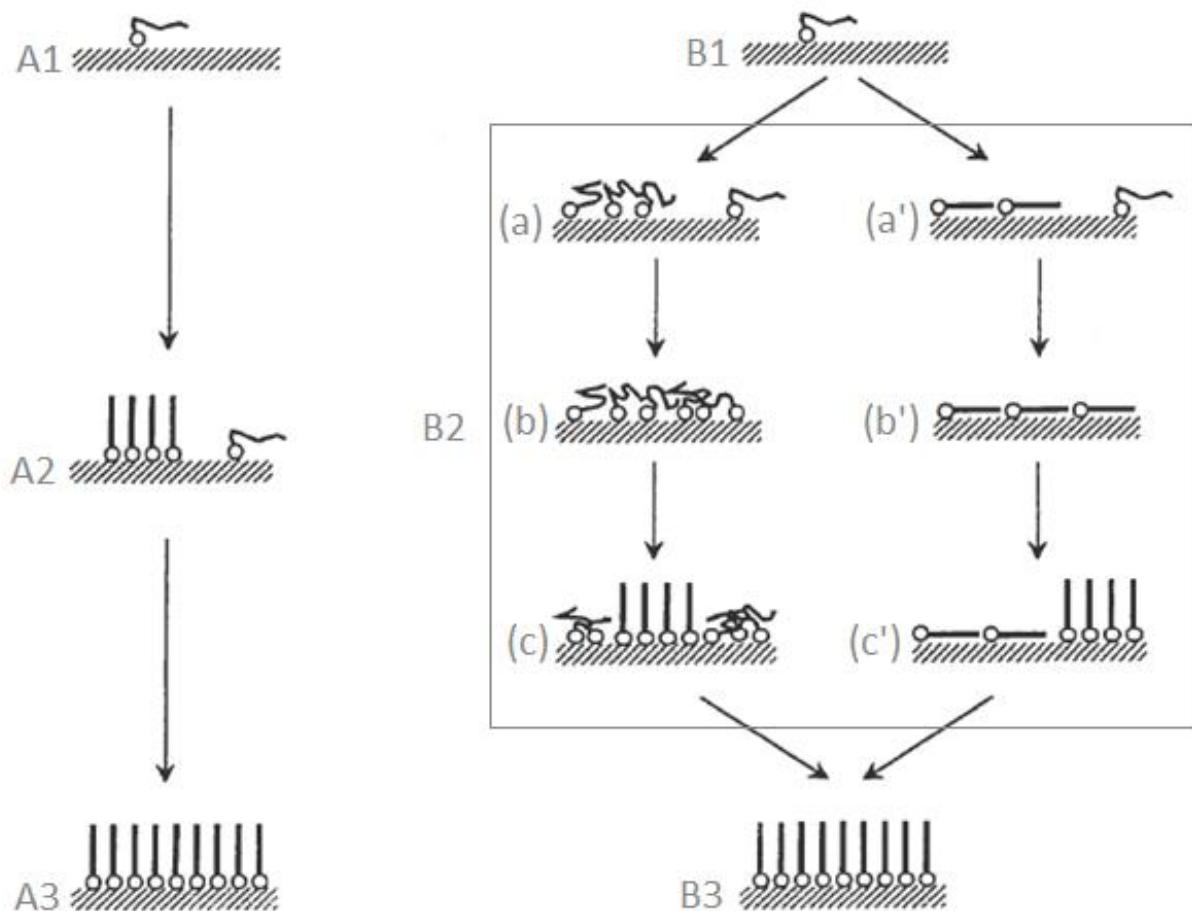


Figure 3.2: SAMs growth mechanisms [33].

3.1.3 SAMs from liquid phase

As mentioned in *paragraph 3.1.2*, SAMs are traditionally prepared from liquid phase. In principle, after proper cleaning of the substrate, it is sufficient to submerge it in the solution composed of SAM precursor plus solvent: self-assembling molecules will deposit on the substrate and the monolayer will eventually assemble. The time it takes for the monolayer to assemble is referred to as immersion time [37]. This simple procedure, outlined in the *figure 3.3*, is denominated **dipping**. Although this thesis work did not use dipping methodology but spin coating to deposit SAMs, it was anyway adopted the route from liquid solution.

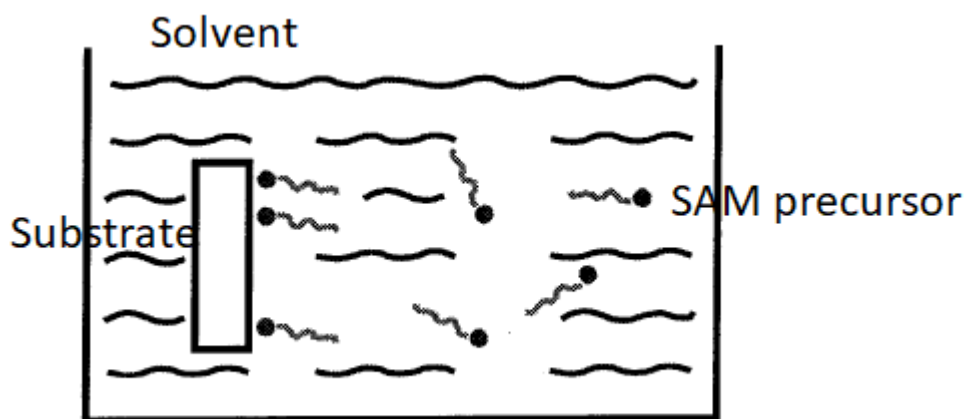


Figure 3.3: dipping methodology for growing SAMs from liquid phase [34].

Many factors can influence the adsorption rate and the good quality of the final layer during SAM deposition from solution [34]:

- Nature of the solvent. Long chain solvents slow down the chemisorption rate due to two reasons: first, SAM precursor mobility in the solution is reduced, and secondly the interactions of solvent molecules with the substrate (from which they have to be displaced) become larger, making the transport of the solute to the substrate more difficult.
- Nature of SAM precursor. The adsorption rate decreases with an increasing length of the backbone, due to the fact that the mobility of the molecules in the solution is reduced.

- Concentration [C] of SAM precursor in the solution. Low concentrations imply slower adsorption rates and require longer immersion times. Anyway, some groups have found out that at very high concentrations, the adsorption rate becomes independent of the concentration itself. [C] is usually chosen in the millimolar or micromolar range.
- Cleanliness of the substrate. Contamination and impurities as well as defects of the substrate can affect the final properties of the self-assembled monolayer.
- Cleanliness of the solution. The purity of the solution, i.e. absence of non-solvent and non-solute particles (often difficult to achieve), strongly influences the successful outcome of the layer formation.
- Temperature. For temperature dependence, still few data exist. In contrast with the deposition from gas phase (which experiences a decrease of chemisorption rate with the temperature increase), the dependence in solution is fairly weak and dipping is usually carried on at room temperature.

3.2 THIOLS SELF-ASSEMBLED MONOLAYERS

3.2.1 Basic notions

Among the great variety of organic compounds that are commonly employed for SAMs fabrication (see *table 3.1*), sulfur derivatives play a very important role, since they have a strong affinity to most of metals (probably because of the possibility to form multiple bonds with surface metal clusters) and some semiconductors [32].

In the case of metals, the geometric arrangement of sulfur moieties on the surface and the lattice parameters of the metal involved are the factors which determine the upper limit in density that the molecules could attain. However, the value may not correspond to density that the same molecules would reach in a pure crystalline form [35].

Thiols⁶ have been the most widely used type of organosulfur SAMs. The scientific literature has many articles concerning the topic, especially about thiols on gold, which represent the archetypal case of self-assembled monolayers on metal substrate. The extensive study of these compounds has led to detailed growth models, which have not been extended yet to

⁶Thiols are sulfur analogues of alcohols, i.e. compounds with generic formula R-SH.

other categories of SAMs. In a first approximation, the adsorption rate ($d\theta/dt$) of thiols should follow the *Langmuir kinetic model*, which states that the rate is proportional to the amount of residual free space on the surface θ and a constant R , according to the following equation:

$$\frac{d\theta}{dt} = R(1 - \theta) \quad \text{Eq. 3.1}$$

Equation 3.1 gives rise to the following growth law:

$$\theta = 1 - e^{-R(t-t_c)} \quad \text{Eq. 3.2}$$

Where t_c is a possible time off-set, which is unequal to 0 only if the nucleation starts with a certain delay [34]. Obviously alternative models with more complex laws do exist, but they won't be described because they go beyond the topic of this thesis.

3.2.2 Alkanethiols

The simplest category of thiols is constituted by *n*-alkanethiols, molecules whose tails are some alkane-derivatives: their structural formula is $\text{CH}_3(\text{CH}_2)_n\text{SH}$.

The SAM used in this thesis work was the **octadecanethiol** (in short ODT) and it belongs to this group of compounds. ODT chemical structure $[\text{CH}_3(\text{CH}_2)_{16}\text{CH}_2\text{SH}]$ is represented in the *figure 3.4* below.

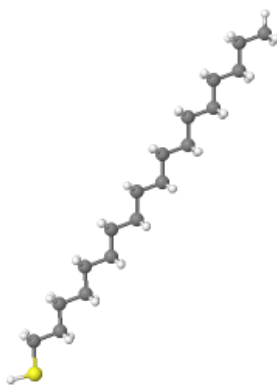


Figure 3.4: ODT molecular structure.

SAMs derived from *n*-alkanethiols present a quasi-crystalline structure, with the chains almost fully-extended in a nearly-all trans conformation. Due to their linear structure, a simple single-chain model can be used to describe the molecules orientation within the monolayer. As shown in *figure 3.5* two parameters are needed: the tilt angle (α) that the linear backbone forms with the surface normal and the twist angle (β) which indicates the rotation of the carbon-carbon bonds plane with respect to the plane containing the surface normal and the tilted chain. Values of α range from 0° to 30° , according to the metallic substrate [35].

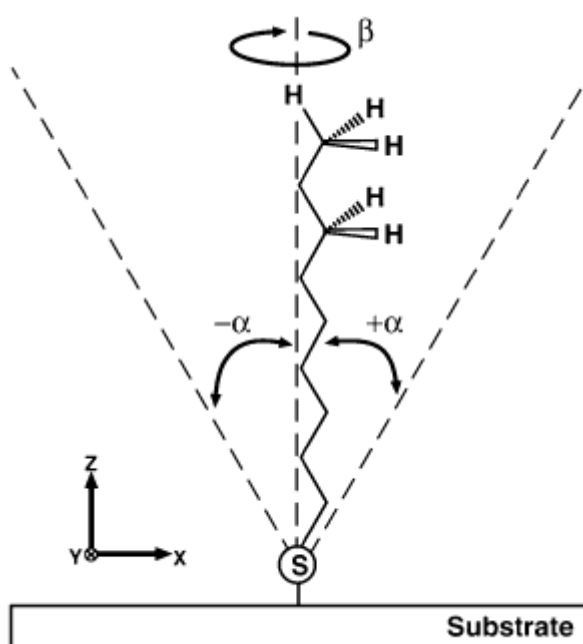


Figure 3.5: schematic view of a fully extended single chain (in an all-trans conformation) of an alkanethiol adsorbed on a substrate [35].

CHAPTER 4. EXPERIMENTAL METHOD

All the experiments of this thesis project were performed at the headquarter of **IMEC**⁷, located in Leuven (Belgium).

4.1 PROCEDURAL STEPS

4.1.1 Preparation of the samples

The first step of each experiment was the metal samples preparation. Both cobalt and copper wafers were fabricated directly at IMEC and stored in an appropriate FOUPs inside the clean room (CR). It is important to underline that the realization of pure metal wafers would be very inconvenient due to the extremely high costs of pure metals, therefore Co and Cu actually made up only the upper layers of more complex stacks.

The stack of the cobalt wafers, from the bottom to the top, was:

- 1 mm of Si substrate;
- 1,5 nm of SiO₂;
- 10 nm of TaN;
- 5 nm of pure cobalt (deposited by physical vapor deposition);
- Co_xO_y (to be taken into account because of the exposure to the oxygen of CR atmosphere).

The stack of the copper wafers, from the bottom to the top, was:

- Si substrate;
- 100 nm of SiO₂;
- 3 nm of TaN;
- 200 nm of pure copper (deposited by electrochemical deposition and thereafter planarized by chemical mechanical polishing).
- Cu_xO_y (to be taken into account because of the exposure to the oxygen of CR atmosphere).

⁷The acronym stands for “Interuniversitair Micro-Electronica Centrum” (Interuniversity Micro-Electronics Center). The company is an international research & development hub, active in the fields of micro- and nano-electronics for the last 35 years.

Managing the wafers with great care, small square-shaped coupons of side 3 cm were cleaved and then stored in specific trays.

4.1.2 Glassware cleaning

As seen in *paragraph 3.1.3*, the cleanliness of the solution is an essential requirement for the good quality of the SAMs, therefore only personal glassware was used for preparing the solution itself, in order to avoid as much as possible external contaminations.

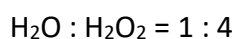
The glassware, carefully stored in a locker of the cleanroom, underwent a hard cleaning on a monthly basis: flask, beakers, funnel, jars were filled first with “regia” and then “piranha” solutions.

The aqua regia was used to remove possible metallic contaminations and it was prepared by mixing water (H₂O), hydrochloric acid (HCl) and nitric acid (HNO₃) with the following ratio:



After at least two hours of wetting time, the solution was trashed in the contaminated acid waste and the glassware rinsed with deionized water (DIW) to neutralize possible acid residuals.

Piranha solution was used to remove the organic contaminants and it was prepared by mixing water (H₂O) and hydrogen peroxide (H₂O₂) at the following ratio:



Due to the strongly exothermic nature of the reaction, at least four hours were waited before trashing the solution in the acid waste, to let the heat dissipate properly. Once again the glassware was rinsed with DIW, to eliminate residuals.

Additionally, right before making the SAM solution, the glassware always underwent a soft cleaning consisting of thoroughly rinsing it three times with organic solvents: isopropyl alcohol (CH₃CHOHCH₃) for beakers, funnel and jars; ethanol (CH₃CH₂OH) for the flask (the distinction was made to prevent any contact of the flask with other liquids than the solvent used to prepare the ODT solution).

4.1.3 Preparation of the ODT solution

The solution was prepared by mixing ethanol (solvent) and ODT (solute). Ethanol (EtOH) is one of the most widely used solvent for preparing SAMs and it was chosen for different reasons: it is able to solvate a great variety of alkanethiols with different degrees of polar character and chain length, it is inexpensive, available in high purity and it has low toxicity [35].

ODT with a high purity degree (98%) was provided by *Sigma-Aldrich company*. The compound, with the look of a white granular powder, was weighted on a balance accurate to 0,0001 g and subsequently poured in the ethanol. For a chosen value of molarity (M), the quantity (w) of ODT was calculated according to the equation below:

$$w = n_{solute} \cdot m.w. \quad \text{Eq. 4.1}$$

where m.w. and n_{solute} are respectively ODT molecular weight (286,559 g/mol) and number of moles. The number of moles was calculated using the following formula:

$$n_{solute} = M \cdot L \quad \text{Eq. 4.2}$$

where M is the abovementioned molarity and L the liters of solvent, usually equal to 0,1 (L). The solution was prepared in a glove box with an atmosphere of N_2 , to eliminate any possible reaction with oxygen. Empirical evidences, in fact, suggest that O_2 may provoke the oxidation of thiols to sulfonates and other oxygenated species, but an inert atmosphere prevents this phenomenon. The ODT took a certain amount of time to be solvated and a manual stirring of the solution was essential to accelerate the process.

4.1.4 SAM deposition by spin coating

The traditional SAM formation route from liquid solution, namely dipping methodology described in *paragraph 3.1.3*, can attain very good quality layers but it suffers from many drawbacks. First of all, dipping requires long immersion times, which reach up to 48 hours for some couplings of substrates and SAMs [29, 37, 38]. Moreover, the technique is difficult to scale up to full wafers because of the high-volume consumptions of both solvent and precursor and the difficulty to control the profile of solute concentration, that can lead to

wafer inhomogeneities. Deposition from vapor phase is easy to integrate and is compatible with back-end of line process flow but, on the other hand, not all SAMs precursors can be evaporated [39]. In this general context, **spin coating** deposition might be the perfect balance: it makes use of liquid solution such as dipping, but it consumes less quantities of solvent and precursor, it is time-saving and easy to scale up, at least in principle. Unfortunately, this methodology has not been adequately studied yet and just few articles concerning the topic exist. The biggest challenge of SAMs deposition by spin coating is the very short time that self-assembling molecules have to arrange in a dense and well-packed layer.

This work aimed to accomplish a good passivation of cobalt and copper samples by spin coating deposition of ODT, performed with the spin-coater shown in *figure 4.1*.



Figure 4.1: Picture of the spin coater.

After a rapid flush with nitrogen (in order to remove possible deposited particles like contaminants of the atmosphere, powder resulting from wafer cleaving etc.), the coupons were placed with a tweezer on the plate of the spin coater (right on top of the vacuum tube), then the vacuum was activated to make them stick on the plate. Pouring the ODT solution from above with the tool running revealed itself a wrong choice, because at a later

moment no deposition was recorded; it was then decided to first put the solution in contact with the samples for a determined amount of time and then proceed with the spinning. The only parameters to set on the spin coater were basically the spinning time and the spinning velocity: spinning time was set to 60 s, to make the coupons dry properly after the wetting step; as regards the velocity, it was found it did not affect the deposition and the average value of 3000 rpm (rounds per minute) was used. Other factors, such as the pre-treatment of the coupons, were varied from time to time, giving rise to different experimental pathways and results, but that will be discussed in *chapters 5 and 6*.

After spinning, the vacuum was turned off and the samples removed with great care, trying to place the tweezers only on the outer edge of the samples and avoiding any scratches which would have damaged the ODT layer.

4.1.5 Characterization of the samples

After the spin coating step, the coupons were stored in the clean room overnight, to make possible traces of solvent (EtOH) completely evaporate. Subsequently, they were subject to a series of analyses through different characterization techniques, which will be explained in detail in the *paragraph 4.2*. For now, only the general operative sequence will be shown.

A first assessment of samples quality was made using the **Spectroscopic Ellipsometry (ES)** and the **Water Droplet Contact Angle Measurement (WCA)**.

ES was employed to evaluate the thickness of the samples post spin coating with respect to a reference value: the thickness was supposed to increase of ≈ 2 nm due to the presence of the additional layer of ODT. The reference value was set on the basis of a coupon which did not undergo any deposition (referred to as bare coupon) coming from the same wafer of the samples. For every single wafer a different bare coupon was required since each one of them could experience a (slightly) different thickness after the fabrication.

WCA, instead, was used to evaluate the water wettability of the samples post spin coating: they were supposed to be mildly non-wetting due to the ODT hydrophobic chains exposed on their surfaces.

The samples which passed satisfactorily the preliminary studies were more deeply investigated with two more techniques, **Atomic Force Microscopy (AFM)** and **Cyclic Voltammetry (CV)** which provided, respectively, a measurement of samples surface roughness and SAM coverage density of the metallic substrates.

4.1.6 Thermal study of the samples

After the characterization process, the most promising samples were reproduced in multiple copies, which were then heated to different temperatures in order to investigate the thermal stability of the ODT. The tool used for this purpose, called heatpulse, is shown in the *figure 4.2*.

For each of the temperatures to be analyzed, few simple operations had to be done:

- one of the coupons was placed on a carrier wafer, in turn inserted in the heatpulse in such a way to stay in contact with the thermocouple of the tool;
- the temperature to be reached was set;
- the coupon was kept inside for 900 s;
- the coupon was extracted after having waited long enough to make it cool down to T_{room} (the amount of time depended on the reached temperature).

It is noteworthy to say that heating was carried on in a nitrogen inert atmosphere, to avoid unwanted reactions with oxygen.

After the annealing, the samples were characterized again with the techniques mentioned in the *paragraph 4.1.5* to evaluate any modifications of the ODT layer. The thermal stability window of the SAM was so established, an essential data for proceeding with the ALD.



Figure 4.2: Picture of the heatpulse.

4.1.7 ALD attempts

The ALD was performed in a Savannah Reactor provided by Veeco-CNT. As announced in the introduction, the deposited substance was hafnium nitride (Hf_xN_y) and the selected precursors were ammonia and TDMAH [tetrakis-(dimethylamido)-hafnium].

The following cycle was adopted:

- pulse of ammonia (NH_3);
- purge with N_2 ;
- pulse of TDMAH [$((\text{CH}_3)_2\text{N})_4\text{Hf}$];
- purge with N_2 .

Different number of cycles and deposition temperatures were explored.

For each deposition 4 coupons were inserted in the reactor, exactly as shown in *figure 4.3*.

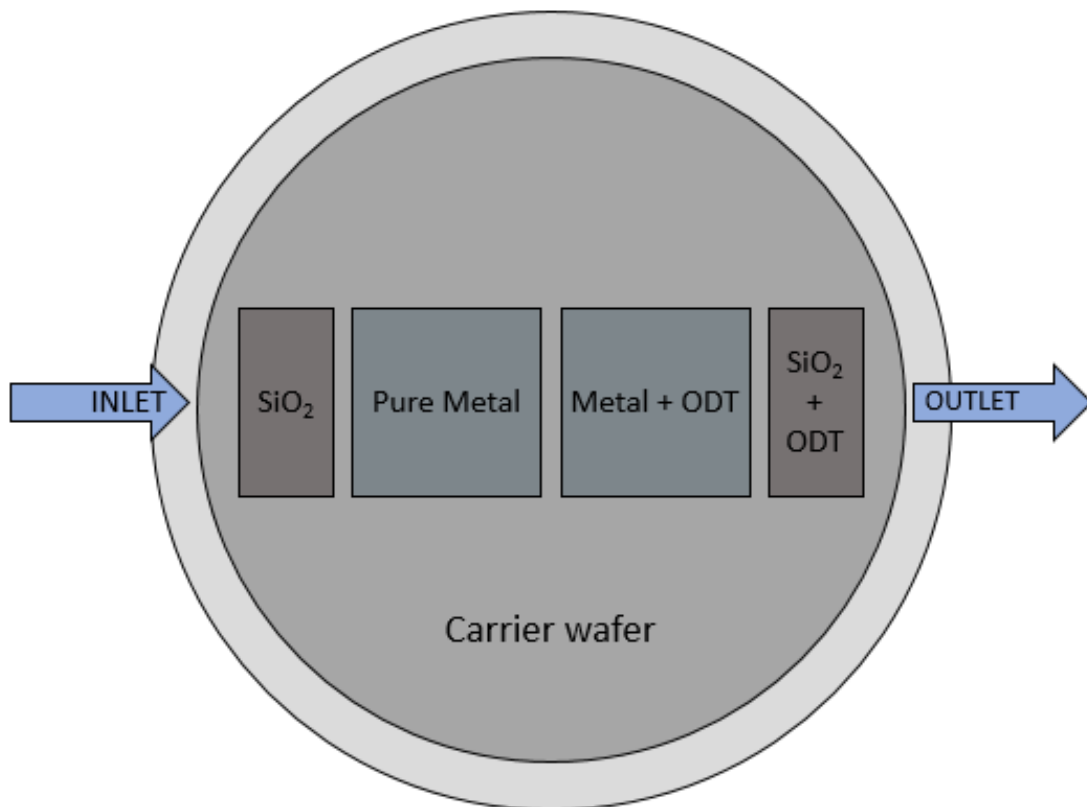


Figure 4.3: arrangement of the coupons in the reactor used to perform the Hf_xN_y ALD.

- Since it was not possible to have patterned substrates of “metal - silicon dioxide”, it was necessary to put distinct samples representative of both materials; half of silica coupons had been subject to the same treatment of the passivated metal ones (“Metal + ODT”), to create the most similar conditions to those of a patterned substrate. This is the reason why one coupon is referred to as “SiO₂ + ODT” in *fig. 4.3*. The ODT, however, did not attach to the SiO₂ due to no chemical affinity, therefore the treated SiO₂ was essentially pure SiO₂.

- The two silica coupons were inserted at the opposite sides of the chamber to check possible variations in the amounts of the deposited Hf_xN_y , which would have meant a difference in the volumetric flowrates of the inflow and outflow reactants streams (but it was not the case).
- The pure metal coupon was placed to evaluate the Hf_xN_y growth on the non-inhibited metal.

The ALD was supposed to occur on “Pure Metal”, “ SiO_2 ” and “ $\text{SiO}_2 + \text{ODT}$ ”, but it had to be blocked on “Metal + ODT” (= Co/Cu functionalized with ODT).

Once the deposition was accomplished, the samples were removed from the reactor and successively analyzed with Spectroscopic Ellipsometry (SE) and **Rutherford Backscattering Spectrometry** (RBS), by which it was possible to calculate, respectively, the changes in thickness experienced by the samples and the quantity of hafnium deposited.

4.2 CHARACTERIZATION TECHNIQUES

4.2.1 Spectroscopic Ellipsometry (SE)

Spectroscopic ellipsometry is a common optical technique mainly employed for investigating thin films. It relies on the polarization change that an incident light beam undergoes when interacting with a sample, like schematically represented in the *figure 4.4* [40].

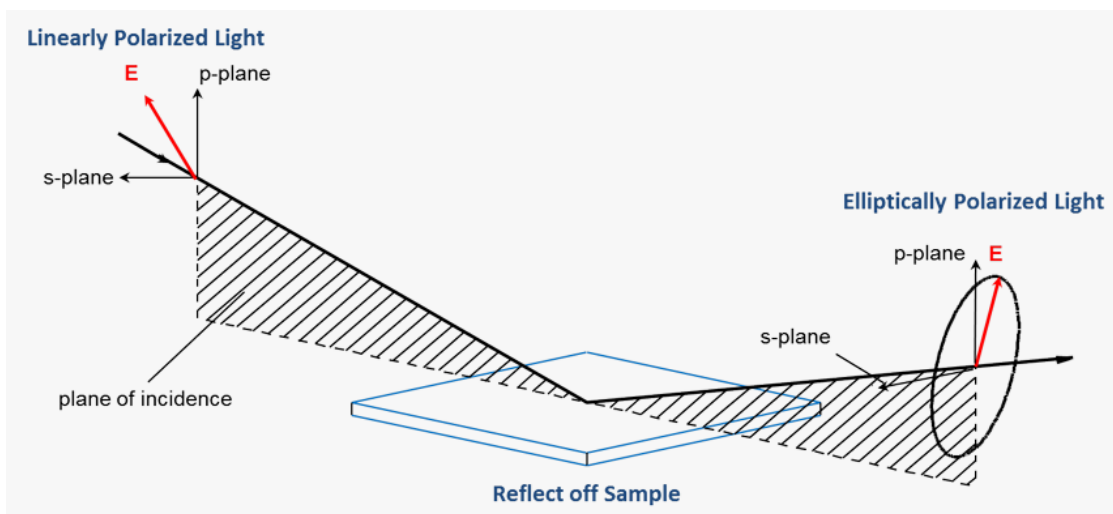


Figure 4.4: Representation of the change in polarization of an incident light beam on a sample.

The incident light beam (whose polarization is known) contains electric fields both parallel (p-) and perpendicular (s-) to the plane of incidence. The surface of the sample differentiates between p- and s- light, provoking a change in polarization of the reflected beam, which is represented by both an amplitude ratio ($\tan \Psi$) and a phase difference (Δ). By themselves, Ψ and Δ are not very informative, but they are exploited in various equations and algorithms which allow to determine many physical properties of the sample, such as surface film thickness, optical constant, refractive index and roughness [40].

The SE data (Ψ and Δ) of this thesis work were collected with the RC2 ellipsometer displayed in the *figure 4.5*, provided by *J.A. Woollam Company*. The thickness values were elaborated with *CompleteEASE software*.

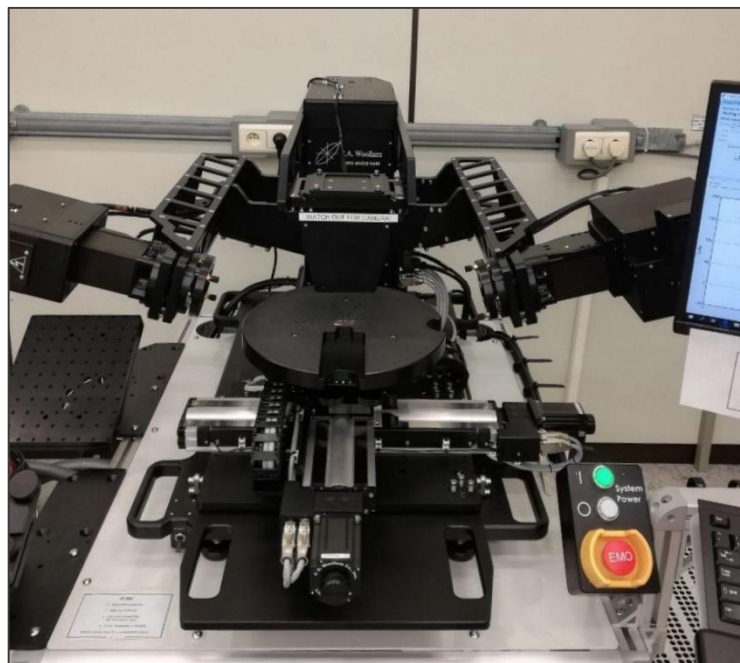


Figure 4.5: Picture of the Woollam RC2 ellipsometer.

4.2.2 Water droplet Contact Angle Measurement (WCA)

The contact angle measurement is performed to determine the wettability of a solid by a liquid; when the liquid involved in the investigation is water, the contact angle determines the hydrophilicity, or conversely the hydrophobicity, of the solid surface.

Strictly speaking, the contact angle is the angle between the solid surface and the tangential to the liquid in the point where liquid-vapor interface meets the solid, such as shown in *figure 4.5*.

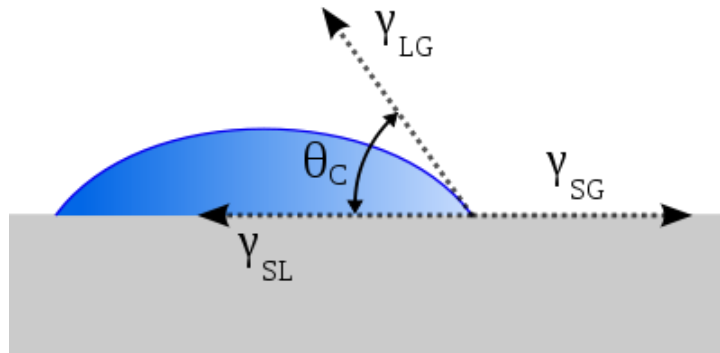


Figure 4.6: schematic of a liquid drop spread on a solid surface, showing the physical quantities involved in Young equation (γ_{SG} , γ_{SL} , γ_{LG} and ϑ) [41].

Denoting the solid-vapor interfacial energy by γ_{SG} , the solid-liquid interfacial energy by γ_{SL} and the liquid-vapor interfacial energy by γ_{LG} (i.e. the surface tension), the value of contact angle θ is calculated via the Young equation [41]:

$$\gamma_{SG} - \gamma_{SL} - \gamma_{LG} \cos \theta = 0 \quad \text{Eq. 4.3}$$

The instrumentation employed for this work is presented in *figure 4.7*.

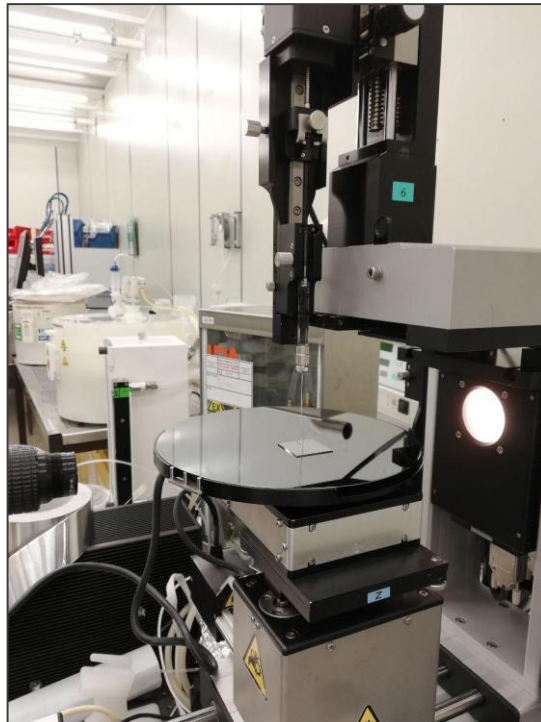


Figure 4.7: picture of the water contact angle tool.

The static sessile drop method was used: 5 droplets per sample were deposited throughout the surface by a syringe positioned above the surface itself and a high-resolution camera captured the images from the lateral profile. The images were afterwards analyzed with a software to obtain the exact values of water contact angles.

From literature it is known that ODT on copper (arranged in a dense and well-packed monolayer) returns a water contact angle of 110° [42]. Although it was not possible to find explicitly the WCA value for ODT on cobalt, a similar value was expected because alkanethiols on metal substrates typically exhibit WCA between 105° and 115° [43].

4.2.3 Atomic Force Microscopy (AFM)

Atomic force microscopy is a versatile and powerful microscopy technology designated for studying samples at the nanoscale. An atomic force microscope uses a cantilever with a very sharp tip to scan the surface of a sample, such as represented in *figure 4.8*. As the tip approaches the surface, close-range attractive forces establish causing the cantilever to deflect towards the surface itself. When the tip is brought too close to the surface, instead, repulsive forces take over, causing the cantilever to deflect away. A laser beam is used to detect the cantilever deflections, which are recorded by a position-sensitive photodiode: since such deflections reflect the valleys and the peaks of the specimen, the AFM can generate a topographic map of it [44].

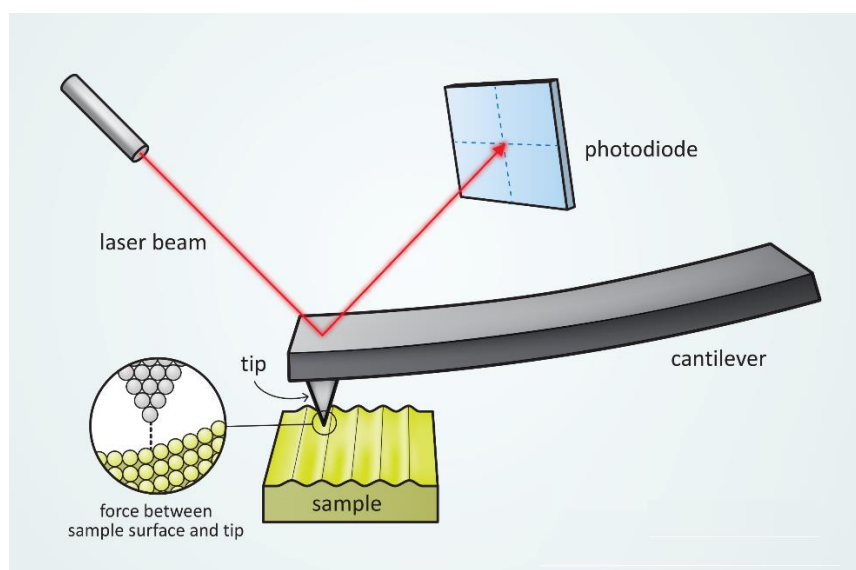


Figure 4.8: representation of atomic force microscopy working principle [45].

Although limited, a certain use of AFM was made in this study to acquire images of samples surfaces. The images, corresponding to small areas of $1 \mu\text{m}^2$, were afterwards analyzed with *Nanoscope Analysis Software* specifically to get surface roughness measurements, typically expressed in terms of two parameters, R_a and R_q .

R_a is defined as the arithmetic average of the absolute values of the surface height deviations (Z_j) measured from the mean plane:

$$R_a = \frac{1}{N} \sum_{j=1}^N |Z_j| \quad \text{Eq. 4.4}$$

R_q is defined as the root mean square of height deviations (Z_i) taken from the mean image data plane:

$$R_q = \sqrt{\frac{\sum_{i=1}^N Z_i^2}{N}} \quad \text{Eq. 4.5}$$

4.2.4 Cyclic Voltammetry (CV)

Cyclic voltammetry is a common electrochemical technique whose aim is to study reduction and oxidation processes of molecular species. CV involves the sweep of an electrode potential as a linear function of time and the determination of the consequent current that flows through the circuit. The results of a cyclic voltammetry measurement provide a plot called cyclic voltammogram or simply voltammogram: the x-axis represents the parameter imposed to the system, i.e. the applied potential (E), whereas the y-axis represents the response, i.e. the current flow [46].

The fundamental components for performing a cyclic voltammetry are:

- Working electrode (WE): it carries out the event of interest, that is the electrochemical reaction;
- Counter electrode (CE): it completes the electrical circuit;

- Reference electrode (RE): it owns a well-defined and stable equilibrium potential and it is used as a reference point against which the potential of the other electrodes can be measured (the applied potential is thus reported as “vs” a specific reference);
- Electrolyte solution: it compensates the electron transfer that occurs between working and counter electrodes via migration of ions in solution.
- Potentiostat: it controls the applied potential of the working electrode, as a function of the reference electrode potential. The experimental parameters are selected through the potentiostat software; the most important ones are the scan rate and the potential window.

CV measurements were used in this thesis in order to estimate the coverage of the ODT on cobalt and copper (the coverage, in fact, can be mathematically related to the current flow throughout the samples). A good passivating SAM was supposed to isolate the substrate from the circuit, obstructing the electron flow and therefore preventing reductions and oxidations to take place. In contrast to EP and WCA, the cyclic voltammetry provided a more reliable quality assessment of the SAMs but, despite this, the technique implied the loss of the samples due to its destructive nature.

The arrangement of the experimental setup, which is shown in the *figure 4.9*, was a little bit time-expensive and went through the steps described below.

- 1) The coupon to be analyzed was placed onto a suitable plate.
- 2) The electrodes (WE, CE, RE) were connected to the potentiostat, which was a *Parstat 3000A* provided by *AMETEK*.
- 3) A sealing O-ring and a matching glass cylinder were positioned on the coupon, covering an area of 1 cm² approximately; they were then fixed in place with a claw.
- 4) The working electrode was connected to the coupon.
- 5) The cylinder was filled with the electrolyte solution, which consisted of sodium hydroxide (NaOH) 0,1 M.
- 6) The counter electrode (a Pt wire) was dipped in the NaOH electrolyte solution.
- 7) The Ag/AgCl reference electrode was dipped in the electrolyte solution too.

Once the setup was accurately prepared, the potential window was set on the parstat software and the measurement was started; the window was established consulting articles which had treated the same metals (Co, Cu) with a similar combination of electrodes and electrolyte solution [47].

First, a reference voltammogram was acquired (by testing a bare Co/Cu coupon), and then the plots of the passivated samples were obtained. Thanks to *Origin Software* it was possible to calculate the areas under the voltammograms curves so that the percent coverage could be extracted, via the following equation:

$$Coverage(\%) = \frac{area_{reference} - area_{sample}}{area_{reference}} * 100 \quad Eq. 4.6$$

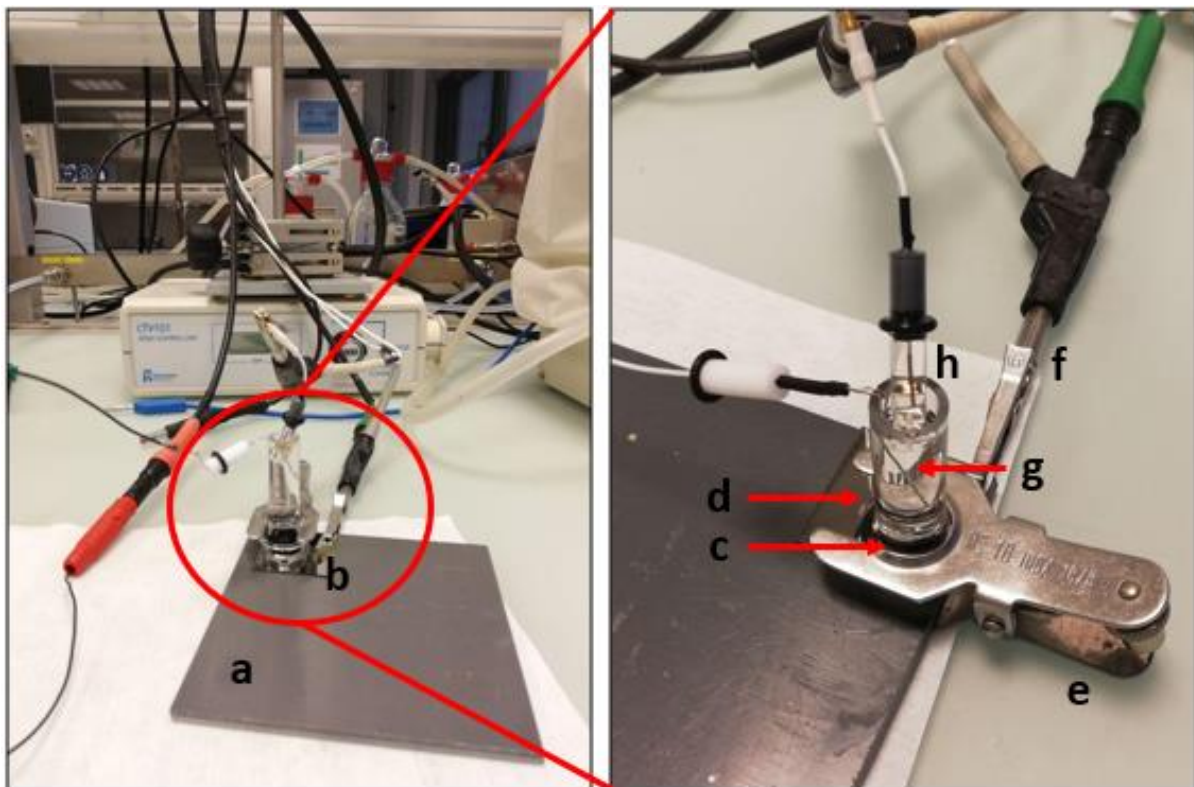


Figure 4.9: picture of the experimental setup for the CV.

(a) supporting plate; (b) specimen; (c) O-ring; (d) glass cylinder filled with NaOH [0,1 M]; (e) claw; (f) working electrode; (g) Pt wire counter electrode; (h) Ag/AgCl reference electrode.

4.2.5 Rutherford Backscattering Spectroscopy (RBS)

RBS is a non-destructive analytical technique by which it is possible to determine the surface structure of a solid material up to several μm depth. The working principle is very simple: the specimen is bombarded with an ion beam in the range of MeV; the beam is elastically back-scattered; a detector records the energy and the angle of backscattered ions, which yield information about the elemental composition of the specimen and its elemental concentration profile in function of the depth [48]. In this work RBS was used to quantify the

amount of hafnium deposited on the samples after the ALD; Hf quantity, expressed in atoms concentration, allowed to calculate the thickness of the hafnium nitride and, consequently, the selectivity.

On the contrary of the other techniques explored so far, the RBS analysis was not carried out personally, but by specialized IMEC operators.

CHAPTER 5. COBALT: RESULTS AND DISCUSSION

5.1 SPIN COATING

The general procedure has been already described in the *paragraphs 4.1.4* and *4.1.5* but some more specifications need to be done.

- Unless otherwise stated, the concentration used for the ODT solution was 0,01 M.
- The first EP measurements were performed with another ellipsometer than the *Woollam RC2* mentioned in the *paragraph 4.2.1*. The tool, unfortunately, did not allow a quantitative analysis of the thickness (due to the absence of a tool-related software), therefore a simple qualitative evaluation was done, by comparing the delta shift on the ellipsometry curves.
- Considering the length of ODT molecules and their orientation on metal substrates characterized by a tilt angle of approximately 30° , the target value for the thickness was ≈ 2 nm, as mentioned in the *paragraph 4.1.5*.
- The plots related to WCA measurements always show error bars since each contact angle was actually obtained by taking the average among 5 different values (as a matter of fact 5 water droplets per coupon were investigated and the angle slightly varied from drop to drop). The plots also display the water contact angle on bare Co, indicated with a red spot ($\approx 47,5^\circ$).
- The target value for the WCA was $\approx 110^\circ$, as said in the *paragraph 4.2.2*.

5.1.1 ODT [different ways for solution deposition] – spinning

The first experiment tested two different ways for depositing the ODT solution on the coupons: dripping it from above, while the spin coater was running, and gently pouring it on the samples, waiting for a certain amount of time before turning on the spin coater.

The latter method proved to be not only less solution-consuming but also much more effective (see *figure 5.1*), therefore it was the only one used from that moment on. The ineffectiveness of the first method can be explained admitting that dripping the solution

from above doesn't give enough time to ODT molecules to interact with the substrate because they are rapidly pushed away from the sample due to its fast rotation.

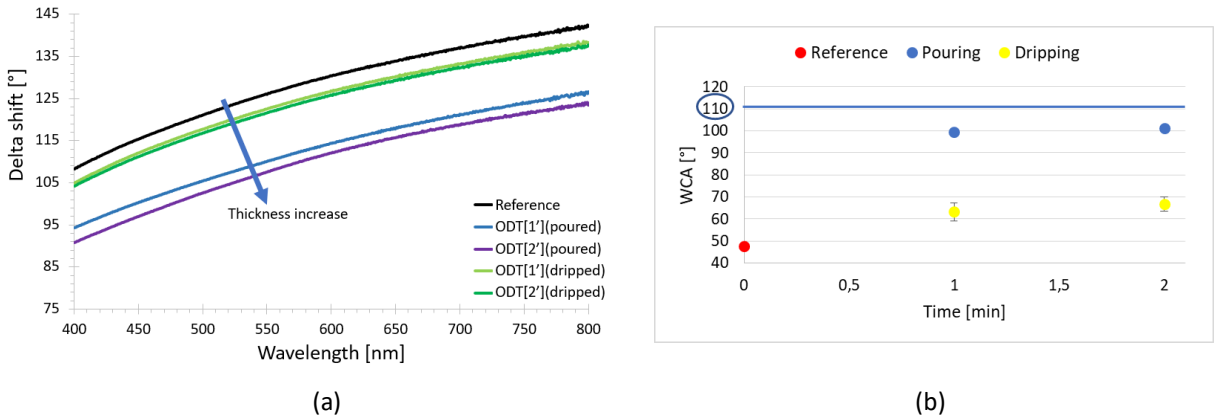


Figure 5.1: experimental results for two different ways of depositing the ODT solution on the coupons. (a) SE curves; (b) WCA values.

5.1.2 ODT [2 min] – spinning [different rpm]

The second experiment was performed to compare the influence of the spinning velocity, keeping the same ODT solution contact time. Four different rounds per minute were set on the spin coater (1000, 2000, 3000, 4000) but almost no differences were found (see figure 5.2), hence for the successive experiments it was decided to use 3000 rpm, a reasonable and intermediate value.

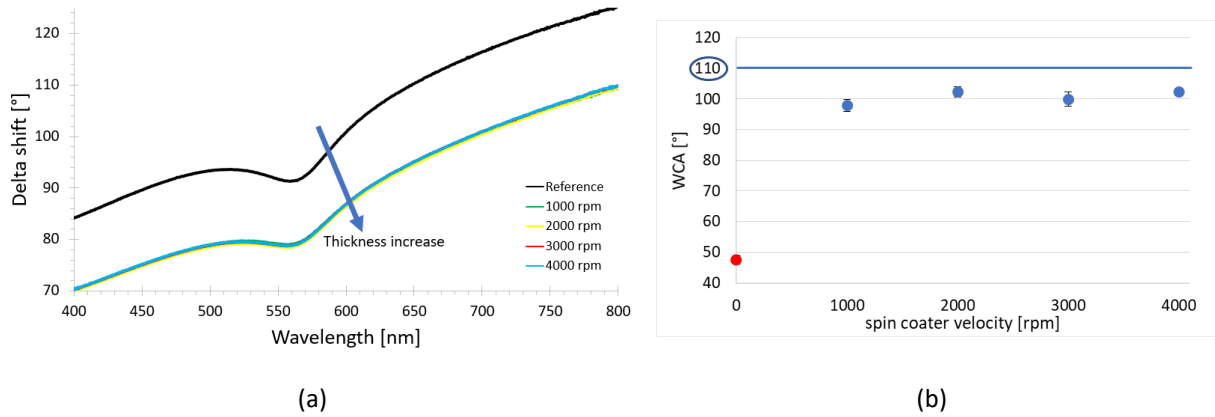


Figure 5.2: experimental results for coupons spun at different rpm (other conditions being equal). (a) SE curves; (b) WCA values.

5.1.3 ODT [different wetting times] – spinning

The third experiment evaluated the effects of the ODT contact time (although partially investigated in the first experiment already). Four different wetting times were chosen (30 s, 1 min, 1 min 30 s, 2 min) and a clearly increasing trend was observed, in both thickness and water contact angle, with the increasing time (see *figure 5.3*).

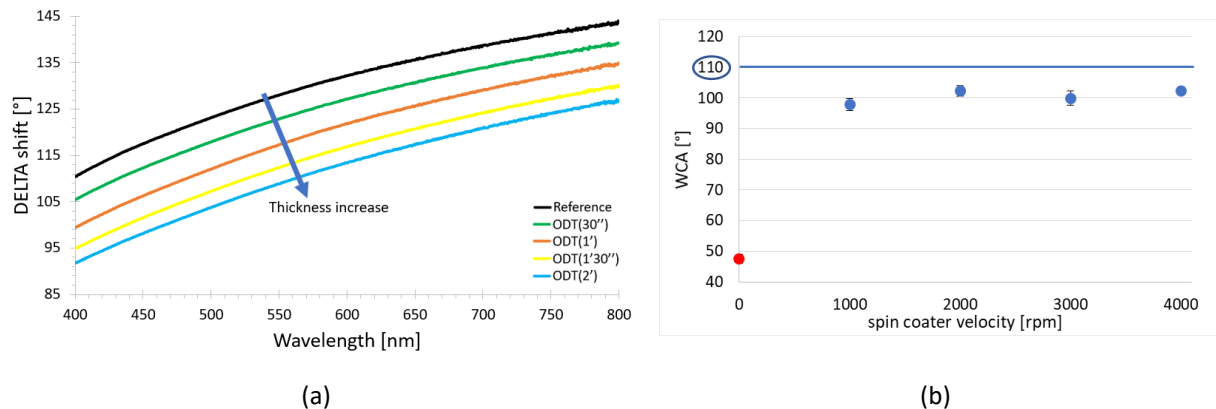


Figure 5.3: experimental results for coupons spun after different contact times of ODT solution.

(a) SE curves; (b) WCA values.

5.1.4 Annealing test

The results of the third experiment were promising and the coupons underwent a quick annealing test (100°C, 10 min) to verify the stability of the deposited ODT; unfortunately, a dramatic decrease in both thickness and water contact angle was observed. This can be explained considering that most probably the ODT was just physically adsorbed on the cobalt, without having established strong chemical interactions.

5.1.5 ODT – rinsing – spinning

Starting from the fourth experiment a rinsing step was introduced in between the wetting and the spinning steps. After having waited for the pre-determined ODT contact time, the coupons were energetically rinsed with pure EtOH to remove the physisorbed chains.

Moreover, it was decided to raise a little bit the contact times, but staying below the threshold of 10 minutes to not make the process too time-expensive, therefore 2 min, 4 min, 6 min and 8 min were used. Not very good results were obtained since both thickness and WCA dropped after the removal of physisorbed ODT (see *figure 5.4*).



Figure 5.4: experimental results, at different ODT solution contact times, for coupons rinsed with EtOH after spinning. (a) thicknesses from SE curves; (b) WCA values.

5.1.6 Pre-treatment_{EtOH} – ODT – rinsing – spinning

In order to help the ODT molecules to chemically interact with the surface, it was thought to deeply clean the samples before pouring the ODT solution, therefore from the fifth experiment onwards a pre-treatment with EtOH was introduced: the coupons were first rinsed with EtOH for 30 seconds, then spun for 60 seconds to make them dry. Slightly better results were obtained (see figure 5.5).

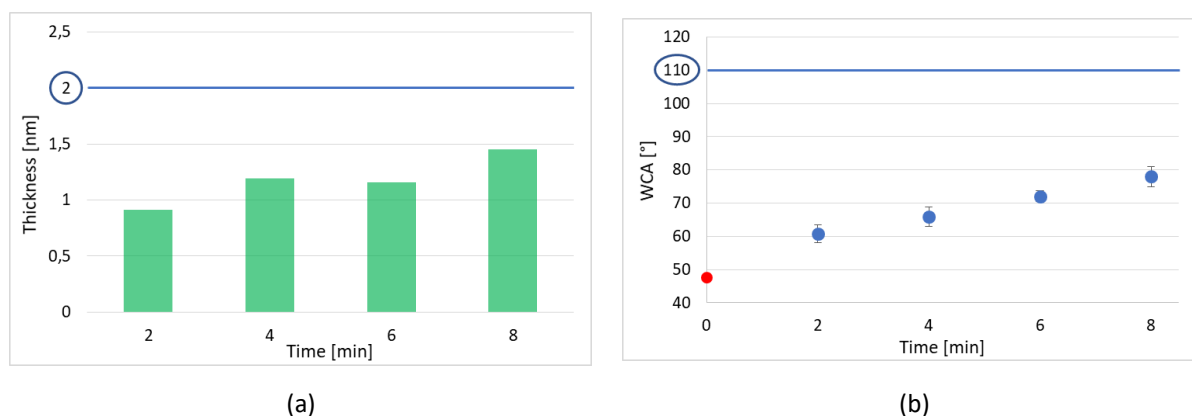


Figure 5.5: experimental results, at different ODT solution contact times, for coupons pre-treated with EtOH and rinsed with EtOH before spinning. (a) thicknesses from SE curves; (b) WCA values.

5.1.7 Pre-treatment_{DMAB} – Pre-treatment_{EtOH} – ODT – rinsing – spinning

Since ODT did not show much chemical affinity towards the cobalt, in the sixth experiment it was decided to add a further pre-treatment to the samples, with the purpose to remove the surface oxide layer (Co_xO_y) whose presence was not taken into account until that moment.

The oxide was reduced via an acidic solution of DMAB, that is dimethylamine borane complex $[(\text{CH}_3)_2\text{NH} \cdot \text{BH}_3]$, provided by *Sigma-Aldrich* with a high purity degree (97%). The acidic solution was prepared by dissolving the compound (in the form of small white crystals) in deionized water (DIW), using a concentration of 0,5 M. The pre-treatment with DMAB consisted of dipping the coupons in the solution of DIW + DMAB for 90 seconds, then rinsing the coupons with DIW and finally spinning them for 60 seconds to let them dry. Compared to the previous cases much better results were obtained, especially at longer times (6 min, 8 min), even if they were still far from the ones to be achieved (see *figure 5.6*).

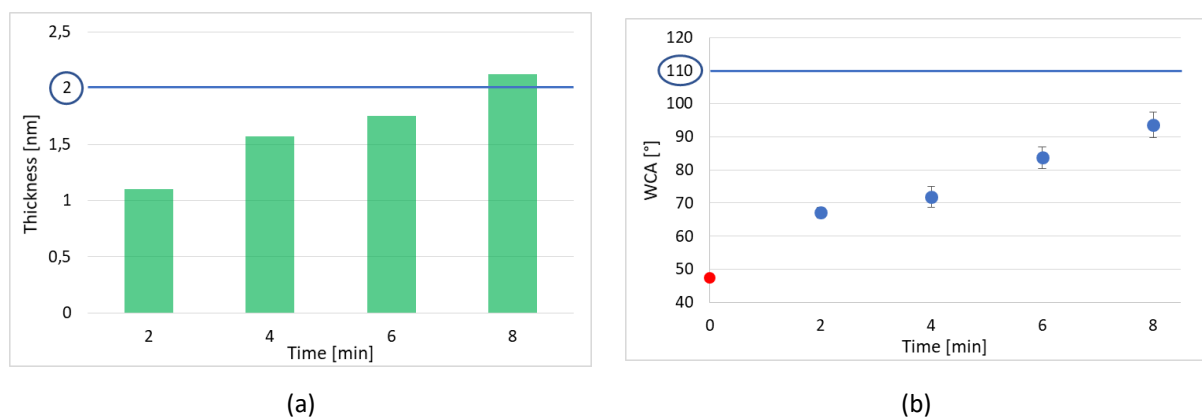


Figure 5.6: experimental results, at different ODT solution contact times, for coupons pre-treated with DMAB solution and EtOH, and rinsed with EtOH before spinning. (a) thicknesses from SE curves; (b) WCA values.

5.1.8 Pre-treatment_{DMAB} – Pre-treatment_{EtOH} – ODT – rinsing – spinning [other attempts]

The sequence adopted in the sixth experiment (pre-treatment with DMAB + pre-treatment with EtOH + ODT solution wetting + rinsing with EtOH + spinning) was repeated many other times but including some variations.

- A more concentrated solution of ODT was employed (0,05 M rather than 0,01 M) but this led to thick layers of physisorbed ODT, even visible to the naked eye (the coupons looked like very blurry).
- The coupons were heated onto a hot metallic plate before the pre-treatments, in order to give to the cobalt some thermal energy, hoping to make it more reactive towards the ODT molecules.
- The ODT solution was poured and spun twice after the pre-treatments.

These other approaches gave quite disappointing results and they were discarded.

5.1.9 Pre-treatment_{DMAB} – Pre-treatment_{EtOH} – ODT [wet annealing] – rinsing – spinning

Since the long series of experiments described above provided unsatisfactory results, a new operating methodology was tried, referred to as “wet annealing”. After the pre-treatments with DMAB and EtOH, the coupons were placed into a Petri dish heated through a hot metallic plate and the solution was poured directly during heating. In this way ODT molecules in solution had much more thermal energy to react with the cobalt. Different temperatures were tested (30°C, 35°C, 40°C, 45°C) and quite good results were obtained, especially at higher temperatures (see the *figures 5.7 and 5.8*).

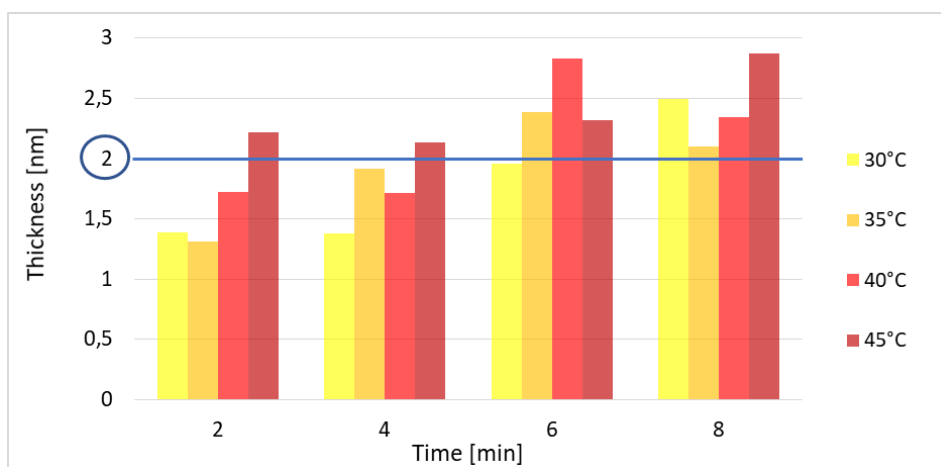


Figure 5.7: thicknesses from SE curves, at different ODT solution contact times, for coupons pre-treated with DMAB solution and EtOH, treated with wet-annealing at different temperatures, and rinsed with EtOH before spinning. The ideal value of thickness to be reached (≈ 2 nm) is marked by a blue line.

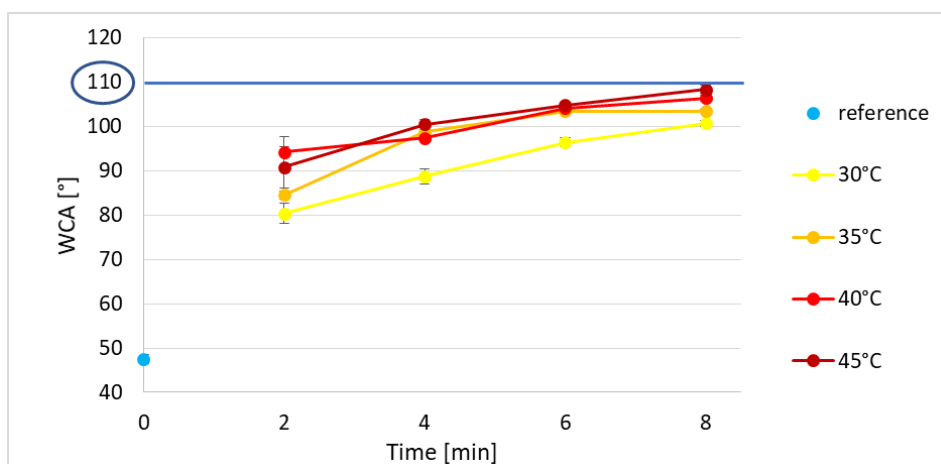


Figure 5.8: WCA values, at different ODT solution contact times, for coupons pre-treated with DMAB solution and EtOH, treated with wet-annealing at different temperatures, and rinsed with EtOH before spinning. The ideal value of WCA to be reached ($\approx 110^\circ$) is marked by a blue line.

Through the wet annealing, samples thickness began to approach (and sometimes exceed) the 2 nm (see *figure 5.7*) whereas the water contact angles started to overcome the value of 100° (see *figure 5.8*). However, the technique had also a drawback: during the heating the solvent⁸ evaporated constantly, especially at 45°C, therefore it was necessary to add droplets of solution to avoid the drying of the coupon. This is the reason why temperatures above 45°C were not explored.

Anyway, relying on SE and WCA, the most promising samples appeared to be the ones treated at higher temperatures (40°C, 45°C) for longer times (6 min, 8 min). Those samples were analyzed with AFM. *Figure 5.9* shows the images acquired.

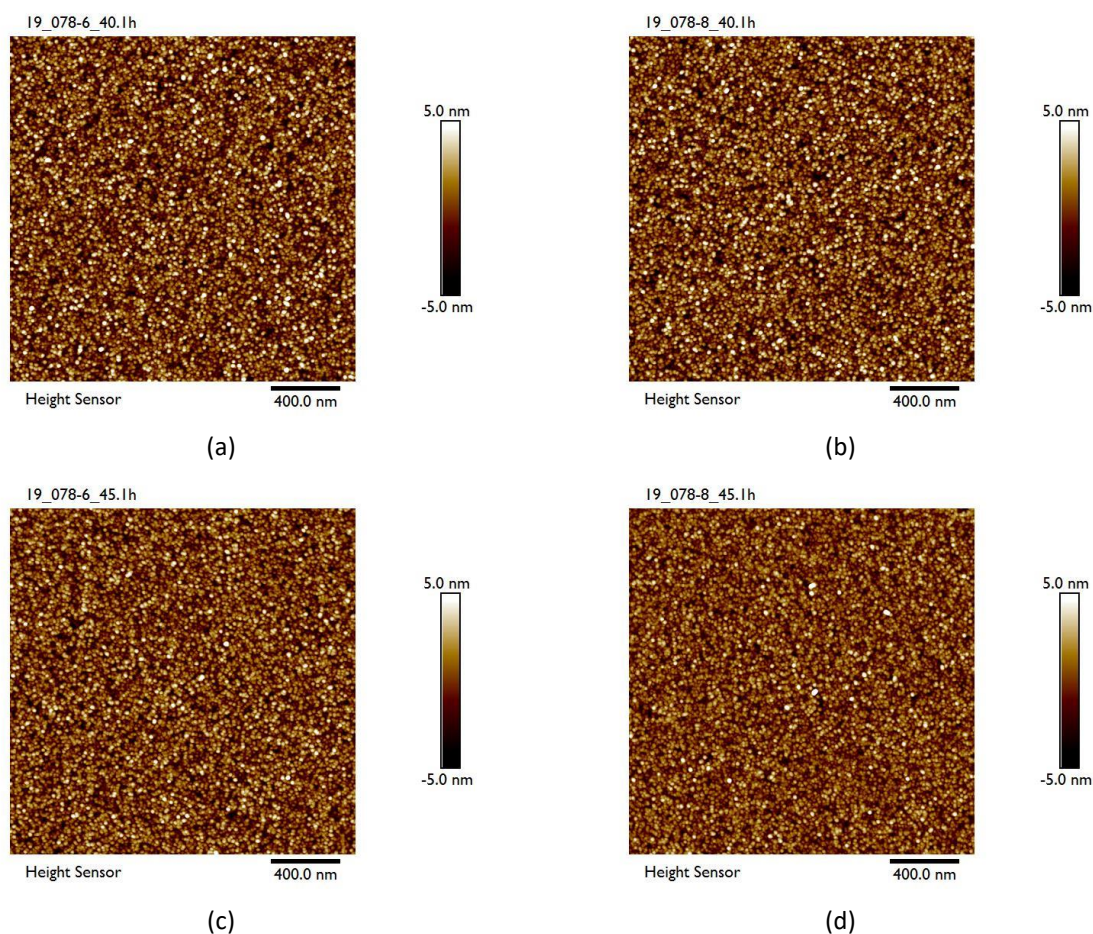


Figure 5.9: AFM images for coupons pre-treated with DMAB solution and EtOH, treated with wet-annealing (at different temperatures and contact times) and rinsed with EtOH before spinning.

(a) Wet-annealing for 6 min at 40°C; (b) wet annealing for 8 min at 40°C; (c) wet annealing for 6 min at 45°C; (d) wet annealing for 8 min at 45°C.

⁸The boiling point of EtOH is 78,2°C [49].

Both the images and the roughness values (presented in *table 5.1*) were consistent with the data available for the bare cobalt. This meant that the ODT layer had covered with conformality the underlying substrate, without forming any islands.

Table 5.1: Roughness values for bare cobalt and 4 coupons pre-treated with DMAB solution and EtOH, treated with wet-annealing (at different temperatures and contact times) and rinsed with EtOH before spinning.

Sample	R_q	R_a
Pure Cobalt	1,07	0,89
ODT wet annealing [40°C, 6 min]	1,80	1,43
ODT wet annealing [40°C, 8 min]	1,76	1,39
ODT wet annealing [45°C, 6 min]	1,66	1,32
ODT wet annealing [45°C, 8 min]	1,32	1,36

The samples were further examined with the CV. As it can be seen from the voltammograms shown in *figure 5.10*, the ODT prevented only marginally the current flow through the metal, meaning that the passivation did not occur properly. This can be explained admitting that the ODT did assemble on cobalt in a conformal monolayer, but not in a dense and well-packed array, such as testified by the extrapolated coverage values presented in *figure 5.11*.

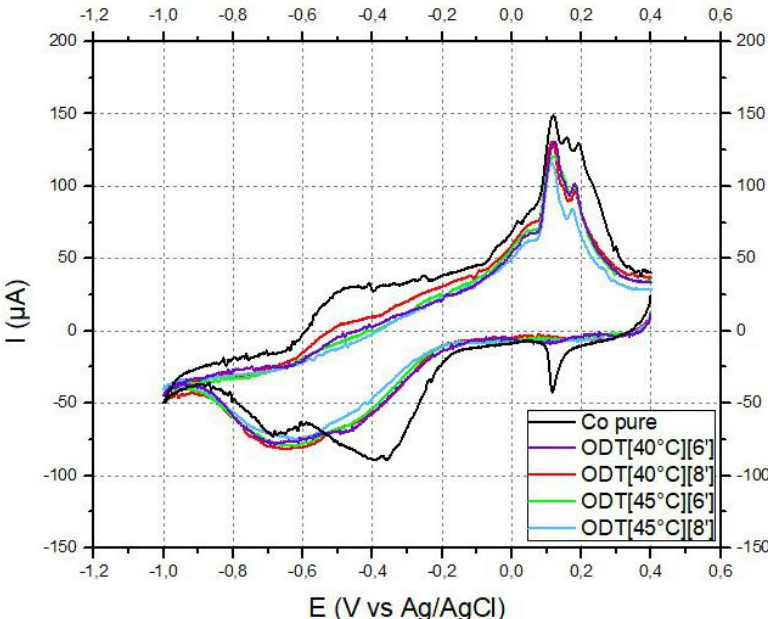


Figure 5.10: CV voltammograms for bare cobalt and 4 coupons pre-treated with DMAB solution and EtOH, treated with wet-annealing (at different temperatures and contact times) and rinsed with EtOH before spinning.

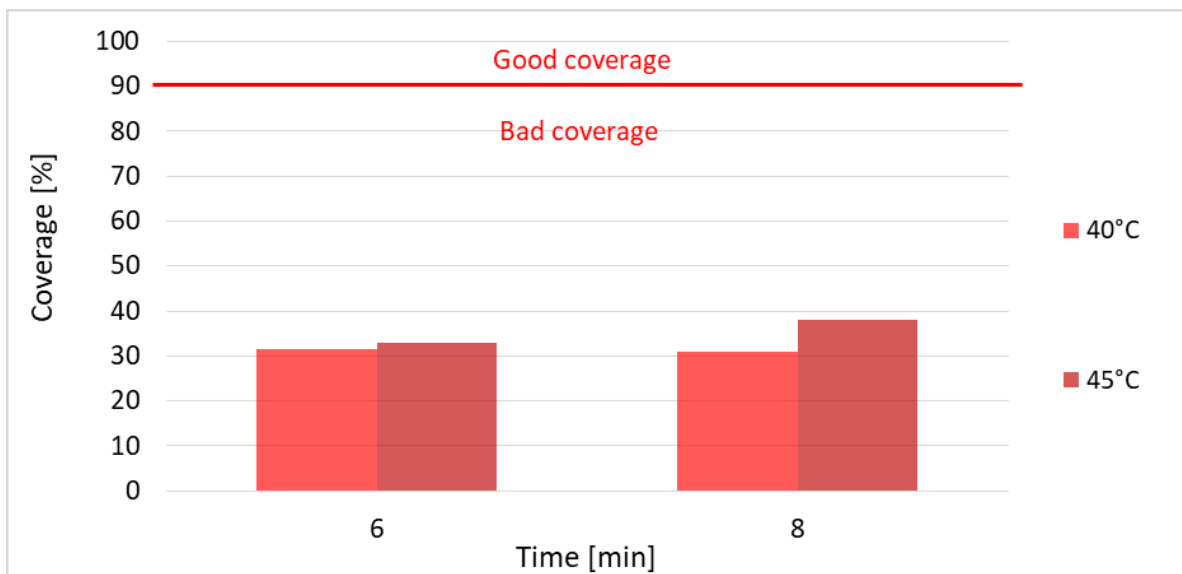


Figure 5.11: percentage coverage values, extrapolated from CV voltammograms, for 4 coupons pre-treated with DMAB solution and EtOH, treated with wet-annealing (at different temperatures and contact times) and rinsed with EtOH before spinning. The limit between good and bad coverage is marked by a red line.

5.2 POST SPIN COATING

5.2.1 Thermal study on the best Co sample

Although the good passivation of the cobalt with the SAM was actually not achieved, it was decided to study anyway the thermal stability of the monolayer. Among the best samples, it was chosen the one wet-annealed at 40°C for 6 minutes. This choice was dictated by a matter of convenience. At 45°C the ethanol evaporated too quickly and a constant action of adding solution was needed. As regards the amount of minutes, it is obvious that, under the same results, the less time-consuming process was preferred.

Summing up what stated above and in the previous paragraph, the thermal stability was investigated only for the coupon subjected to the following treatment:

- pre-treatment of DMAB = DMAB wetting (90 s) + rinsing with DIW + spinning (60 s, 3000 rpm);
- pre-treatment with EtOH = EtOH rinsing (30 s) + spinning (60 s, 3000 rpm);
- wet annealing = ODT solution wetting (300 s) at 40°C;
- rinsing with EtOH;
- spinning (60 s, 3000 rpm).

Six copies of the sample were heated up to 100°C, 125°C, 150°C, 200°C, 250°C and 300°C.

SE, WCA and CV measurements were performed before and after the annealing on each sample. *Figure 5.12* presents the variations of both thickness (calculated from the SE curves) and WCA. Looking at the plots it was possible to identify the safe temperature window for the ODT on cobalt, i.e. the temperature range where it does not undergo degradation or desorption. The ODT turned out to be stable more or less until 150°C.



Figure 5.12: experimental results of thermal study, carried on at 6 different temperatures, for a Co coupon pre-treated with DMAB solution and EtOH, treated with wet-annealing (at 40°C, for 6 minutes) and rinsed with EtOH before spinning. (a) Thickness loss from SE curves; (b) WCA decrease.

Figure 5.13, instead, shows the voltammograms resulting from CV and the extrapolated values of coverage. The data confirmed the stability of the SAM up to 150°C.

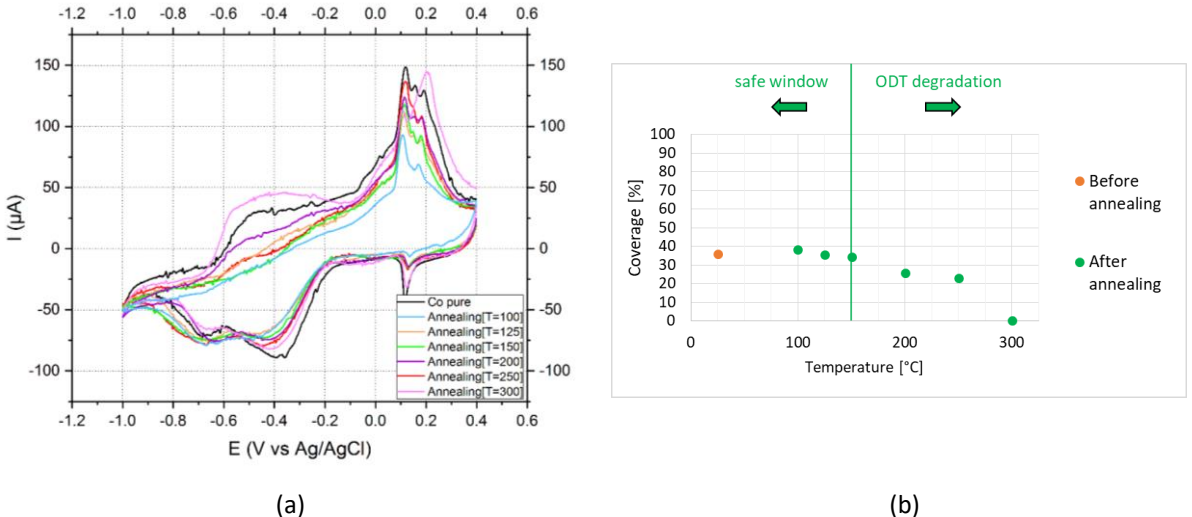


Figure 5.13: CV results of thermal study, carried on at 6 different temperatures, for a Co coupon pre-treated with DMAB solution and EtOH, treated with wet-annealing (at 40°C, for 6 minutes) and rinsed with EtOH before spinning. (a) Voltammograms; (b) coverage values extrapolated from CV.

5.2.2 ALD on the best Co sample

Once verified the thermal stability of the ODT, it was decided to perform the ALD despite the negative results concerning the percentage coverage provided by the CV. Two temperatures (in accordance with the safety thermal window) were tested, 120°C and 150°C, with four different numbers of cycles per each, namely 10, 20, 30 and 40.

SE measurements performed before and after the ALD allowed to evaluate the variation in thickness experienced by the coupons. The greater the increase in thickness, the greater the amount of hafnium nitride deposited.

The plots showing the thickness change of the samples versus the number of cycle are portrayed in *figures 5.14* and *5.15*. Recalling the *paragraph 4.1.7*, each deposition involved 4 coupons: pure cobalt, cobalt + ODT, pure silicon dioxide, silicon dioxide + ODT.

Both at 120°C and 150°C a linear growth (versus number of cycles) was observed for the “SiO₂” and “SiO₂ + ODT” samples, with no thickness differences in between them (as it had to be). Unfortunately, almost no differences as well were found between the “Co” and “Co + ODT” samples. It was only noticed that the thickness increase of the “Co + ODT” was, per each number of cycles, slightly smaller than the one experienced by the pure Co. This was maybe due to a larger nucleation delay, probably induced by the ODT. However, the passivation of the metal was clearly ineffective, this is the reason why no further analyses were done on the samples.

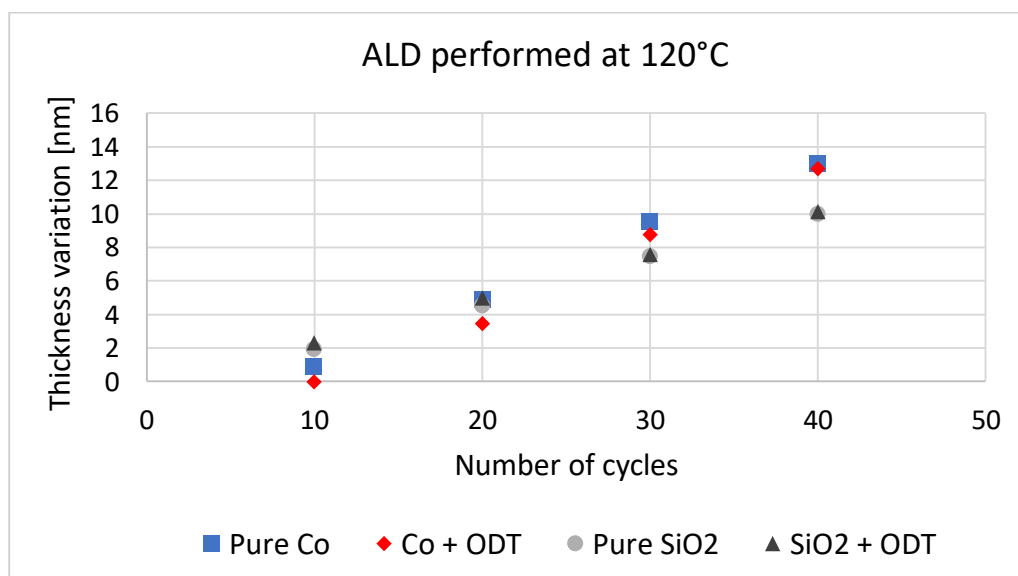


Figure 5.14: plot of thickness change experienced by 4 different coupons (pure cobalt, cobalt + ODT, pure silicon dioxide, silicon dioxide + ODT) versus number of cycles of Hf_xN_y ALD performed at 120°C.

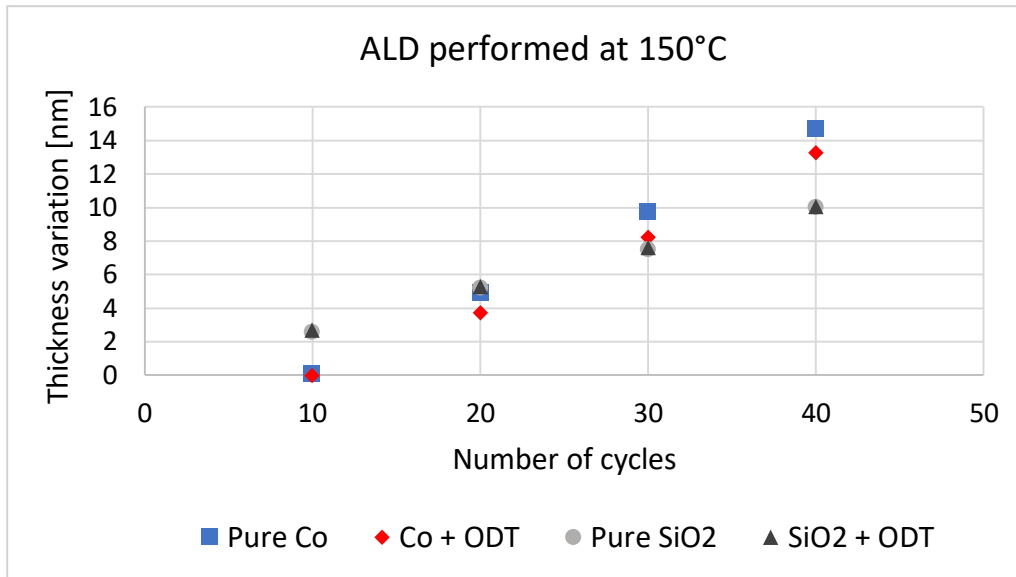


Figure 5.15: plot of thickness change experienced by 4 different coupons (pure cobalt, cobalt + ODT, pure silicon dioxide, silicon dioxide + ODT) versus number of cycles of Hf_xN_y ALD performed at 150°C.

CHAPTER 6. COPPER: RESULTS AND DISCUSSION

6.1 SPIN COATING

The same specifications done at the beginning of *chapter 5* still hold:

- the concentration used for the ODT solution was 0,01 M;
- the target value for the thickness was ≈ 2 nm;
- the target value for the WCA was $\approx 110^\circ$;
- WCA plots display error bars;
- WCA plots display the contact angle on bare Cu, indicated with a red spot ($\approx 52,8^\circ$).

6.1.1 Pre-treatment_{EtOH} – ODT – rinsing – spinning

Basing on the previous experience with the cobalt, the first experiment with the copper already included a pre-treatment with EtOH (for cleaning the samples surface) and a rinsing step before spinning (to avoid useless islands of physisorbed molecules). As usual the solution was poured on the coupons, and different ODT solution contact times were tried (30 s, 1 min, 2 min, 4 min). The results provided by SE and WCA (presented in *figure 6.1*) showed thicknesses much higher than 2 nm (approaching almost 14 nm), and contact angles bigger than 110° . Besides, they did not seem much related with the increasing contact time.

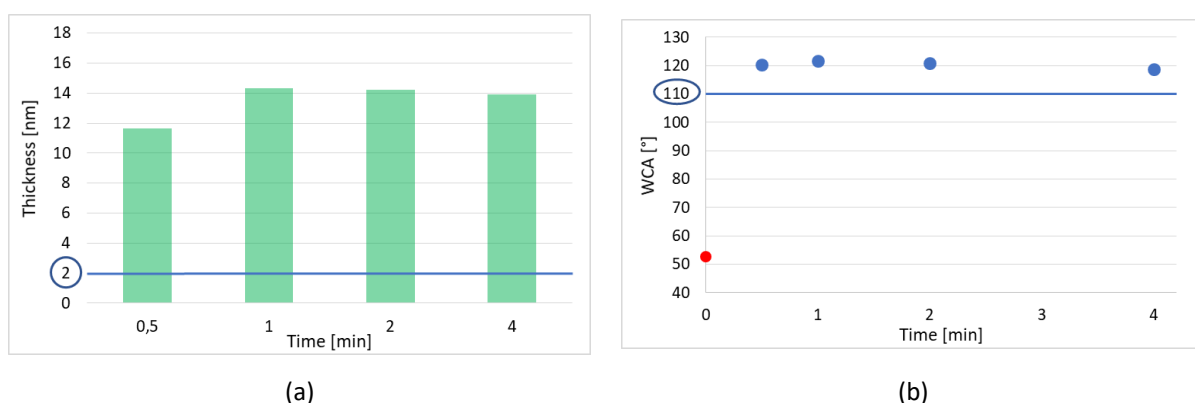


Figure 6.1: experimental results, at different ODT solution contact times, for coupons pre-treated with EtOH and rinsed with EtOH before spinning. (a) thicknesses from SE curves; (b) WCA values.

The idea of an ODT monolayer on copper was obviously discarded since those results could be explained only by contemplating the formation of a multilayer.

On one hand, the presence of a multilayer assures a very good coverage of the underlying substrate or, in other words, an excellent passivation. On the other hand, it poses a problem in view of an ALD process, because the molecules of the upper layers could detach due to the high temperature, and eventually end up on the growth-areas, slowing down the deposition.

The excellent passivation of the copper was supported by the voltammograms of the CV, displayed in the *figure 6.2* together with the extrapolated values of percentage coverage. The curves belonging to the ODT-treated coupons were completely flat, meaning no current flow through the samples. Consequently, the coverage resulted to be over 99,99%.

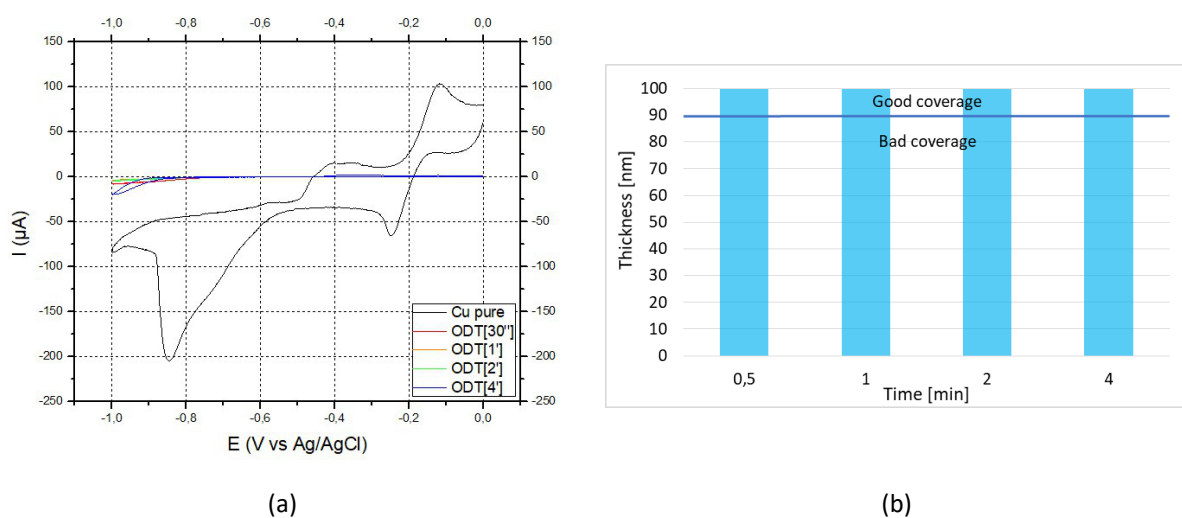


Figure 6.2: CV results, at different ODT solution contact times, for coupons pre-treated with EtOH and rinsed with EtOH before spinning. (a) Voltammograms; (b) coverage values extrapolated from CV.

6.1.2 Pre-treatment_{EtOH} – ODT [wet annealing] – rinsing – spinning

In order to accomplish a specular study with respect to the one made for the cobalt, the second experiment on the copper involved the procedure of wet annealing, performed at 40°C. The results, presented in the *figure 6.3*, suggested that an even thicker multilayer had formed, bringing evidence about the positive role of the heat during the self-assembling mechanism.

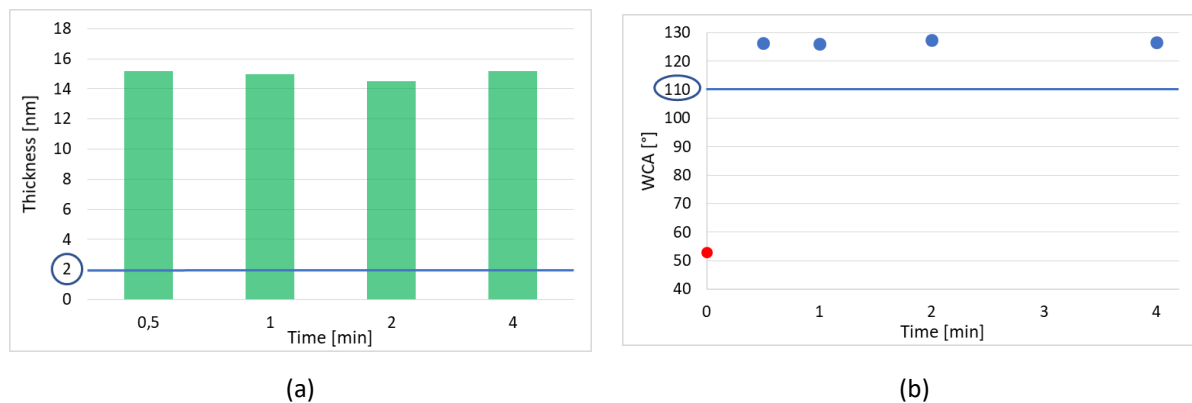


Figure 6.3: experimental results, at different ODT solution contact times, for coupons pre-treated with EtOH, treated with wet-annealing (at 40°C) and rinsed with EtOH before spinning. (a) thicknesses from SE curves; (b) WCA values.

6.1.3 Pre-treatment_{EtOH} – ODT – rinsing – spinning – annealing

The third experiment was basically a repetition of the first one, but with the implementation of an additional step: after the spinning, the samples were annealed in the heatpulse at 140°C for 15 minutes. Two things were observed: a slight decrease in thickness and the approach of the WCA to the ideal value of 110°C, as shown in the *figure 6.4*.

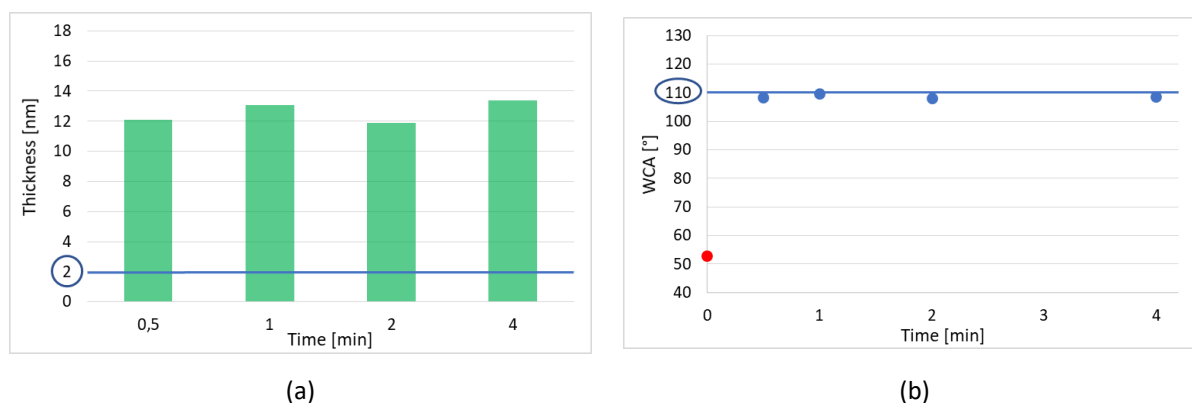


Figure 6.4: experimental results, at different ODT solution contact times, for coupons pre-treated with EtOH, rinsed with EtOH before spinning and annealed after spinning. (a) thicknesses from SE curves; (b) WCA values.

Most probably the thermal energy supplied by the annealing provoked the evaporation of the ODT molecules either physisorbed or mechanically stuck on the upper layer. This fact involved a smoothing of the multilayer, as testified by the data acquired with the AFM, through which a decrease in roughness was recorded (see *figure 6.5*).

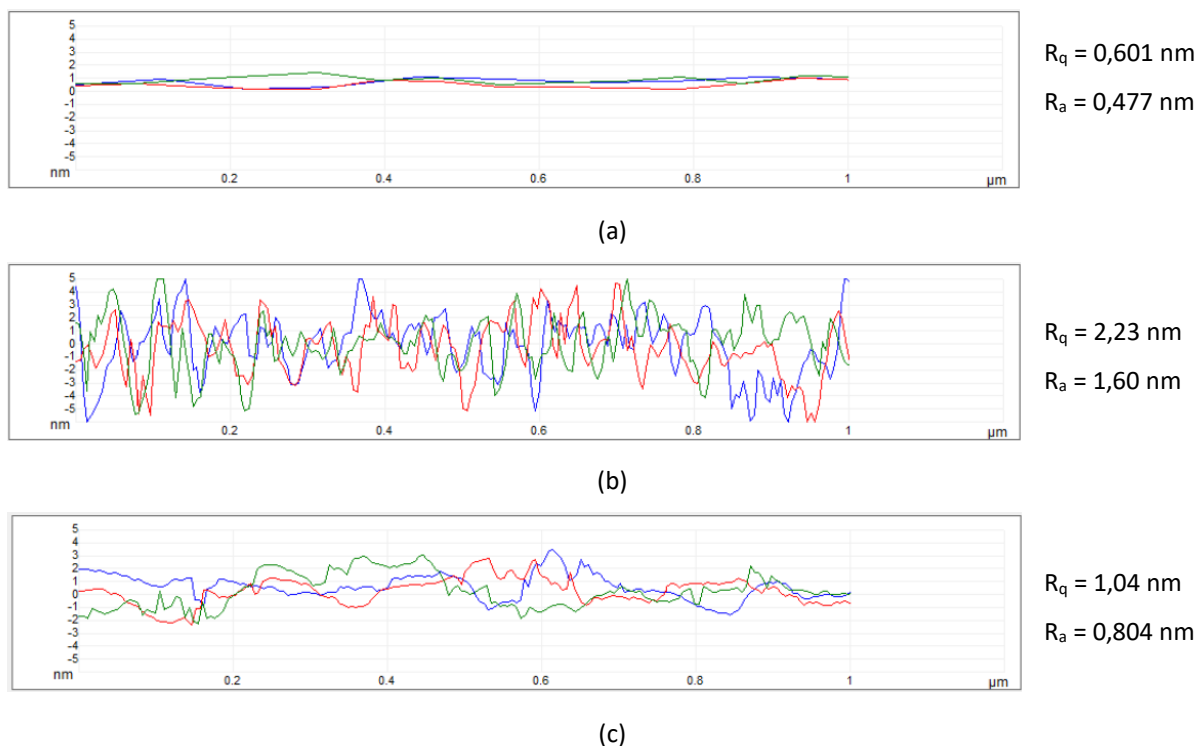


Figure 6.5: roughness profiles with related parameters of three distinct sections of a blanket copper coupon and an ODT-treated copper coupon before and after the annealing.
 (a) Pure Cu; (b) Cu + ODT before the annealing; (c) Cu + ODT after the annealing.

As regards the CV, no differences were found in the percentage coverage after the annealing, such as shown in figure 6.6.

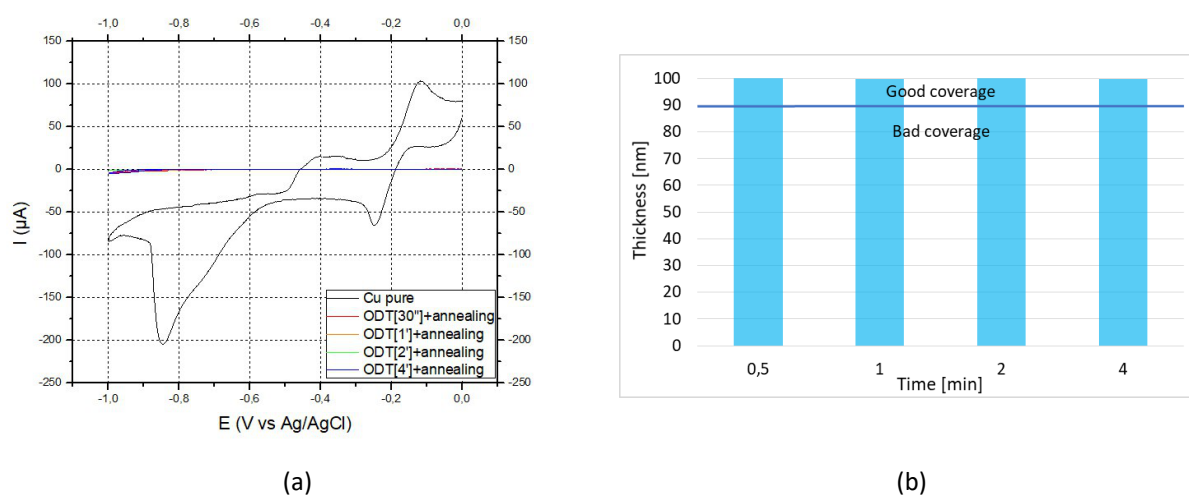


Figure 6.6: CV results, at different ODT solution contact times, for coupons pre-treated with EtOH, rinsed with EtOH before spinning and annealed after spinning.
 (a) Voltammograms; (b) coverage values extrapolated from CV.

6.2 POST SPIN COATING

6.2.1 Thermal study on the best Cu sample

Among the copper samples, it was chosen to investigate the thermal stability only for the coupon subjected to the following treatment:

- Pre-treatment with EtOH = EtOH rinsing (30 s) + spinning (60 s, 3000 rpm);
- ODT solution wetting (60 s) at T_{room} ;
- rinsing with EtOH;
- spinning (60 s, 3000 rpm);
- annealing (15 min, 140°C).

The choice was dictated by practical reasons: 1 minute was definitively not time-consuming; adopting a temperature higher than T_{room} would not have brought real benefits; the annealing post spinning had proved to be effective for the quality of the multilayer. Five copies of the sample were heated up to 100°C, 150°C, 200°C, 250°C and 300°C.

SE, WCA and CV measurements were performed before and after the annealing on each sample. *Figure 6.7* presents the variations of both thickness (calculated from the SE curves) and WCA. Looking at the plots it was possible to identify the safe temperature window for the ODT on copper. As in the case of cobalt, the ODT turned out to be stable until 150°C. This was confirmed by CV, whose results are shown in *figure 6.8*.

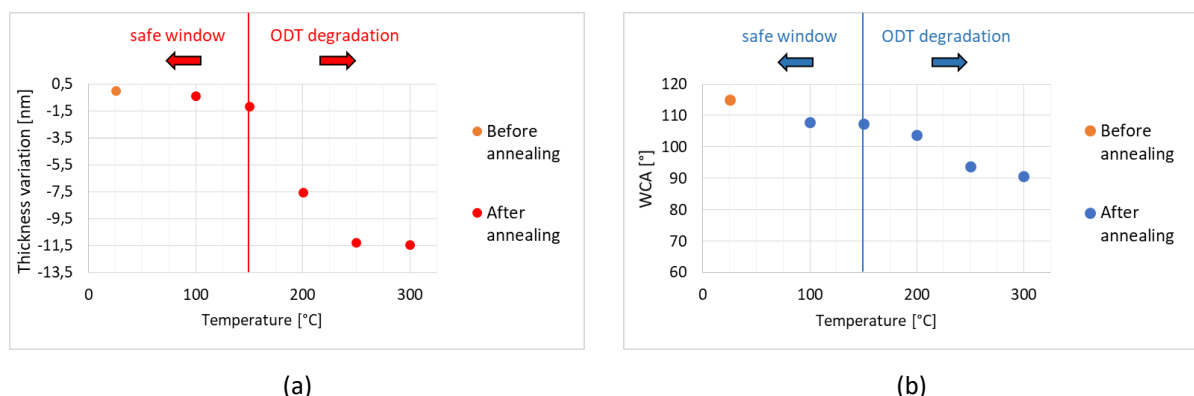


Figure 6.7: experimental results of thermal study, carried on at 5 different temperatures, for a Cu coupon pre-treated with EtOH, treated with ODT solution (at 25°C, for 1 minute), rinsed with EtOH before spinning and annealed after spinning. (a) Thickness loss from SE curves; (b) WCA decrease.

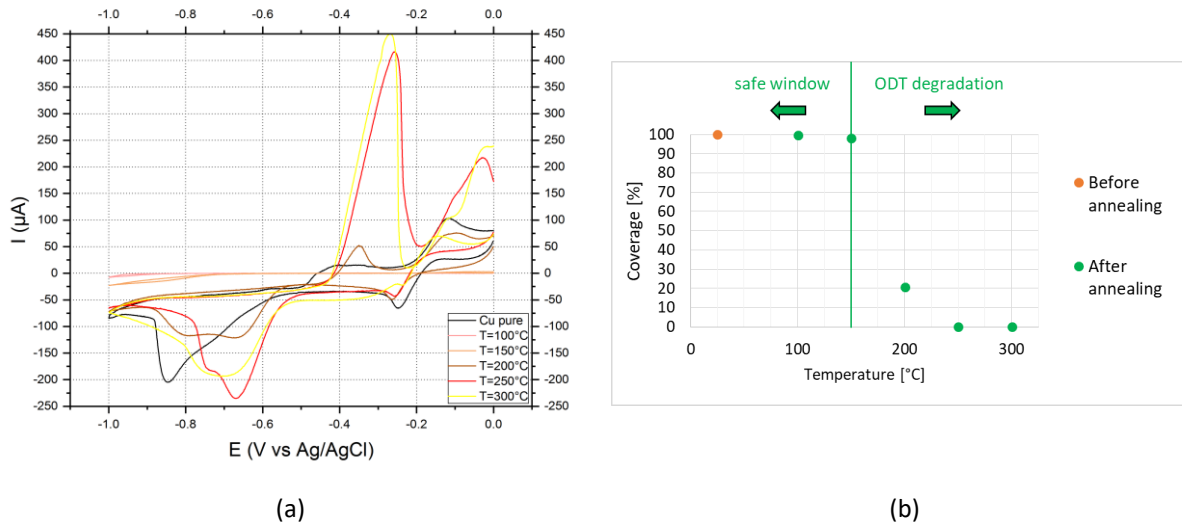


Figure 6.8: CV results of thermal study, carried on at 5 different temperatures, for a Cu coupon pre-treated with EtOH, treated with ODT solution (at 25°C, for 1 minute), rinsed with EtOH before spinning and annealed after spinning. (a) Voltammograms; (b) coverage values extrapolated from CV.

6.2.2 ALD on the best Cu sample

As in the cobalt case, two temperatures (in accordance with the safety thermal window) were tested, 120°C and 150°C, with four different numbers of cycles per each, namely 10, 20, 30 and 40. SE measurements performed before and after the ALD allowed to evaluate the variation in thickness experienced by the coupons. The plots showing the thickness change of the samples versus the number of cycle are portrayed in figures 6.9 and 6.10.

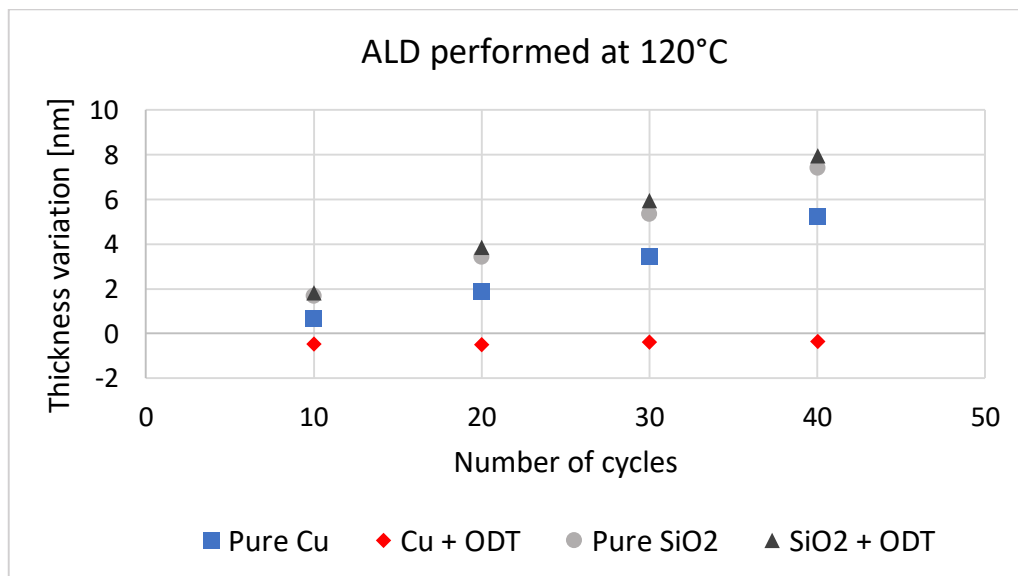


Figure 6.9: plot of thickness change experienced by 4 different coupons (pure copper, copper + ODT, pure silicon dioxide, silicon dioxide + ODT) versus number of cycles of Hf_xN_y ALD performed at 120°C.

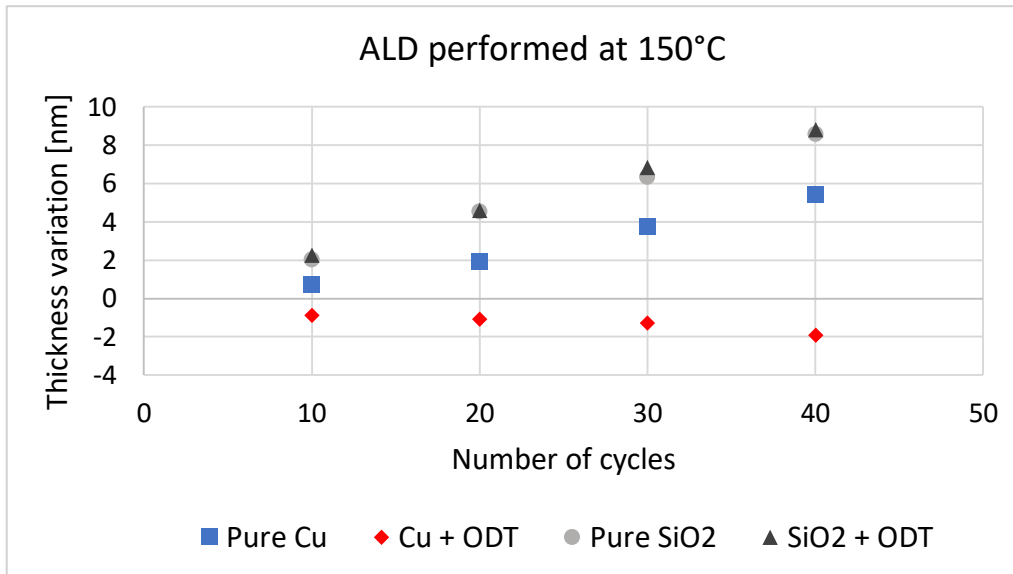


Figure 6.10: plot of thickness change experienced by 4 different coupons (pure copper, copper + ODT, pure silicon dioxide, silicon dioxide + ODT) versus number of cycles of Hf_xN_y ALD performed at 150°C.

Recalling the *paragraph 4.1.7*, each deposition involved 4 coupons: pure copper, copper + ODT, pure silicon dioxide, silicon dioxide + ODT. As it can be seen from the plots, both the silicon dioxide coupons and the pure copper ones were interested by a linear increase in thickness with the increasing number of cycle. Once again, no differences were recorded between the “SiO₂” and “SiO₂ + ODT” samples, as it had to be. However, the most interesting data were the ones about the passivated copper, which clearly underwent a decrease in thickness. The non-increase could be explained only admitting that the deposition of hafnium nitride was successfully prevented. The reduction in thickness (slightly more accentuated at 150°C rather than 120°C), instead, was certainly due to the loss of ODT from the upper levels of the multilayer, probably due to the beginning of desorption phenomena caused by the high temperatures used in the Savannah reactor. Since the process had given the desired results, pure “SiO₂” and “Cu + ODT” samples were more deeply investigated with the RBS technique in order to evaluate the exact amount of hafnium. This was necessary not only to estimate the selectivity, but also to exclude the possibility that the thickness decrease (on passivated copper) was the result of two opposite effects, namely the desorption of the ODT and the deposition of Hf_xN_y . RBS results are presented in *figures 6.11 and 6.12*.

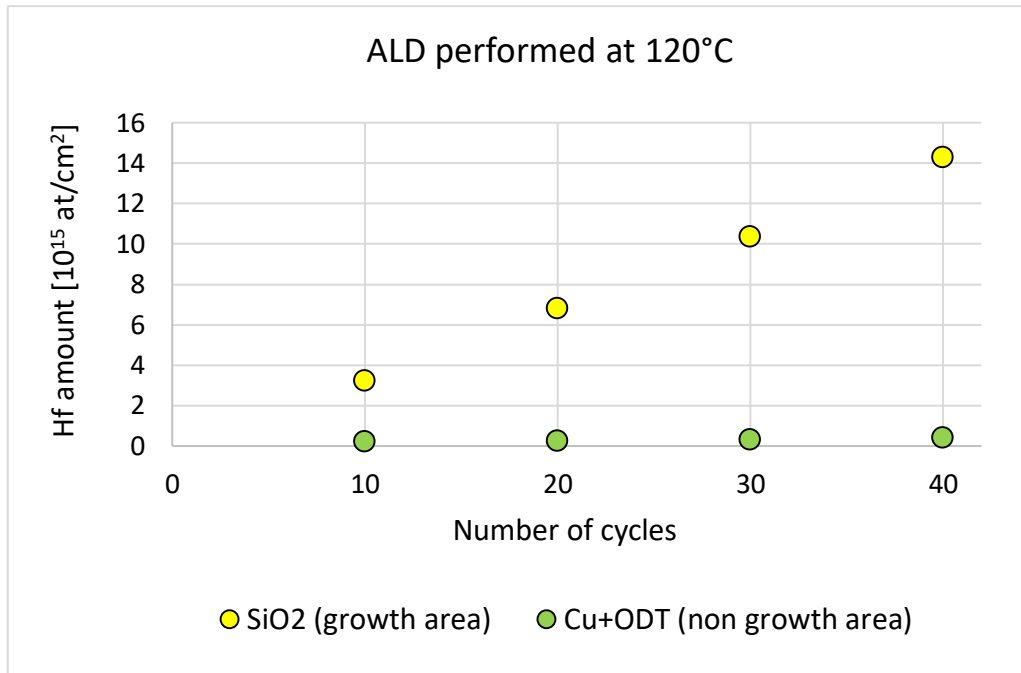


Figure 6.11: plot of Hf amount (calculated by RBS technique) on growth and non-growth areas versus number of cycles of Hf_xN_y ALD performed at 120°C.

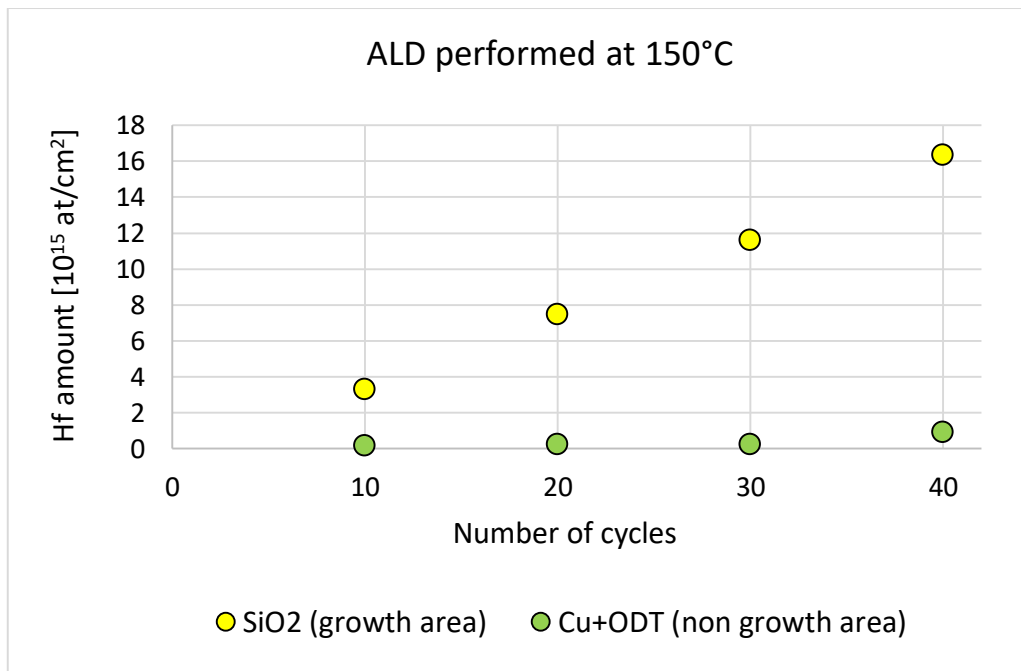


Figure 6.12: plot of Hf amount (calculated by RBS technique) on growth and non-growth areas versus number of cycles of Hf_xN_y ALD performed at 150°C.

Knowing the amounts of material present after the deposition on growth and non-growth areas thanks to the RBS analysis, it was possible to apply the *equation 2.2* in order to

calculate the selectivity for each of the 8 atomic layer depositions performed. The selectivity values in this way obtained are displayed in the *table 6.1*:

Table 6.1: selectivity values for the 8 different ALD performed.

Nos. of cycle	T = 120°C	T = 150°C
10	90,4%	88,4%
20	94,4%	93,4%
30	96,0%	94,1%
40	89,8%	94,4%

In conclusion the selectivity was, on average, greater than 90%. This result can be considered without any doubt a very encouraging success, even if there is still a long way to go for achieving a truly area-selective ALD by the employment of ODT deposited by spin coating. Moreover, other depositions should be done to verify if the desorption of ODT molecules from passivated copper (non-growth area) hinders in some ways the Hf_xN_y growth on SiO_2 (growth areas), slowing down the GPC.

CONCLUSIONS

The aim of this thesis was to successfully passivate cobalt (Co) and copper (Cu) surfaces with a self-assembled monolayer, namely octadecanethiol (ODT), in order to create a barrier layer able to block the atomic layer deposition (ALD) of hafnium nitride (Hf_xN_y). In this way the process would have occurred on silicon dioxide (SiO_2) but not on Co/Cu, thus becoming area-selective.

The ODT was deposited on the metals by spin coating, a methodology different from the ones traditionally employed. Many experimental pathways were tried to make the ODT react with the cobalt, but few progresses were obtained. Eventually a monolayer did form, but it was not dense enough to effectively prevent the ALD.

The ODT successfully attached to the copper because of an extraordinary chemical affinity, even if it was not possible to avoid the formation of multiple layers. The blocking ability of the ODT multilayer over the Cu was tested, and the results were quite positive. In particular, selectivity values higher than 90% were achieved.

Moreover, the thermal stability of ODT on both metals was investigated, finding out that it resists until 150°C , after which it undergoes desorption independently from the underlying substrate (Co/Cu).

REFERENCES

- [1] Brock D.C., 2006, *Understanding Moore's law: four decades of innovation*, Chemical Heritage Press, Philadelphia, Pennsylvania.
- [2] Baker R.J., 2010, *CMOS: Circuit design, Layout and Simulation*, Wiley-IEEE Press, Piscataway, New Jersey.
- [3] Zhao L., 2017, *All about interconnects*, Semiconductor Engineering, <https://semiengineering.com/all-about-interconnects/>.
- [4] Courtesy of Imec Academy, IMEC, <https://www.imec-int.com/en/home>.
- [5] Lapedus M., 2016, *Interconnects challenges rinsing*, Semiconductor Engineering, <https://semiengineering.com/interconnect-challenges-grow-3/>.
- [6] Loke A., 1999, *Scaling of interconnects*, PhD Thesis, Stanford University, Stanford, California.
- [7] Gall D., 2016, Electron mean free path in elemental metals, *Journal of applied physics* **119**, 1-5. [<http://dx.doi.org/10.1063/1.4942216>]
- [8] Zhang W., Brongersma S.H., Richard O., Brijs B., Palmans R. *et al.*, 2004, Influence of Electron Mean Free Path on the Resistivity of Thin Metal Films, *Microelectronic Engineering* **76(1-4)**, 146-152.
- [9] Hu C.K., Kelly J., Chen H.C., Huang H., Ostrovski Y. *et al.*, Electromigration and resistivity in on-chip Cu, Co and Ru damascene nanowires, *2017 IEEE International Interconnect Technology Conference (IITC)*, Hsinchu, Taiwan, 16-18 May 2017. [DOI: [10.1109/IITC-AMC.2017.7968977](https://doi.org/10.1109/IITC-AMC.2017.7968977)]
- [10] Kimura Y., Saka M., 2019, Prediction of Electromigration Critical Current Density in Passivated Arbitrary Configuration Interconnect, *Journal of Electronic Packaging* **141(2)**, 1-7. [DOI: [10.1115/1.4042980](https://doi.org/10.1115/1.4042980)]
- [11] Bekiaris N., Wu Z., Ren H., Naik M., Park J.H. *et al.*, Cobalt fill for advanced interconnects, *2017 IEEE International Interconnect Technology Conference (IITC)*, Hsinchu, Taiwan, 16-18 May 2017. [DOI: [10.1109/IITC-AMC.2017.7968981](https://doi.org/10.1109/IITC-AMC.2017.7968981)]
- [12] Schor D., IEDM 2017 plus ISSCC 2018: Interl's 10nm, switching to cobalt interconnects, *IEEE International Electronic Devices Meeting*, San Francisco, California, 17 Feb 2018.
- [13] Zhang L., Kraatz M., Aubel O., Hennesthal C., Zschech E. *et al.*, 2010, Grain Size And Cap Layer Effects On Electromigration Reliability Of Cu Interconnects: Experiments And Simulation, *Stress induced phenomena in metallization: 11th International Workshop* **1300**, 3-7. [DOI: [10.1063/1.3527136](https://doi.org/10.1063/1.3527136)]
- [14] Mackus A.J.M., Merckx M.J.M., Kessels W.M.M., 2019, From the Bottom-Up: Toward Area-Selective Atomic Layer Deposition with High Selectivity, *Chem. Mat.* **31**, 2-12.

- [15] Cheng Y.L., Lee C.Y., Huang Y.L., 2018, Copper Metals for Semiconductor Interconnects in *Noble and Precious Metals – Properties, Nanoscale Effect and Applications*, chapter 10, edited by Mohindar Seehra, IntechOpen. [ISBN: [978-1-78923-293-6](#)]
- [16] Kim J., Kim T.W., 2009, Initial Surface Reactions of Atomic Layer Deposition, *JOM* **61**, 17-22.
- [17] Zyulkov I., Krishtab M., De Gendt S., Armini S., 2017, Selective Ru-ALD as a Catalyst for Sub-Seven-Nanometer Bottom-Up Metal Interconnects, *ACS Appl. Mater. Interfaces* **9**, 31031-31041.
- [18] Gregorczyk K., Knez M., 2016, Hybrid nanomaterials through molecular and atomic layer deposition: Top down, bottom up, and in-between approaches to new materials, *Progress in Surface Science* **75**, 1-37.
- [19] Puurunen R.L., 2014, A Short History of Atomic Layer Deposition: Tuomo Suntola's Atomic Layer Epitaxy, *Chem. Vap. Dep.* **20**, 332-344.
- [20] Johnson R.W., Hultqvist A., Bent S.F., 2014, A brief review of atomic layer deposition: from fundamentals to applications, *Materials Today* **17(5)**, 236-246.
- [21] George S.M., 2009, Atomic Layer Deposition: An Overview, *Chem. Rev.* **110(1)**, 111-131.
- [22] Fei C., Liu H., Wang X., Fan X., 2015, The influence of process parameters and pulse ratio of precursors on the characteristics of La_{1-x}Al_xO₃ films deposited by atomic layer deposition, *Nanoscale Res. Lett.* **10**, 180-186. [DOI: [10.1186/s11671-015-0883-6](#)]
- [23] Puurunen R.L., Vandervorst W., 2004, Island growth as a growth mode in atomic layer deposition: A phenomenological model, *J. Appl. Phys.* **96**.
- [24] Leskelä M., Ritala M., 2002, Atomic layer deposition (ALD): from precursors to thin film structures, *Thin solid films* **409**, 138-146.
- [25] Wilson C.A., Grubbs R.K., George S.M., 2005, Nucleation and Growth during Al₂O₃ Atomic Layer Deposition on Polymers, *Chem. Mater.* **17**, 5626-5634.
- [26] Matero R., 2004, Atomic Layer Deposition of Oxide Films Growth, Characterisation and Reaction Mechanism Studies, Academic dissertation, University of Helsinki, Helsinki, Finland.
- [27] Wojtecki R., Mettry M., Nathel N.F., Friz A., De Silva A. *et al.*, 2018, 15nm Resolved Patterns in Selective Area Atomic Layer Deposition – Defectivity Reduction by Monolayer Design, *ACS Appl. Mater. Interfaces* **10(44)**, 38630-38637.
- [28] Xu Y., Yan X., 2010, Thermodynamics and Kinetics of Chemical Vapour Deposition in *Chemical Vapour Deposition. Engineering Materials and Processes*, Chap. 4, Springer, London, United Kingdom.
- [29] Bobb-Semple D., Nardi K.L., Draeger N., Hausmann D.M., Bent S.F., 2019, Area-Selective Atomic Layer Deposition Assisted by Self-Assembled Monolayers: A comparison of Cu, Co, W, and Ru, *Chem. Mater.* **31(5)**, 1635-1645.

- [30] Schubert U., Hüsing N., 2000, *Synthesis of Inorganic Materials*, Wiley-VHC Verlag GmbH & Co. KGaA,, Weinheim, Germany.
- [31] Hashemi F.S.M., Prasittichai C., Bent S.F., 2015, Self-Correcting Process For High Quality Patterning By Atomic Layer Deposition, *ACS Nano* **9(9)**, 8710-8717. [DOI: [10.1021/acsnano.5b03125](https://doi.org/10.1021/acsnano.5b03125)]
- [32] Ulman A., 1996, Formation and Structure of Self-Assembled Monolayers, *Chem Rev.* **96**, 1533-1554.
- [33] Schwartz D.K., 2001, Mechanisms and Kinetics of Self-Assembled Monolayer Formation, 2001, *Annu. Rev. Phys. Chem.* **52**, 107-137.
- [34] Schreiber F., 2000, Structure and growth of self-assembling Monolayers, *Progress in Surface Science* **65**, 151-256.
- [35] Love J.C., Estroff L.A., Kriebel J.K., Nuzzo R.G., Whitesides G.M., 2005, Self-Assembled Monolayers of Thiolates on Metals as a Form of Nanotechnology, *Chem. Rev.* **105**, 1103-1169.
- [36] Chaki N.K., Aslam M., Sharma J., VijayaMohanan K., 2001, Applications of self-assembled monolayers in materials chemistry, *Proc. Indian Acad. Sci. (Chem. Sci.)* **113**, 659-670.
- [37] Färm E., Venkamäki M., Ritala M., Leskelä M., 2012, Passivation of copper surfaces for selective-area ALD using a thiol self-assembled monolayer, *Semicond. Sci. Technol.* **27**. [DOI: [10.1088/0268-1242/27/7/074004](https://doi.org/10.1088/0268-1242/27/7/074004)]
- [38] Nie H.Y., 2017, Self-assembled monolayers of octadecylphosphonic acid and polymer films: Surface chemistry and chemical structures studied by time-of-flight secondary ion mass spectrometry, *Surf. Interface Anal.* **49**, 1431-1441. [DOI: [10.1002/sia.6296](https://doi.org/10.1002/sia.6296)]
- [39] Sun Y., Negreira A.R., Meersschaut J., Hoflijk I., Vaesen I. *et al.*, 2017, Optimization and upscaling of spin coating with organosilane monolayers for low-k pore sealing, *Microelectronic Engineering* **167**, 32-36.
- [40] Ellipsometry FAQ, J.A. Woollam, Ellipsometry Solutions, <https://www.jawoollam.com/resources/ellipsometry-faq>.
- [41] Ismail A., Khulbe K., Matsuura T., 2019, *Reverse Osmosis*, Elsevier, Amsterdam, The Netherlands.
- [42] Lecordier R., Herregods S., Armini S., 2018, Vapor-deposited octadecanethiol masking layer on copper to enable area selective Hf₃N₄ atomic layer deposition on dielectrics studied by in situ spectroscopic ellipsometry, *J. Vac. Sci. Technol.* **36(3)**, 031605(1)-031605(8).
- [43] Ishida T., Tsuneda S., Nishida N., Hara M., Sasabe H. *et al.*, 1997, Surface-Conditioning Effect of Gold Substrates on Octadecanethiol Self-Assembled Monolayer Growth, *Langmuir* **13**, 4638-4643.
- [44] De Oliveria R.R.L, Albuquerque D.A.C., Cruz T.G.S., Yamaji F.M., Leite F.L., 2012, Measurement of the Nanoscale Roughness by Atomic Force Microscopy: Basic Principles and Applications in *Atomic Force Microscopy – Imaging, Measuring and Manipulating Surfaces at the Atomic Scale*, chapter 7, edited by Dr. Victor Bellitto, IntechOpen. [ISBN [978-953-51-0414-8](https://doi.org/10.5772/intechopen.978-953-51-0414-8)]

- [45] Scientific Image – Atomic Force Microscope Illustration, NISE National Informal Stem Education Network, <https://www.nisenet.org/catalog/scientific-image-atomic-force-microscope-illustration>.
- [46] Elgrishi N., Rountree K.J., McCarthy B.D., Rountree E.S., Eisenhart T.T. *et al.*, 2018, A Practical Beginner's Guide to Cyclic Voltammetry, *J. Chem. Educ.* **95**, 127-206.
- [47] Jayaraman T.R., Venkatesan V.K., Udupa H.V.K., 1975, Cyclic voltammetries studies of electroless cobalt in naoh, *Electrochimica Acta* **20(3)**, 209-213.
- [48] Mayer M., Rutherford Backscattering Spectrometry, *Workshop on Nuclear Data for Science and Technology: Materials Analysis*, Trieste, Italy, 19-30 May 2003.
- [49] PubChem, Ethanol, <https://pubchem.ncbi.nlm.nih.gov/compound/702>.